Non-linear effects in the universe

by

Hui-Ching (Teresa) Lu

A thesis

presented to the University of Cape Town

for the degree of

Doctor of Philosophy

in

Applied Mathematics

Supervised by

Dr. Chris Clarkson

December 1, 2009

Abstract

One of the distinct trends in modern cosmology is in testing its theoretical aspects against the high precision data available in recent years. Although the standard cosmological model has already shown certain satisfactory results in matching the data from observations of the Cosmic Microwave Background and Large Scale Structure, we are by far unable to be convinced of its ability in describing the complete nature of the universe. Therefore, detailed study has to be done in the theory of higher order cosmological perturbation to enable us the ability in describing the non-linear aspects of the universe. Only then we shall be equipped with better knowledge/understanding to begin to appreciate better the vastness of the history/evolution of the universe. What is more troubling in being satisfied with the standard cosmological model is that the very foundation of the building blocks in the standard model - namely the Copernican principle - has yet to be tested against data with high accuracy.

In this thesis, a few contributions have been made in advancing these topics in the study of modern cosmology. Chapter 2 exams validity of the Copernican principle. We propose a principle test for the Copernican assumption. The proposed test does not depend on any theory of gravity nor on our understanding of dark energy, but relies only on the geometry of the Friedmann-Lemaître-Robertson-Walker models themselves. It is by definition that our proposed Copernican function should obtain a zero value at each redshift for the standard cosmological model - Friedmann-Lemaître-Robertson-Walker model, which assumes Copernican principle in its model building. In general, this Copernican function should yield a non-zero value at each redshift for an inhomogeneous model, for example the Lemaître-Tolman-Bondi model. We also present two alternative approaches that might help us in testing the validity of Copernican principle and hence further understand the underlying issues of dark energy.

Since one of the aims of this thesis is to address the non-linear aspects of the universe, we briefly review the Friedmann-Lemaître-Robertson-Walker model and its linear order perturbation. We will present its line element and all the components required for calculating the trace-reversed Einstein field equations at background and linear order. We also briefly look at the issue of coordinate transformation and gauge choices. Furthermore, it is necessary to present the power spectrum, the matter transfer function and introduce the features of the scalar, vector and tensor modes in linear theory. Last but not least, some basic ideas of the 1+3 covariant formalism are also presented and it should be of great help to us when we present our analysis on second order vorticity generation.

Chapter 4 outlines our investigation in second order vector modes from coupled linear scalar modes. We present the expressions for components needed for calculating the second order trace-reversed Einstein field equations. This should in term provides us with a constraint equation and an evolution equation for the second order vector modes. Vector perturbations typically produce vorticity and a transverse shear in the fluid four velocity.

Expressions for vorticity and vector shear are calculated at second order in order to better understand the issue of vorticity generation at second order. We investigate, first of all, how the vector modes are generated from individual scalar modes at radiation era by assuming the form of two delta functions for an input scalar power spectrum in the vector mode power spectrum expression. We find that the vector modes are efficiently produced when the two scalar modes are outside the Hubble radius. Furthermore, we realise that once one of the scalar modes is inside and the other outside the Hubble radius, there is effectively no generation of vector modes. We then move on to looking at the power spectrum of vector modes from power-law scalar input power spectrum. We also investigate the feature of the power spectra of vector metric perturbations and vector shear, and present our analysis on the issue of vorticity generation at second order during the dust era with a non-zero cosmological constant.

Preface

The work presented in this thesis is based on the collaboration with Kishore Ananda, Chris Clarkson, Roy Maartens and Bruce Bassett. Much of chapter 2 is based on the paper "A general test of the Copernican Principle", Chris Clarkson, Bruce Bassett and Teresa Hui-Ching Lu, *Phys. Rev. Lett.* 101 (2008) 011301. And chapter 4 is based on the two papers "Vector modes generated by primordial density fluctuations", Teresa Hui-Ching Lu, Kishore Ananda and Chris Clarkson, *Phys. Rev.* **D** 77 (2008) 043523, and "The cosmological background of vector modes", Teresa Hui-Ching Lu, Kishore Ananda, Chris Clarkson and Roy Maartens, JCAP 02 (2009) 023.

I hereby declare that this thesis has not been submitted, either in the same or different form, to this or any other university for a degree, and it represents my work.

Hui-Ching (Teresa) Lu

Acknowledgements

I am about done with PhD now. Next year out to the BUSINESS WORLD. Scary...

I would like to thank Chris Clarkson who is my official supervisor for his help, guidance, understanding and support during my PhD. It would not be possible to complete it without him.

I would like to thank my unofficial supervisor Kishore Ananda for his help and very calming advices and also his cool attitude toward things. He is a balancing factor between me and Chris sometimes.

I would like to thank everyone in the cosmology group and the Maths department at UCT as well for their tolerance toward me and my noisy self.

I would like to thank my family for their understanding and support. Without them, I would not be able to complete my PhD.

I would like to thank University of Cape Town and National Research Foundation (NRF South Africa) for their financial support during my PhD. I would like to thank the Royal Society and NRF South Africa for a joined grant from them for making my visits to the ICG possible.

I would like to thank my friends: Diane, Emma, Will, Oliver, Martin, Bonita, Nawahl, Viv and many many more for their support and tolerance toward me. It's very good to have them...

I would like to thank Tim as well. After all, he has very high tolerance and lots of support toward all my ups and downs during my PhD.

I would like to thank everyone at the ICG and Geneva cosmology group for their hospitality during my visits. I had a wonderful time during my stays. In particular, I would like to thank Roy Maartens and Ruth Durrer for their support and guidance. The visits would not have been made possible without encouragement from them.

I hope I have not forgotten anyone... Oh dear, I am not sure...

Contents

List of Abbreviations

CP	Copernican Principle
FLRW	Friedmann-Lemaître-Robertson-Walker
CMB	Cosmic Microwave Background
LSS	Large Scale Structure
SNIa	type Ia supernova
LTB	Lemaître-Tolman-Bondi
EOS	equation of the state
CDM	cold dark matter
BAO	Baryon Acoustic Oscillations
EFEs	Einstein field equations
EMT	energy momentum tensor
AP	Alcock-Paczynski

List of Symbols

ds	Infinitesimal line element
$g_{\mu\nu}$	Metric tensor
t	Coordinate time
a	Scale factor
K	Curvature of background spacetime
η	Conformal time, $d\eta = dt/a(t)$
$H(t)$	Hubble parameter in proper time, $H = \frac{\dot{a}}{a}$
$\mathcal{H}(\eta)$	Hubble parameter in conformal time, $\mathcal{H}(\eta) = aH(t)$
z	Redshift
G	Newton's constant
κ	$\kappa^2 = 8\pi G$
Λ	Cosmological constant
ρ	Energy density
Ω_m	Matter density parameter
Ω_Λ	Cosmological constant parameter
Ω_k	Curvature parameter
$d_A(z)$	Angular diameter distance/Area distance
$d_L(z)$	Luminosity distance
$R(t,r)$	Areal radius in LTB model
$E(r)$	Energy/geometric function in LTB model
$M(r)$	Gravitational mass function in LTB model
$t_B(r)$	Bang time function in LTB model
$\mathcal{C}(z)$	Copernican function
$w(z)$	Time varying equation of the state
q_0	Deceleration parameter
$H_\perp(t,r)$	Angular Hubble rate in LTB model
$H_\parallel(t,r)$	Radial Hubble rate in LTB model
γ_{ij}	Flat background spatial metric tensor
$\Gamma^\alpha_{\beta\gamma}$	Christoffel symbols
$R_{\alpha\beta}$	Ricci tensor
R	Ricci scalar
$G_{\alpha\beta}$	Einstein tensor
$T_{\alpha\beta}$	Energy momentum tensor
P	Pressure
u^α	Fluid four-velocity
w	Constant equation of the state
$\bar{g}_{\alpha\beta}$	Full perturbed metric (background + perturbed metric at each order)
$\delta^{(1)}g_{\alpha\beta}$	Perturbed metric at first order

$\phi^{(1)}$	Lapse function (scalar metric perturbation at first order)
$\psi^{(1)}$	Curvature perturbation (scalar metric perturbation at first order)
$B^{(1)}$	Scalar metric perturbation at first order
$E^{(1)}$	Scalar metric perturbation at first order
$F_i^{(1)}$	Vector metric perturbation at first order
$S_i^{(1)}$	Vector metric perturbation at first order
$h_{ij}^{(1)}$	Tensor metric perturbation at first order
$\delta^{\alpha}_{\ \beta}$	Kronecker delta
$\Phi^{(1)}$	Bardeen potential (lapse function in longitudinal gauge)
$\Psi^{(1)}$	Bardeen potential (curvature perturbation in longitudinal gauge)
$\bar{\Gamma}^{\alpha}_{\beta\gamma}$	Full perturbed Christoffel symbols (background + perturbed expressions)
$\delta^{(1)}\Gamma^{\alpha}_{\beta\gamma}$	Christoffel symbols at linear order
$\bar{R}_{\alpha\beta}$	Full perturbed Ricci tensor (background + perturbed expressions)
$\delta^{(1)}R_{\alpha\beta}$	Ricci tensor at linear order
$\delta^{(1)}R$	Ricci scalar at linear order
$\bar{T}_{\alpha\beta}$	Full perturbed energy momentum tensor (background + perturbed expression)
$\delta^{(1)}T_{\alpha\beta}$	Energy momentum tensor at linear order
$\bar{u}^{\alpha}$	Full perturbed four-velocity (background + perturbed expressions)
$\delta^{(1)}u^{\alpha}$	Four-velocity at linear order
$\bar{\rho}$	Full perturbed energy density (background + perturbed expressions)
$\delta^{(1)}\rho$	Energy density at linear order
$\bar{P}$	Full perturbed pressure (background + perturbed expressions)
$\delta^{(1)}P$	Pressure at linear order
$\bar{q}_{\alpha}$	Full perturbed energy flux (only perturbed expressions)
$\delta^{(1)}q_{\alpha}$	Energy flux at first order
$\bar{\pi}_{\alpha\beta}$	Full perturbed anisotropic pressure (only perturbed expressions)
$\delta^{(1)}\pi_{\alpha\beta}$	Anisotropic pressure at first order
k^i	Comoving wave vector
k	Comoving wave number $k^2 \equiv k^i k_i$
$\mathcal{P}_f(k,\eta)$	Dimensionless power spectrum of f
$n_s(k)$	Effective spectral index
c_s	Adiabatic sound speed
δ	Density contrast $\delta = \frac{\delta^{(1)}\rho}{\rho}$
$g(z)$	Growth suppression function
$\mathcal{R}$	Curvature perturbation in comoving gauge
$\Delta^2_{\mathcal{R}}$	Primordial power spectrum for curvature perturbation
$T(k)$	Transfer function
z_{eq}	Time at matter-radiation equality
z_d	Drag epoch
k_{eq}	Scale at matter-radiation equality
k_{silk}	Silk damping scale
Ω_b	Baryon density parameter
Ω_c	CDM density parameter
$h_{\alpha\beta}$	Projection tensor (projects orthogonal to the four velocity vector)
$U^{\alpha}_{\ \beta}$	Projection tensor (projects parallel to the four velocity vector)
Θ	Expansion scalar
$\sigma_{\alpha\beta}$	Shear tensor

$\omega_{\alpha\beta}$	Vorticity tensor
ω_{α}	Vorticity vector
$R_{\alpha\beta\mu\nu}$	Riemann tensor
$C_{\alpha\beta\mu\nu}$	Weyl tensor
$E_{\alpha\beta}$	Electric part of Weyl tensor
$H_{\alpha\beta}$	Magnetic part of Weyl tensor
$\delta^{(2)}g_{\alpha\beta}$	Perturbed metric at second order
$S_i^{(2)}$	Vector metric perturbation at second order
$\delta^{(2)}\Gamma^{\alpha}_{\beta\gamma}$	Connection coefficients at second order
$\delta^{(2)}R_{\beta\gamma}$	Second order Ricci tensor
$\delta^{(2)}T_{\beta\gamma}$	Second order energy momentum tensor
$\delta^{(2)}u^{\beta}$	Second order four velocity
$v_{(2)i}$	Second order vector velocity perturbation
$\bar{\omega}_{\alpha\beta}$	Full perturbed vorticity tensor (only perturbed expressions)
$\delta^{(1)}\omega_{\alpha\beta}$	First order vorticity tensor
$\delta^{(2)}\omega_{\alpha\beta}$	Second order vorticity tensor
$\bar{\sigma}_{\alpha\beta}$	Full perturbed shear tensor (only perturbed expressions)
$\delta^{(1)}\sigma_{\alpha\beta}$	First order shear tensor
$\delta^{(2)}\sigma_{\alpha\beta}$	Second order shear tensor
$\sigma_{(2)i}$	Second order vector shear perturbation
$\mathcal{P}_{\mathcal{V}}(k,\eta)$	Dimensionless vector mode power spectrum in radiation era
$\mathcal{P}_{\mathcal{S}}(k,\eta)$	Dimensionless vector mode power spectrum in dust era with non-zero Λ
Ω_{σ}	Dimensionless shear density
$h_{ij}^{(2)}$	Tensor metric perturbation at second order
$\hat{\mathcal{S}}^{ij}(\boldsymbol{k},\boldsymbol{x})$	Fourier space scalar projection operator
$\hat{\mathcal{V}}^{ij}(\boldsymbol{k},\boldsymbol{x})$	Fourier space vector projection operator
$\hat{\mathcal{T}}^{ij}(\boldsymbol{k},\boldsymbol{x})$	Fourier space tensor projection operator
$\mathcal{S}^{ij}(\boldsymbol{x},\boldsymbol{x}')$	Real space scalar projection operator
$\mathcal{V}_l^{\ ij}(\boldsymbol{x},\boldsymbol{x}')$	Real space vector projection operator
$\mathcal{T}_{lm}^{\ \ ij}(\boldsymbol{x},\boldsymbol{x}')$	Real space tensor projection operator

List of Figures

Chapter 1

Introduction

The Copernican principle

The Copernican principle (CP) has played a pivotal role from the beginning of modern cosmology. The modern day CP is the two assumptions that when averaged over large enough scales, the universe is homogeneous and isotropic. One of the most successful and commonly adopted model in cosmology is the Friedmann-Lemaître-Robertson-Walker (FLRW) model. The FLRW model describes a spatially expanding homogeneous and isotropic background, and therefore it is a model built on the foundation of the CP. Together with its linear perturbations, it has been shown to match the current high precision data from observations of the Cosmic Microwave Background (CMB) [206, 207, 117] and Large Scale Structure (LSS) [212]. The data provides strong evidence for a nearly spatially flat universe on large scales with a primordial spectrum of adiabatic, Gaussian and close to scale invariant density perturbations. However, this simple adoption of the CP in any cosmological model costs us dearly: for example in matching observational data from the CMB or from the type Ia supernova (SNIa) [82, 11, 190] to the model, a cosmological constant (or in general a dark energy component) is introduced without knowing its exact nature. Therefore, exploration of its validity has been in many researchers' focus especially in recent years when at last vast quantity of observational data with reasonable accuracy has become available to us.

The issue of testing the CP has been looked at by various authors and a few tests have been proposed. Here we will look at a couple of these tests in more details. In chapter 2 of this thesis we will consider the issue of testing the CP and propose a principle test for the Copernican assumption and two alternative approaches in testing the CP.

Inspired by the idea mentioned by Goodman in 1995 [87] on the possibility of testing the CP with the distortions of the blackbody spectrum of the CMB, authors in [44] took this idea a step further and demonstrated how this test can be implemented in a more practical approach. They chose to consider a low amplitude void with the profile that is known as a Hubble bubble (local void) embedded in a flat Einstein-de Sitter matter dominated universe

and calculated the constraints on the CMB blackbody spectrum distortion. They showed that their results rule out large voids with large density contrasts and in term ruled out the ones that were violating the CP the most.

Another idea on testing the CP was introduced in [227]. They proposed a method that uses the time drift of redshift (change of redshift with respect to time on observer's past light cone) in spacetimes with less symmetries than the FLRW universe, for example the spherically symmetric but radially inhomogeneous Lemaître-Tolman-Bondi (LTB) metric. Together with the distance data, they were able to demonstrate how the observation of time drift of redshift can be used to test the CP. In [55], another approach to test the CP was put forward. They showed that the local redshift dependence of the luminosity distance from the SNIa observation can be used to indicate if we live in a large void or if the dark energy is appropriate in explaining the cosmic expansion in the coming years. Other studies related to the CP have been done as well as the ones mentioned in more details above, see for example [31, 108, 221].

Dark energy/cosmological constant problem

Instead of trying to test the CP, dealing with the more direct problem at hand - understanding the nature/property of this dark energy/cosmological constant component, is a far more common practice. Ever since the discovery of the accelerated expansion of the universe from the observation of the luminosity distance to SNIa [192, 187, 178], people have been trying to explain this observed feature with a dark energy component which takes up about 70% of the total energy density with limited success. This limitation mainly comes from our lack of understanding in the underlying physics of dark energy. When at first the dark energy component was proposed to explain the accelerated expansion of the universe, it was addressed as a cosmological constant Λ (sometimes also considered as a negative pressure fluid with the equation of the state (EOS) $w = -1$). Soon afterward, the ΛCDM model, in particular the flat ΛCDM model, became the standard model in the study of the universe. See Fig. 1.1 for observational evidence for a flat universe.

This model provides a reasonably good fit to the high precision observational data, based on a small number of cosmological parameters that characterise it [63]. A consistent set of best fit model parameters coming from independent data sets such as CMB anisotropies, galaxy surveys and supernova luminosities marks a remarkable achievement for the ΛCDM models (see Fig. 1.2 for constraints from joint data sets). However, anything that contributes to the energy density of the vacuum acts just like a cosmological constant since it enters the Einstein field equations via an energy momentum tensor $T^{vac}_{\mu\nu} = -(\Lambda/8\pi G)g_{\mu\nu}$. With our current understanding of particle physics, it is still extremely difficult to explain as to why the theoretical expectations for the cosmological constant exceed observational limits by approximately 120 orders of magnitude [237, 229, 230].

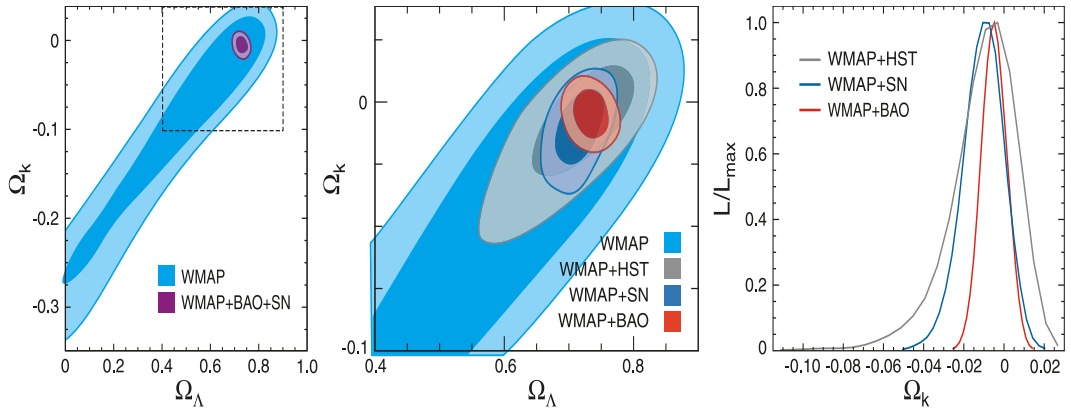

Figure 1.1: In the (Ω_Λ,Ω_k) plan: evidence for a flat universe from the combined data analysis from two observations: CMB and LSS. Figure taken from [117].

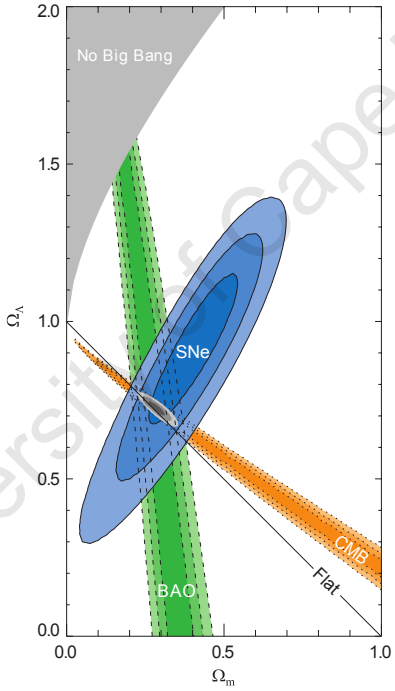

Figure 1.2: In the $(\Omega_m, \Omega_\Lambda)$ plane: joint constraints from CMB [63], baryon acoustic oscillations (BAO) [70] and Union supernovae data set including samples from the Supernova Legacy Survey and ESSENCE Survey, the older datasets, and HST. Showing in the figure are their 68.3%, 95.4% and 99.7% confidence level contours (figure taken from [118]).

This has a lead to a variety of approaches which attempt to explain the accelerated expansion. For example, instead of a rather limited constant EOS, one should perhaps consider a time varying EOS $w(z)$ for the dark energy. Common parameterisations of $w(z)$ include a linear variations with redshift, $w(z) = w_0 + w_z z$, as proposed in [58], an evolution that reaches a constant w at high redshift, $w(z) = w_0 + w_a z/(1+z)$, as proposed in [132] or

an evolution with an EOS that has the form $w(z) = w_0 - \alpha \ln(1+z)$ such as the one used in [68, 85]. Here w_0 is the present value of the EOS and $\alpha \equiv dw/d\ln a$ with a being the scale factor. However from the data fitting point of view, the assumption of a functional form can lead to possible biases in statements made about the dark energy and its evolution. This is especially so should the true dark energy EOS behave very differently from its assumed functional form [124]. More importantly the far fetched relation of the parameterisation to the physical parameters is of a greater cause of concern, see for example [193, 145].

This is not the only concern that has been raised related to the issue of dark energy. We also have to bear in mind that cosmic observations also depend on other cosmological parameters such as the curvature density Ω_k and the total matter density Ω_m. It has long been known that there are degeneracies between Ω_k, Ω_m and $w(z)$ and this issue has been under intense investigation, see for example [133, 54, 100, 97]. It has also been argued that should it turn out that we have an interaction between the dark components - dark energy and dark matter (see [27, 79, 228] for a few proposed models), it is possible to create new features to structure formation. These include a possible bias as pointed out in [5] and also a possible violation in the weak equivalence principle by dark matter [25]. Another concern regarding the dark components is raised in [119]. It has been argued that current background observations cannot distinguish beyond the combination of dark matter and dark energy evolution since they degenerate at a level that is sensitive to the total energy momentum tensor. Without additional assumptions, we cannot measure either of them by purely gravitational observations.

Seeing such difficulty in understanding the nature of dark energy and the complexity of the problem (see Fig. 1.3 for an illustration of some of the possible dark energy model classes and how they have grown from the simplest model - ΛCDM), this leads some to search for an alternative explanation to the observed accelerated expansion of the universe. For example, if the accelerated expansion of the universe is actually caused by the geometry of the universe being inhomogeneous, this might fool us wrongfully into the conclusion that there should be dark energy by *mimicking* a non-zero cosmological constant behaviour in a homogeneous universe. This gives us an alternative way of explaining as to why there should be no cosmological constant and yet at the same time possibly with minimal new physics introduced. Due to the apparent needs in finding alternative explanation to dark energy, the inhomogeneous models have only received renewed interests in recent years even though the idea was put forward as early as in the 1990s (see e.g. [175]).

Some alternative explanations to dark energy

There are a few proposed ways as to how the inhomogeneities could in principle mimic dark energy. One of which has gained momentum in recent times is the so-called 'back-reaction' approach (see for example [43] for a review). This back-reaction comes from the

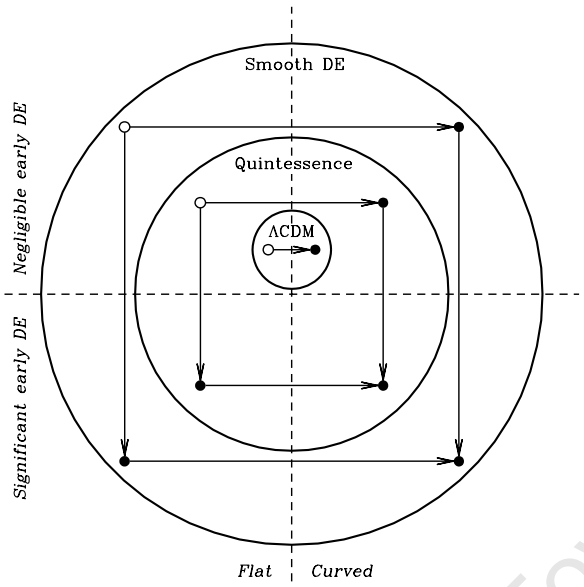

Figure 1.3: Illustration of the model classes (large circles) and subclasses (represented by points within different regions of the circles). Open points mark the initial (simplest) type of model within each class, and arrows indicate paths to the more complex models in the class. Note that in the figure models with constant EOS are under the category of "Negligible early DE". Figure taken from [158].

fact that the operations of spatial averaging do not commute with the time evolution [42]. Therefore, in an inhomogeneous universe the averaged quantities satisfy modified Friedmann equations that contains these back-reaction terms. These back-reaction terms increase as inhomogeneities develop since they depend on the variance of the local expansion rate. Whether one can explain away the cosmic acceleration with back-reaction is still unclear at the moment and it is hotly debated [107, 174, 185, 233]. Even if $\Lambda = 0$ and acceleration is due to back-reaction, one would still need to explain the cosmological constant problem [56] and this is yet another open question in modern cosmology.

Another interesting proposal is the idea of having a local void (a local underdense region) around us and hence our universe is in fact an inhomogeneous universe. This way it is conceivable that we do not have to assume an accelerated expansion in order to fit the data as we have done for the homogeneous and isotropic models.

Several authors have investigated the local void idea before [3, 4, 83, 215, 216, 217, 48, 28] and most have used a LTB model to describe the void. At the moment, the most exigent problem in the void modelling is our ability in determining the correct void size that is able to match up with all the current data from various sources, for example data from the CMB, supernovae observation, and baryon acoustic oscillations. So far there has been no success in fitting all three data sets despite many attempts. More complicated scenarios have also been considered already. For example instead of having the observers in the centre of the void,

we have off-centre observers. Unfortunately, there has been limited success in that direction as well and in reality more investigation is still required in order to model the void correctly.

Linear perturbation theory

Despite the unsolved cosmological constant problem in the standard model in cosmology, it is not without its merits. As mentioned earlier, it has been shown after all that it is able to fit the current data to a reasonable degree. What is more is that the background FLRW model plus its linear perturbation has shown its ability in developing the basic theory of structure formation. Of course given the complexity of the universe, no linear theory will have the capacity to fully describe it. Consequently, developing the perturbation theory to at least second order becomes a necessity since only then we will have the tools to be able to study the mildly non-linear features we observe in the universe.

The key idea in the theory of structure formation is that in the early universe if there existed small energy density fluctuations (also called seeds), then they could be amplified by gravitational instability. It is possible to study the induced fluctuations and their time evolution using linear perturbation theory because the linear theory uses inhomogeneous perturbations about a homogeneous background and these seeds are an inhomogeneously distributed form of energy density that contributes only a small fraction of the total energy density of the universe. This idea is very appealing since it is consistent with what we can see from the CMB observation (see Fig 1.4).

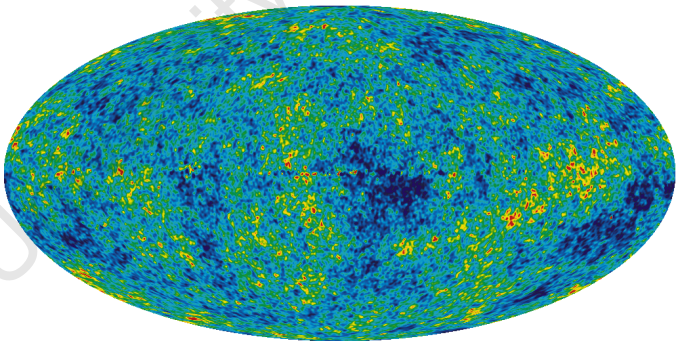

Figure 1.4: From the CMB anisotropies we can see that there are small inhomogeneities in the early universe. Therefore, the idea of studying the theory of structure formation using the inhomogeneous linear perturbations around a homogeneous background is feasible. Figure taken from [96].

Linear cosmological perturbations were initially studied in quite significant details by Lifshitz [128]. It was later extended and with some errors corrected by authors in [129]. However, synchronous gauge was used in both publications and their analysis was plagued by some ambiguity caused by the gauge modes. This further caused some misinterpretation and misuse of their results by many authors at the time without realising this problem. But

some did recognise this gauge mode problem and tried to develop methods that are gauge independent. For example, in [94, 170] they tried to develop a formulation that deals with curvature tensor perturbation instead of the perturbation in the metric tensor. However, it was not a complete success and they couldn't solve the ambiguity caused by a gauge mode in their expression with a zero pressure cosmic fluid.

In the meantime, equations for density perturbations in a longitudinal gauge was derived in [92]. It was then discovered that the gauge modes problem that was plaguing the synchronous gauge analysis was not appearing in the longitudinal gauge expressions. Then it was shown in [168, 189] that the derive perturbative expressions are free of gauge modes in a comoving gauge. They also used various gauge conditions to investigate the evolutionary behaviour of density perturbations and hence clarified the issue of gauge dependence in the growth rate of the density perturbation.

All of the papers mentioned above focused on the situation where we have adiabatic perturbations without sources. Therefore, there remained the issues of what could possibly be sourcing these density perturbations on super horizon scales and the size of their amplitudes still need to be considered. It was only in 1980 that these issues were addressed thoroughly. In [184], they managed to show how one can remove the two unphysical gauge modes in synchronous gauge that were causing much unwanted confusions and hence interpreted results on density perturbations on super horizon scales erroneously. This provided them with renewed understanding in the study of density perturbations and hence allowed them the freedom to take one step further to investigate the idea of generating density perturbations with an entropy perturbation.

Then in [12] Bardeen formulated the completely gauge invariant perturbation equations that took the study of the theory of linear perturbation to the next level. He not only studied the density perturbations in the linear theory, but also focused on the vector and tensor types of perturbations. To some extent, he also examined the criterion for the validity of the linear perturbation analysis by comparing the perturbation amplitudes between several physical quantities. His equations for gauge invariant variables were later on re-derived in [35] in a straightforward manner starting from the synchronous gauge.

Taking full advantage of these gauge invariant perturbation equations formulated by Bardeen, in [116] they reformulated the expressions extensively and paid special attention to the geometrical meaning of the perturbation. Furthermore, they also looked at the application of the linear theory to some cosmological models, including for example examining the effect of isotropic and anisotropic stress perturbations, behaviour and generation of density perturbations in the radiation and dust universe and so on. Since then gauge invariant perturbative approach received more and more popularity and has been applied to various areas in cosmology, for example it has been used to study the dynamics of inflationary universe models [81], to study fluctuations in the CDM model of structure formation [157] and used for a gauge invariant analysis of perturbations through the decoupling epoch [90].

And it has now become a fundamental tool for any modern cosmologist.

Alternative approaches to cosmological perturbations have been worked on as well. One of which that is a competitive contender to the usual metric approach is a gauge invariant formalism based on covariant approach. This covariant approach has the idea of defining exact variables that are meaningful in any spacetime such that their values vanish on the background [74, 76, 75, 105] (see [64, 37] for the extension to multi-fluid an scalar field models in the covariant approach). These variables are gauge invariant perturbations of the FLRW background and their physical meanings are apparent through the covariant definition. However, due to the technical complication when working with the covariant approach, it has not been able to reach the popularity that the metric approach has achieved in the study of cosmological perturbation theory.

The upsurge of interest in linear perturbation theory pushed it into its maturity, since then it has provided us with a means to explain the origin of structures such as galaxies and clusters in the inflationary universe model. The important recognition that quantum fluctuations in an expanding universe could lead to classical density perturbations was pointed out in [51]. Also, it was pointed out in [183, 191] that in an inflationary universe scales inside the Hubble radius $H^{-1}(t)$ (or comoving scales that are smaller than the comoving Hubble radius $(aH)^{-1}$) at the beginning of the inflation will expand rapidly and exit the Hubble radius (the horizon). However, they will re-enter the Hubble radius at a time after the period of inflation and form the large scale cosmological perturbations and it was pointed out in [93, 239] that they have a scale invariant power spectrum in the simplest inflationary models. See Fig 1.5 for a schematic demonstration on the creation and evolution of perturbations in the inflationary universe.

The proposal that the universe went through a period of inflationary phase was originally introduced in [91] in order to deal with a variety of cosmological problems: the horizon problem, the flatness problem, and the unwanted relic problem. The horizon problem arise when we see the same CMB temperature on patches that we believe have never been in causal contact before the photons have been emitted. The flatness problem is also called the fine-tuning problem. With the geometry of the universe observed by the CMB to be nearly flat today, this implies that an extremely fine-tune conditions will be needed for early times since the curvature grows in time in the standard model of cosmology. The unwanted relic problem is also known as the monopole problem. The prediction (from currently known particle physics models) that some stable relics (magnetic monopoles) produced at very high temperatures such as the ones experienced in the early universe are not observed today. It is therefore still an open question if they exist at all. See [126] for more details on these issues and for the different proposed inflationary models. Although the inflationary universe model has shown an ability in addressing the three cosmological problems, many have considered it to be merely a toy model. However since its proposal, the theory has gone from strength to strength and it has now become part of the standard model

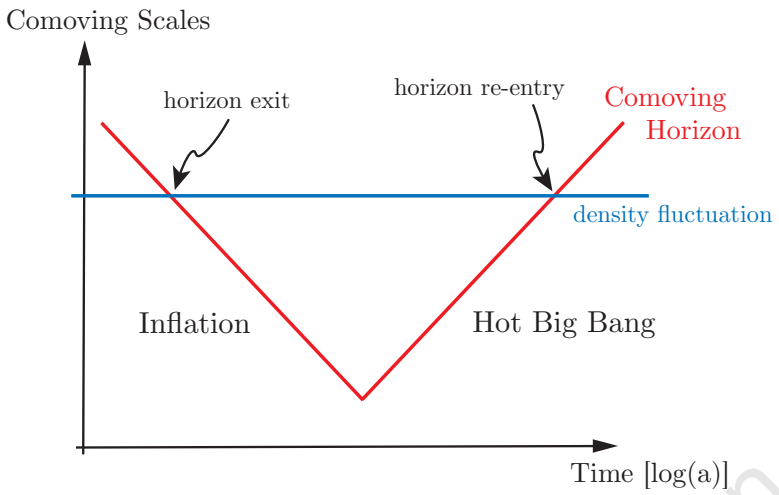

Figure 1.5: Schematic demonstration on the creation and evolution of perturbations in the inflationary universe. Perturbations are inside the horizon at first then expand rapidly and exit the horizon. However, they re-enter the horizon at a later time when the period of inflation has ended. Figure taken from [21].

of cosmology that cannot be dismissed lightly. The realisation that it has shown success in explaining the production mechanism for the large scale structure such as clusters of galaxies in the universe and the CMB temperature anisotropies, which was first detected by the Cosmic Background Explorer (COBE) satellite [23, 89, 204], through the linear theory of cosmological perturbation, has allowed us the possibility of testing some aspects of inflationary scenario.

In cosmological perturbation theory, the metric tensor can have three different types of perturbations: scalar, vector and tensor perturbations/modes. Scalar modes are related to the matter density perturbation, vector modes are also known as the rotational perturbations and tensor modes are the so-called gravitational waves (which are yet to be detected directly). At linear order in the usual inflationary models, scalar and tensor modes have been studied by many [232, 223, 224, 138] and predictions have been made on a specific relationship between the spectrum of the scalar and tensor modes [127]. However, so far vector modes have received little attention because a scalar field cannot support vector modes at linear order as illustrated in [19, 152]. Even if vector modes are produced during inflation, once they leave the Hubble radius during the inflationary phase they will decay very rapidly. Therefore, in the inflationary paradigm the vector modes at linear order are considered to be insignificant when compared with scalar and tensor modes.

Throughout the years some authors have proposed other contenders to the usual early universe inflationary models, for example the pre big bang scenario or the cyclic/ekpyrotic models [84, 208, 213]. Although some have become highly disfavoured (or even ruled out) by our current observation, others have survived. In this regard, gravitational wave ob-

servations become one of the most crucial experiments in the modern cosmology since for example in the cyclic/ekpyrotic scenario it has been shown to have a very different gravitational wave production when compared with a single field inflationary models [34]. Due to the significant impact that the existence of gravitational waves would have on modern cosmology, there have been a few experiments designed for its direct detection. Two of such experiments are the ground based Advanced Laser Interferometer Gravitational-Wave Observatory (Advanced LIGO) [130] and the space mission Laser Interferometer Space Antenna (LISA) [134, 135, 151].

An alternative search of these tensor perturbation is from the CMB polarization. It was pointed out in [111, 112, 196, 197] that for the CMB polarization via Thomson scattering the tensor perturbations produce both E-modes (curl-free) and B-modes (curl type) while the scalar perturbations create only E-modes and the vector perturbations create mainly B-modes. This could provide us with an indirect probe of the tensor perturbations and a unique opportunity to disentangle the effect of the tensor perturbations from the scalar perturbations. However, the greatest obstacle in this approach is our ability to clean the B-mode signals from the contamination caused from the effect of weak gravitational lensing on the CMB by the matter distribution. This is because weak lensing on the CMB transforms the E-mode into B-mode polarization and hence obscure the tensor perturbations signal. However, it has been shown in [195] that this lensing effects can be largely cleaned using high resolution data (10 arcmin or better), thus permitting us to probe inflationary models with tensor to scalar power spectrum amplitude ratios to be $r \sim 10^{-6}$.

Non-linear perturbation theory

With the level of technological advancement that we have achieved in recent years and we will be able to achieve in the future, many have realised that we should start looking into the non-linear aspects of our universe. From the analysis done on observational data using the linear theory, the universe is revealed to have approximately adiabatic and Gaussian fluctuations. Should one be required to better constrain the accuracy of these first order results or study the primordial non-Gaussian features of the universe, one would have to go beyond linear order.

Physical observable such as the three point correlation function (or its Fourier counterpart, the bispectrum) of the scalar perturbations that is able to distinguish non-Gaussian from Gaussian perturbations on various cosmological scales. It requires us to do a perturbative expansion up to second order in order to obtain a self-consistent result and we would find it hard to compute and understand the bispectrum for the primordial scalar perturbations without our understanding on a gauge invariant definition of the comoving curvature perturbation (which is conserved on large scales) at second order in the perturbative approach [142, 137] (see also [14] for a review on primordial non-Gaussianity). Therefore, it

would be timely for us to develop and gain a comprehensive insight in the theory of non-linear cosmological perturbation. Indeed, it has been one of the rapidly growing fields in modern cosmology in recent years.

Although we have achieved quite an ample understanding in the linear perturbation theory, development of the second order perturbation theory has not been straightforward. Part of it is due to the sheer enormity of the algebraic expressions involved at second order. Issues relating to gauge transformation and gauge invariance at second order has been looked at using rigorous mathematics [205, 40, 38, 39]. In a series of papers [162, 163, 164, 165, 166, 167], Nakamura followed and principally expanded these work in an attempt to lessen the complicated formulation usually involved when one goes beyond linear order. Some authors even dedicated themselves into presenting a large set of expressions in hopes that they would aid any who wishes to work on non-linear perturbation theory [103, 104, 169].

Similar to the linear theory, the metric tensor can also have scalar, vector and tensor perturbations at second order. Owing to the important implications the tensor modes might have in modern cosmology, they have received much interest to date. In the linear theory, the amplitude of the first order gravitational waves depends on the energy scale of inflation and may not be observable should inflation occur at a scale much below the GUT scale [114]. However, second order tensor mode generation does not depend on which early universe model that we adopt in our analysis, e.g. inflation versus ekpyrotic/cyclic. This is because the observed Gaussian distribution of the linear matter density perturbations could in fact generate second order tensor modes via a quadratic mode-mode coupling mechanism and provide us with a χ^2-distribution for the second order tensor modes.

Some authors have investigated along this direction. In [7], they investigated second order tensor modes generated from a quadratic scalar modes coupling in the radiation era. They first studied the second order gravitational wave generation by a single scalar mode. This can be done by choosing a delta function form at a single scale for the input power spectrum. This has allowed them to gain insight into the generation mechanism of second order tensor modes induced by linear scalar modes. They also computed the gravitational wave background generated by a power law spectrum on all scales and found that the linear scalar modes continued to add power to a single tensor mode power spectrum until it is well inside the Hubble radius, but then tensor mode oscillates at almost constant amplitude at later times. They also found that on a given scale only a narrow range of the linear scalar modes with well defined phase make the dominant contribution to the second order tensors. Finally, they concluded that it is possible to place independent limits on the scalar tilt from the proposed future detectors such as LISA or DECIGO [113].

Authors in [22] expanded the work done in [7] and they derived the complete power spectrum of the second order gravitational waves induced by scalar modes ranging over all observable wavelengths. They first gave the analytical solutions to the energy densities of both the second order scalar induced gravitational waves and first order gravitational waves

in inflationary models. Then they numerically integrate the equation of motion directly and confirmed their analytical results with the numerics (see Fig. 1.6 for a comparison between energy density spectra of first and second order gravitational waves). Note that as pointed out in [22], with fine tuning the primordial inflationary contribution can be suppressed below the current scalar induced contribution for the gravitational wave energy density spectra. This can be seen in Fig. 1.6 where we have the red thick curve (today) crosses the black dotted curve (primordial) at intermediate wavelengths.

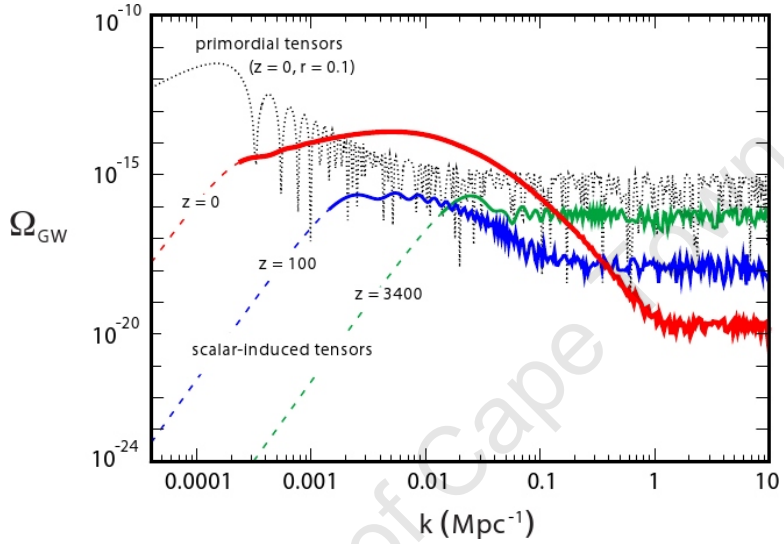

Figure 1.6: The red, blue and green curves represent the energy density spectra of the scalar induced tensors at today, redshift $z = 100$ and redshift $z = 3400$. Note that the dashed range of these three curves represent large scale modes that are outside the horizon at each given epoch. The black curve is the energy density spectra of scale invariant primordial tensor modes for an inflationary model with tensor-to-scalar ratio $r = 0.1$. Figure taken from [22].

Work has been done on investigating the effects of these second order gravitational waves, generated on very large scales, on CMB polarization [155]. Similar to the way that primordial black hole formation has been used to constrain over-densities on small scales, some have also studied how the gravitational waves produced in the radiation dominated era can be used as a constraint on the primordial density perturbation on the scales that are not directly observable by the CMB or LSS [86, 125, 10].

Note that what we have mentioned here regarding second order gravitational waves is only the tip of an iceberg and we cannot go through everything in much detail due to the vast quantities of literature one can find relating to tensor modes in perturbation theory. See for example [45, 46, 148, 149, 146, 172, 67, 62, 9, 8] for a list of relevant work.

As pointed out earlier, vector (rotational) perturbations at linear order are considered to be insignificant since scalar field cannot support linear vector modes. This might lead

one to have the naive expectation that second order vector modes would be the same as in the linear case, so that a generic prediction arise from inflation is that there is no vector modes. However, this expectation could not be more wrong because the same mechanism that generates second order tensor modes from coupled linear scalar modes can apply to second order vector modes as well.

There are a variety of other mechanisms which also predict vector modes and they have been studied by various authors before. Some examples of such include fine-tuned anisotropies in collisionless neutrinos [122], cosmic strings [182, 234] and the presence of a primordial magnetic field [210, 123]. Also, in [152] they studied how the second order vector modes are generated by first order scalar modes but in a collapsing universe scenario. Authors in [147] considered the generation of primordial magnetic fields and vorticity from second order cosmological perturbations. However, a detailed investigation of the generation mechanism that produces second order vector modes from coupled linear scalar modes in the standard (inflationary) scenario remains a missing puzzle in the theory of cosmological perturbation until the work done for this thesis which is presented in chapter 4.

It must be emphasised that it is important to better understand these vector perturbations since they are likely to play a more prominent role in cosmology in the coming years. This is because of their contributions to the CMB (see for example [15, 16, 156, 218, 219, 220] for some relevant work) [1]. As a result, it will impact on the B-mode polarization in the CMB and could become the dominant contribution when compared with the second order gravitational waves [155].

The work presented in this thesis is in the following order: in chapter 2 the issue of testing the Copernican principle is considered and a Copernican function is proposed. This Copernican function does not depend on any theory of gravity nor on our understanding of dark energy, but relies only on the geometry of the FLRW models themselves. It is demonstrated that our Copernican function is zero for the homogeneous FLRW models and it is non-zero for the inhomogeneous LTB models. In chapter 3, some basics in standard cosmological perturbation theory are briefly outlined. These include introducing the basic features of the flat FLRW model and its linear perturbation. The definition of power spectrum and the matter transfer function are also presented. Features of scalar, vector and tensor modes in linear theory are introduced. Chapter 4 deals with another important part of this thesis. In this chapter, our investigations in second order vector modes from coupled linear scalar modes both in the radiation and dust (with a cosmological constant) eras are presented. The power spectra of these vector modes at both eras are calculated and the issue of vorticity generation at second order are discussed. Finally, in chapter 5 a brief summary of the work presented in this thesis and discussion of possible future work is also presented.

[1] Note that [15, 16] gives an incorrect description of the Boltzmann equation at second order. See [179, 180, 181] for the correct expressions and derivations.

Chapter 2

Testing the Copernican Principle

The CP has stood as one of the fundamental assumptions in the heart of the study of modern cosmology without being properly tested for decades. However as we approach the age of being able to harvest a significant amount of high precision data, it is perhaps timely for us to give the issue of testing the Copernican principle a more serious consideration.

In this chapter, we shall propose a general method that might help us in testing the CP. Before we introduce it, we shall firstly look at some basics of the FLRW model which is a homogeneous model and the LTB model which is the simplest inhomogeneous model. Using the test we proposed here, we will demonstrate the difference in the Copernican function between the FLRW model which has adopted the CP and the LTB model which has not had the CP embedded in its foundation. Lastly, we shall propose a few alternative methods that might also help us justify the validity of the CP.

2.1 Homogeneous model - Friedmann-Lemaître-Robertson-Walker model

The FLRW model is spatially homogeneous and isotropic. When using the FLRW model, it is automatically assumed that the CP is valid. Here we will briefly introduce some basics of the FLRW model.

Throughout this thesis, we use units where the speed of light is $c = 1$. Also, the Greek indicies run from 0 to 3 and the Latin indices run from 1 to 3. The general FLRW metric is given as (note that we have used the signature (–, +, +, +) throughout this thesis):

$$ds^2 = g_{\mu\nu}dx^\mu dx^\nu = -dt^2 + a^2(t)\left[\frac{1}{1-Kr^2}dr^2 + r^2 d\Omega^2\right], \tag{2.1}$$

where t is the cosmic time, $a(t)$ is the scale factor, and $d\Omega^2 = d\theta^2 + \sin^2\theta d\phi^2$.

We can define the Hubble parameter in cosmic time to be $H(t) = 1/a(t)\ da(t)/dt = \dot{a}(t)/a(t)$. The variables r, θ and ϕ are polar coordinates. Constant K represents curvature

of the spatial geometry. For $K > 0$, $K = 0$ and $K < 0$, we have positive spatial curvature (closed), zero spatial curvature (Euclidean) and negative spatial curvature (hyperbolic) universe respectively. We can relate proper time to conformal time η via the relation $d\eta = 1/a(t)dt$. The conformal Hubble parameter is just $\mathcal{H} = 1/a(\eta)\ da(\eta)/d\eta = a'(\eta)/a(\eta)$.

Another commonly used presentation of the FLRW metric is

$$ds^2 = -dt^2 + a^2(t)\left[d\check{r}^2 + f^2(\check{r})d\Omega^2\right], \tag{2.2}$$

where we have $f(\check{r}) = \check{r}$, $f(\check{r}) = 1/\sqrt{K}\sin(\sqrt{K}\check{r})$ and $f(\check{r}) = 1/\sqrt{K}\sinh(\sqrt{|K|}\check{r})$ for $K = 0$, $K > 0$ and $K < 0$ respectively.

2.1.1 The cosmological redshift and the density parameter

The cosmological redshift, z, is defined in terms of the ratio of the observed and emitted wavelengths, λ_o and λ_e respectively, in the radiation spectrum of an observed galaxy. This definition can be related to the scale factor since the wavelength scales linearly with the scale factor, i.e. $\lambda \propto a$.

$$z = \frac{\lambda_o}{\lambda_e} - 1 = \frac{a_o}{a_e} - 1, \tag{2.3}$$

where a_o represents the value of the scale factor at the time of observation and a_e is the value of the scale factor at the time of emission. At present time t_0, we can set $a_o = a_0$.

This provides us a way to relate cosmic time t, conformal time η, scale factor and redshift z:

$$d\eta = \frac{dt}{a(t)} = \frac{da}{H(a)a^2} = -\frac{1}{a_0}\frac{dz}{H(z)}. \tag{2.4}$$

This relation is very useful to us since in all our analysis presented later, we will convert all our expressions from functions of conformal time η to redshift z because this is what we can obtain from observational data.

From the Einstein field equations (EFEs), we can calculate the Friedmann equation. We will show in more detail as to how this can be done in chapter 3 and we will only present expression for the Friedmann equation here:

$$3H^2 = \kappa^2\rho + \Lambda - \frac{3K}{a^2}, \tag{2.5}$$

Note that here we have $\kappa^2 = 8\pi G$, Λ is the cosmological constant and ρ is the energy density. This is particularly useful to us when we need to define the density parameter introduced next.

Besides redshift, another parameter that is widely used in cosmology is the density parameter. When we have a 'flat' universe with zero cosmological constant, a critical density ρ_c arise from it. The critical density is defined through the first term in the Friedmann

equation Eq. (2.5)

$$\rho_c = \frac{3H^2(t)}{\kappa^2} = \frac{\mathcal{H}^2(\eta)}{a^2(\eta)}\frac{3}{\kappa^2}. \tag{2.6}$$

Current value of the matter density parameter is just that

$$\Omega_{m0} = \frac{\rho_0}{\rho_{c0}} = \frac{\kappa^2\rho_0}{3H_0^2}, \tag{2.7}$$

where ρ_0 is the current density of the universe and ρ_{c0} is the present day critical density and H_0 is the Hubble parameter today. Similarly, one can also define a parameter that is associated with the cosmological constant

$$\Omega_\Lambda = \frac{\Lambda}{3H_0^2}. \tag{2.8}$$

If we consider any constant background curvature K, we can then define a parameter that is associated to it such as

$$\Omega_k = -\frac{K}{3H_0^2}. \tag{2.9}$$

In this case, we have $\Omega_{m0} + \Omega_\Lambda + \Omega_k = 1$. Note that if $K > 0$ then $\Omega_k < 0$ and vice versa. New expression for the Hubble parameter is

$$H^2(z) = H_0^2\left[\Omega_{m0}(1+z)^3 + \Omega_\Lambda + \Omega_k(1+z)^2\right]. \tag{2.10}$$

Since we look at the flat FLRW background in chapter 3, we shall have $\Omega_{m0} + \Omega_\Lambda = 1$. Using Eqs. (2.4), (2.3), (2.7), (2.8) and (3.14), we can obtain a new expression for the Hubble parameter:

$$H^2(z) = H_0^2\left[\Omega_{m0}(1+z)^3 + \Omega_\Lambda\right]. \tag{2.11}$$

2.1.2 Distance relations

In this subsection, we present two important distance relations in cosmology: angular diameter distance (also known as the area distance) and luminosity distance. They can be found in any textbooks on cosmology (see e.g. [61]).

Angular diameter distance/Area distance

If we consider a non-expanding background, the angular diameter distance is the measure of the distance between a source with known physical size $\mathcal{D}$ and an angle ϑ subtended by the source at the observer. This distance can be expressed as

$$d_A = \frac{\mathcal{D}}{\vartheta}. \tag{2.12}$$

However, in the case of FLRW background which describes an expanding universe, it is slightly more complicated than what is shown in Eq. (2.12). Now we need to take into consideration that the comoving size of the source is $\mathcal{D}/a$ where again a is the scale factor. Consider the observer's position is at $r = 0$ (with time being $t = t_o$) without loss of generality and the source is at position $r = r_e$ emitting a signal at time $t = t_e$. The comoving distance out to the source is defied as

$$\chi = \int_{t_e}^{t_o} \frac{dt}{a(t)} = \int_{a_e}^{a_o} \frac{da}{a^2 H(a)} = \int_{z_o}^{z_e} \frac{1}{a_o} \frac{dz}{H(z)}, \tag{2.13}$$

where we have used Eq. (2.4). Now the angle subtended by the source at the observer is then $(\mathcal{D}/a)/\chi$. The angular diameter distance in flat FLRW background is

$$d_A(z) = \frac{\chi}{1+z}. \tag{2.14}$$

This can be arrived at by substituting an expression for $H(z)$ using Eq. (2.10). If we consider non-zero curvature background, then the angular diameter distance is

$$\begin{aligned} d_A(z) &= \frac{1}{(1+z)H_0\sqrt{\Omega_k}} \sin\left(H_0\sqrt{\Omega_k}\chi\right), \text{ for } \Omega_k > 0. \\ d_A(z) &= \frac{1}{(1+z)H_0\sqrt{-\Omega_k}} \sinh\left(H_0\sqrt{-\Omega_k}\chi\right), \text{ for } \Omega_k < 0. \end{aligned} \tag{2.15}$$

One thing worth noting is that from Eqs. (2.14) and (2.15) we can see that the flat case ($\Omega_k = 0$) is essentially the same as considering $\frac{\chi\sqrt{x}}{\sqrt{x}} \approx \chi$. This property was used in presenting Eq. (2.36) and hence only one expression is shown instead of three.

Luminosity distance

In a non-expanding background, the observed flux $\mathcal{F}$ at a distance $\boldsymbol{d}$ from a source of known luminosity L is

$$\mathcal{F} = \frac{L}{4\pi \boldsymbol{d}^2}, \tag{2.16}$$

where $4\pi\boldsymbol{d}^2$ is the area (of the telescope) where the emitted light goes through at observer and distance $\boldsymbol{d}$ is the luminosity distance in this case. If we consider expanding flat FLRW background, then the observed flux $\mathcal{F}$ from a source of known luminosity L is

$$\mathcal{F} = \frac{La^2}{4\pi\chi^2}. \tag{2.17}$$

If we compare Eqs. (2.16) and (2.17), then the luminosity distance in flat FLRW background is

$$d_L(z) = (1+z)\chi. \tag{2.18}$$

Note that from Eqs. (2.14) and (2.18) we can conclude that a relation between the diameter distance and luminosity distance in flat space is

$$d_L(z) = (1+z)^2 d_A(z). \tag{2.19}$$

However, this relation is true in curved spacetime as well. This was proved generally in [72] and tested later in [18, 225].

2.2 Inhomogeneous model - The Lemaître-Tolman-Bondi model

The general spherically symmetric metric for an irrotational dust matter source in synchronous comoving coordinates is the Lemaître-Tolman-Bondi [120, 214, 32] metric

$$ds^2 = -dt^2 + \frac{[R'(t,r)]^2}{1+2E(r)}\, dr^2 + R^2(t,r)d\Omega^2, \tag{2.20}$$

where $R'(t,r) = \partial R(t,r)/\partial r$, and $d\Omega^2 = d\theta^2 + \sin^2\theta d\phi^2$ is the unit 2-sphere. The function $R = R(t,r)$ is the areal radius, since the proper area of a sphere of coordinate radius r on a time slice of constant t is $4\pi R^2$. The function $E = E(r) \geq -1/2$ is an arbitrary function of the LTB model, representing the local geometry.

Solving the EFEs gives us a generalised Friedmann equation for $R(t,r)$,

$$H(t,r) \equiv \partial_t \ln R(t,r) = \frac{1}{R(t,r)}\sqrt{\frac{2M(r)}{R(t,r)} + 2E(r)}, \tag{2.21}$$

where $H(t,r)$ is the local Hubble rate and an expression for the density

$$4\pi G\rho(t,r) = \frac{M'(r)}{R^2(t,r)R'(t,r)}, \tag{2.22}$$

where $M(r)$ is another arbitrary function of the LTB model that gives the gravitational mass within comoving radius r. Here $E(r)$ also plays a dynamical role, it determines the local energy per unit mass of the dust particles. This can be seen if we compare Eq. (2.21) with the Newtonian analogue of a dust cloud, we see that E(r) also acts as an energy potential [161].

Here we also relate the LTB free functions, $M(r)$ and $E(r)$, to the more familiar density parameter today $\Omega_{M_0}(r)$ and the Hubble constant $H_0(r)$ as presented in [78]. We then have

$$2M(r) \equiv H_0^2(r)\Omega_{M_0}(r)R_0^3(r), \text{ and } 2E(r) \equiv H_0^2(r)(1-\Omega_{M_0}(r))R_0^2(r), \tag{2.23}$$

where $H_0(r) = H(t_0,r)$, $\Omega_{M_0}(r) = \Omega_M(t_0,r)$ and $R_0(r) = R(t_0,r)$. Note that we have also ignored the cosmological constant. With these Friedmann friendly framework defined LTB

free functions, we can then re-express Eq. (2.21) in a more familiar form:

$$H^2(t,r) = H_0^2(r)\left[\Omega_{M_0}(r)\left(\frac{R_0(r)}{R(t,r)}\right)^3 + (1-\Omega_{M_0}(r))\left(\frac{R_0(r)}{R(t,r)}\right)^2\right]. \tag{2.24}$$

Eq. (2.21) can also be solved in terms of a parameter $\eta = \eta(t,r)$, and a third arbitrary function $t_B(r)$:

$$R = \frac{M}{2E}\,(\cosh\eta - 1), \qquad \sinh\eta - \eta = \frac{(2E)^{3/2}(t-t_B)}{M}; \qquad E > 0, \tag{2.25}$$

$$R = M\left(\frac{1}{2}\,\eta^2\right), \qquad \frac{1}{6}\,\eta^3 = \frac{(t-t_B)}{M}; \qquad E = 0, \tag{2.26}$$

$$R = \frac{M}{(-2E)}\,(1-\cos\eta), \qquad \eta - \sin\eta = \frac{(-2E)^{3/2}(t-t_B)}{M}; \qquad E < 0, \tag{2.27}$$

for hyperbolic, parabolic and elliptic solutions respectively [1]. Even if a non-zero cosmological constant had been retained, Eq. (2.21) can still be solved in terms of Weierstrass elliptic functions as has been discussed in [120, 171]. The third arbitrary function $t_B = t_B(r)$ is the local time at which $R = 0$, i.e. the local time of the big bang, so we have a non-simultaneous bang surface (this assumes we take $t > t_B$ above). The time reverse of the above equations are also possible solutions, in which case t_B is the time of the big crunch, and the hyperbolic and parabolic cases are collapsing models. Specification of the three arbitrary functions - $M(r)$, $E(r)$ and $t_B(r)$ - fully determines the model. They constitute a radial coordinate choice, and two physical relationships. If we differentiate Eq. (2.25) to get $\dot{R}$ and R' in terms of η and eliminate η from R' we get

$$R' = \left(\frac{M'}{M} - \frac{E'}{E}\right)R - \left\{t_B' - \left(\frac{3E'}{2E} - \frac{M'}{M}\right)(t-t_B)\right\}\dot{R}. \tag{2.28}$$

We can also get the same equation from (2.27), and starting from (2.26) we get (2.28) with $E'/E = 0$.

One thing worth mentioning is that there is a difference between the arbitrary function $M(r)$ we have here, and the sum of the masses of the particles that formed the gravitating body. The former is the mass that generates the gravitational field (hence called the gravitational mass). If we integrate (2.22) at constant time, then we get an expression for $M(r)$:

$$M = 4\pi\int_0^r \rho R^2 R' dr. \tag{2.29}$$

The total rest mass of the matter is found by integrating the density with respect to the

[1] However, near the origin, it is the sign of RE/M that determines the type of solution.

volume element on a constant time surface. We use $\overline{M}$ to denote it:

$$\overline{M} = 4\pi \int_0^r \rho \, \frac{R^2 R'}{\sqrt{1+2E}} \, dr. \tag{2.30}$$

The difference between M and $\overline{M}$ depends on the sign of E, which is the energy. When $E > 0$ or $E = 0$ or $E < 0$ over the whole integral, M would be larger than or equal to or smaller than $\overline{M}$, as pointed out in [32].

2.2.1 The Friedmann-Lemaître-Robertson-Walker case

In the homogeneous FLRW case, we have $\rho = \rho(t)$ only. If η is to be independent of r at all times in Eqs. (2.25) and (2.27), this implies that one needs to have the bang time t_B constant and E proportional to $M^{2/3}$, since the three arbitrary functions are functions of r only:

$$t_B = \text{constant}, \qquad E^{3/2}/M = \text{constant}. \tag{2.31}$$

These two equations define the FLRW case invariantly. For an FLRW universe, $R(t,r) = a(t)b(r)$ gives the FLRW scale factor, $a(t)$. When we exercise our freedom in choosing the radial coordinate to be $b(r) = r$, we then have $R'(t,r) = a(t)$. Together with the choice that $2E(r) = -kr^2$, the resulting RW metric looks like

$$ds^2 = -dt^2 + a^2(t)\left[\frac{dr^2}{1-kr^2} + r^2\left(d\theta^2 + \sin^2\theta d\phi^2\right)\right], \tag{2.32}$$

where k is an arbitrary constant such that $k = +1$, $k = 0$ and $k = -1$ give us positively curved, flat and negatively curved spatial sections respectively. Another common choice is to have $2E(r) = -\sin^2 r$ and $2E(r) = -\sinh^2 r$ for the $k = +1$ and $k = -1$ cases respectively.

If we integrate Eq. (2.29), we then get

$$M = \frac{4\pi}{3}\rho R^3$$

as expected for the FLRW cases.

2.2.2 Behaviour near the origin

In the LTB model, an origin occurs at $r = r_0$ if we have $R(t, r_0) = 0$ for any t. Without loss of generality, we will assume $r_0 = 0$ throughout this thesis since what we are really interested in is the behaviour of the three arbitrary functions near the origin of the spherical coordinates because they are functions of r only.

If one looks at Eq. (2.25) or (2.27), in the case when we have $r = 0$ and $R(\eta(t,0),0) = 0$

for every $0 < \eta < 2\pi$, it is essential to have

$$\frac{M}{2E} \to 0 \text{ as } r \to 0. \tag{2.33}$$

In other words, this means that $2RE/M$ also has to be finite here. Of course, if we require the term $t - t_B$ remain finite when $r \to 0$, then we must also have

$$\frac{2E^{3/2}}{M} = \text{finite as } r \to 0. \tag{2.34}$$

And the evolution Eq. (2.21) tells us that if we have $\dot{R}(t, 0) = 0$ at all times, i.e. our origin remains an origin at all times, this requires that

$$E \to 0 \text{ and } \frac{M}{R} \to 0 \text{ as } r \to 0. \tag{2.35}$$

Using the conditions (2.35) and (2.34) in conjunction with the fact that $2RE/M$ remains finite near the origin, we can then deduce that $M \propto E^{3/2}$ to the lowest order in r and also $E \sim R^2$ and $M \sim R^3$ on a constant time slice. From these conditions, one can easily see that the LTB model assumes FLRW form near the origin. However, this is not surprising at all since the LTB model is based on the spherical symmetry assumption.

2.3 A principle test for Copernican assumption

In this section, we first present a principle test for the CP which relies on a consistency relation of the homogeneous and isotropic FLRW models between distances and the Hubble rate, both as a function of redshift. We show that this is not satisfied for radially inhomogeneous models – the LTB models, providing just such a mechanism to test if we live in an approximation to an FLRW universe or near the centre of a spherically symmetric one. We then present two alternative tests. We also present a figure demonstrating that our Copernican function is non-zero for some LTB classses. We then introduce two possible alternative tests to our proposed principle test for the CP.

2.3.1 Consistency relation

In FLRW models with constant curvature, the luminosity distance may be written as (in units where $c = 1$)

$$d_L(z) = \frac{(1+z)}{H_0\sqrt{-\Omega_k}} \sin\left(\sqrt{-\Omega_k}\int_0^z \mathrm{d}z' \frac{H_0}{H(z')}\right), \tag{2.36}$$

where Ω_k is the curvature parameter today, and the expansion rate $H(z)$ takes the value $H_0 = H(0)$ today. The area distance is defined using $d_L = (1+z)^2 d_A$, and another distance measure we will use is $D = (1+z)d_A$. We may rearrange Eq. (2.36) to give an expression

for the curvature parameter in terms of $H(z)$ and $D(z)$:

$$\Omega_k = \frac{[H(z)D'(z)]^2 - 1}{[H_0 D(z)]^2}, \tag{2.37}$$

where a prime denotes that $' = \mathrm{d}/\mathrm{d}z$ (not to be confused with earlier notation). This tells us how to measure the curvature from distance and Hubble rate observations, independently of any other model parameters or dark energy model. Remarkably this tells us the curvature today from these measurements at any single redshift.

Given that the curvature parameter is independent of redshift, we may differentiate Eq. (2.37) to obtain an expression which must equal zero. The factor responsible for this is

$$\mathcal{C}(z) = 1 + H^2\left(DD'' - D'^2\right) + HH'DD', \tag{2.38}$$

which must be zero in any FLRW model at all redshifts, by virtue of Eq. (2.36). As shown in [54], this function may also be derived by equating the two reconstructed functions for $w(z)$ given by Eqs. (2.37) and (2.38).

As we have not utilised the Friedmann equation, the derivation of $\mathcal{C}(z)$ relies only on the metric of spacetime, and not on the theory of gravity, nor on any matter model present – it is therefore a purely geometric function. Consequently, if the FLRW models are indeed the correct background model, then we should expect to measure $\mathcal{C}(z) \approx 0$ (up to the amplitude of perturbations) in the real universe at all redshifts.

The errors on $\mathcal{C}(z)$ may be roughly estimated using series expansions for $D(z)$ and $H(z)$, but with different FLRW parameter values, and dark energy equations of state. From this estimation, at leading order, it can be seen that the error on $\mathcal{C}(z)$ is then the difference between the deceleration parameter measured separately using D and H:

$$\mathcal{C}(z) = \left[q_0^{(D)} - q_0^{(H)}\right] z + \mathcal{O}(z^2). \tag{2.39}$$

This in term tells us that at low redshift, our error on $\mathcal{C}(z)$ is roughly the same as q_0 as estimated using $H(z)$. Therefore, an aspect of our test is that $H(z)$ measurements must come from a different data set than used for distance data.

Presently most estimates of $H(z)$ rely implicitly on Eq. (2.37) or some other aspect of the FLRW models themselves. However, passively evolving objects such as luminous red galaxies provide a family of roughly synchronised clocks at moderate to high redshift, from which we can measure $H(z)$ directly using $H(z) = -1/(1+z)t(z)$ [109, 201]. Alternatively, measuring the change of redshift, $\dot{z}(z)$, of an object over a period of several years can also provide $H(z)$ [226], and so be used as a probe of the Copernican Principle based on the arguments presented here [227].

Another possible approach in estimating $H(z)$ is proposed in [33]. They showed that the dipole of the luminosity distance data from the supernova measurements can be used

to determine $H(z)$ and discussed the accuracy with which the Hubble parameter can be measured from. Although it was concluded that a large number of supernovae is needed in order to achieve an accuracy of 30% in $H(z)$ measurement, future planned surveys are expected to be able to deliver these. This last approach is of particular interest to us since it allows us to in principle obtain data for both $d_L(z)$ and $H(z)$ that are required in our Copernican function $\mathcal{C}(z)$ from one data set.

Prospects for constraining $\mathcal{C}(z)$ in the near future as an independent confirmation of the standard model are exciting. For example, finding $w(z)$ from distance data requires knowledge of $D''(z)$, while reconstructing it from $H(z)$ alone requires knowing $H'(z)$ [54]. Taking derivatives of observable functions introduces extra errors, so it might in practice be simpler to measure $\{[H(z)D'(z)]^2 - 1\}/[H_0 D(z)]^2$ at different redshifts, and check that it yields the same value as it should by virtue of Eq. (2.37). In FLRW models this tells us the value of the curvature today; in more general models this quantity will not be as simple as this. This is an important consistency check on the FLRW models. If it is found to change with redshift then that is equivalent to finding $\mathcal{C}(z) \neq 0$ [2]. Thus, while we try to search for $w(z)$, we can measure $\mathcal{C}(z)$ at the same time to a similar degree of accuracy.

But what would a measurement $\mathcal{C}(z) \neq 0$ imply, even if only at one redshift? Since it is not dark energy or deviations from general relativity, the origin must be a different cosmological geometry which is not homogeneous. Clearly, then, measuring $\mathcal{C}(z) \neq 0$ at any redshift would pose serious problems for cosmology.

We have given a necessary condition for violation of the CP, but is it sufficient? In other words, could the CP be violated while still having $\mathcal{C}(z) = 0$? Consider LTB models, which can fit the Hubble diagram without invoking dark energy (see e.g. [49] for a review). These are spherically symmetric models with each shell at radius r evolving as a separate FLRW model. Clearly the generic scenario is for each shell to be characterised by a different Ω_k and so have $\mathcal{C}(z) \neq 0$. Indeed, we show in subsection 2.3.2 that $\mathcal{C}(z)$ is a freely specifiable function in these models, so $\mathcal{C}(z) = 0$ which are not FLRW is a very limited subclass within the LTB family.

2.3.2 $\mathcal{C}(z)$ in LTB models

In the previous subsection we have stated that $\mathcal{C}(z) = 0$ for the FLRW case. In this subsection, we will look at $\mathcal{C}(z)$ in the LTB models. We will first discuss as to why $\mathcal{C}(z)$ is a freely specifiable function in the LTB models.

Eq. (2.20) gives us the general LTB metric whereas Eq. (2.21) provides us with a generalized Friedmann equation for the *angular* Hubble rate,

$$H_\perp(t, r) = \partial_t \ln R(t, r). \tag{2.40}$$

[2] We thank Ruth Durrer for pointing this out to us. Note that we must use the relation given by Eq. (2.37) for this to work; measuring curvature at different redshifts by standard tests will be contaminated by our assumptions about the dark energy equation of state.

As mentioned earlier, of the three radial degrees of freedom, one is gauge, while two are genuine physical degrees of freedom, and can be specified arbitrarily. We shall assume that the coordinate degree of freedom specifies the bang time function: thus, specifying $\{M(r), E(r)\}$ fully specifies the LTB model.

In LTB models the expansion in the radial direction, $H_{\parallel}(t,r)$, is not the same as that in the angular direction, but is given instead by [154]

$$H_{\parallel}(t,r) = \frac{\partial_t \partial_r R(t,r)}{\partial_r R(t,r)} = H_{\perp}(t,r) + \frac{\partial_r H_{\perp}(t,r)}{\partial_r \ln R(t,r)}. \tag{2.41}$$

In the FLRW limit $\partial_r H_{\perp} = 0$, so the two Hubble rates are the same and this can be easily verified. From Eq. (2.21) we can derive that

$$\partial_r H_{\perp}(t,r) = -\frac{\partial_r R}{R^2}\sqrt{\frac{2M}{R}+2E} + \frac{1}{R\sqrt{\frac{2M}{R}+2E}}\left(\frac{\partial_r M}{R} - \frac{M\partial_r R}{R^2} + \partial_r E\right). \tag{2.42}$$

From subsection 2.2.1 we have $R(t,r) = a(t)r$, $2E(r) = -kr^2$ and $M(r) = \frac{4\pi}{3}\rho(t)a^3(t)r^3$. Substituting them into Eq. (2.42) we can then see that $\partial_r H_{\perp}(t,r) = 0$, and hence $H_{\perp}(t,r) = H_{\parallel}(t,r)$. A perhaps much easier way to come to this is by looking at the left hand side of Eq. (2.21), which gives us $\partial_r H_{\perp}(t,r) = \partial_r[\partial_t a(t)r/a(t)r] = 0$. This can present different ways to view $\mathcal{C}(z)$ in LTB models, as we can use whichever $H(z)$ we like once we have related r to z on the null cone.

Finding the area distance explicitly in terms of redshift is not simple, and is discussed in detail in [160]. In the usual procedure, one chooses a radial coordinate which flattens out the central observer's null cone. Evaluating the function R on the null cone then turns it into the area distance as a function of redshift: $d_A(z) = R|_{\text{null cone}}$. However, it has been shown in [53] that $d_L(z)$, or equivalently $d_A(z) = R(z)$ (and so $D(z)$), may be considered as a free function of the LTB model instead of $M(r)$. Therefore, the LTB model may be directly specified by the free functions $\{D(z), E(r)\}$. On the null cone we may find the radial coordinate $r(z)$, implying that $E(r(z)) = E(z)$ is a free function instead of $E(r)$. As a free function, we may replace $E(z)$ with $H_{\perp}(z)$ using Eq. (2.40) evaluated on the null cone, which means that an LTB model can in fact be specified instead by $\{D(z), H_{\perp}(z)\}$ or $\{D(z), H_{\parallel}(z)\}$.

So, as far as $\mathcal{C}(z)$ is concerned, we now see that in an arbitrary LTB model, it can be anything one chooses, whether we are to interpret $H(z)$ as $H_{\perp}(z)$ or $H_{\parallel}(z)\}$, or a suitable combination of them [3] If it is zero for both $H_{\perp}(z)$ and $H_{\parallel}(z)\}$, potentially giving a class of LTB models which would fail our Copernican test, then that leaves just one degree of freedom - exactly as in FLRW models with dark energy. If this free function is

[3] In this thesis we show a few $\mathcal{C}(z)$ non-zero cases following the approach and notations to the LTB models used in [78]. However, at the time of working on this project we have verified that $\mathcal{C}(z)$ is non-zero for a class of LTB models, using the code presented in [136].

$H(z) = H_\perp(z) = H_\parallel(z)\}$, say, then $D(z)$ must be given by Eq. (2.36), which can be shown by integrating $\mathcal{C}(z) = 0$. Although we have not shown that these models are necessarily FLRW, this would have to be a very restricted family within the full LTB class. It would be interesting to determine the exact conditions under which $\mathcal{C}(z) = 0$ observed from one location is a sufficient condition for an expanding spacetime to be FLRW. However, this is outside the scope of this thesis.

This 'Copernican function' therefore must be considered, as far as a test for the CP is concerned, as essentially free, and must therefore be determined by observations.

In line with our new understanding in the LTB models, here we demonstrate a few $\mathcal{C}(z)$ cases using the notation used in [78]. In Fig. 2.1, we show the Copernican function for three LTB models and the flat ΛCDM model. For the three LTB models, We choose a homogeneous/simultaneous bang time, i.e. $t_B(r) = 0$. Further assuming the conventional gauge choice $R(t_0, r) = 1$, we are left with just one free function to specify our model with. As pointed out in [78], we can then choose this function to be the radial profile of the dimensionless matter density today $\Omega_{M_0}(r)$. For the Gaussian and Lorentzian cases, the matter density today takes the form of

$$\Omega_{M_0}(r) = \Omega_{out} - (\Omega_{out} - \Omega_{in})e^{-(r/\sigma)^2} \tag{2.43}$$

and

$$\Omega_{M_0}(r) = \Omega_{out} - (\Omega_{out} - \Omega_{in})\frac{\sigma^2}{\sigma^2 + r^2} \tag{2.44}$$

respectively. Ω_{in} and Ω_{out} are the value of $\Omega_{M_0}(r)$ at the centre of the void at infinity, respectively. The parameter σ characterises the size of the void.

For the better origin smoothness case, it is taken from [80] and the matter density today takes the form of

$$\Omega_{M_0}(r) = \Omega_{in} + \frac{\Omega_{out} - \Omega_{in}}{\nu - 1}\left[\nu \tanh\frac{r}{\sigma} - \tanh\frac{r\nu}{\sigma}\right], \tag{2.45}$$

where ν is the parameter that controls the slope of Ω_{M_0} at the origin. Note that these chosen LTB models are from the best-fit models to the SN data [80]. σ used in Fig. 2.1: we have $\sigma = 2.1$, 3.3 and 3.2 Gpc for the "better origin smoothness", Gaussian and Lorentzian models, respectively. Also, we used $\Omega_{out} = 1$ in all cases, but $\Omega_{in} = 0.15$, 0.14 and 0.13 for the "better origin smoothness", Gaussian and Lorentzian models, respectively. Note also that the function $H_0(r)$ can be obtained from Eq. (3.5) in [78] since we have chosen $t_B(r) = 0$. However, we have $H_0 = 64.17$, 64.36 and 64.39 km s^{-1} Mpc^{-1} for the "better origin smoothness", Gaussian and Lorentzian models, respectively.

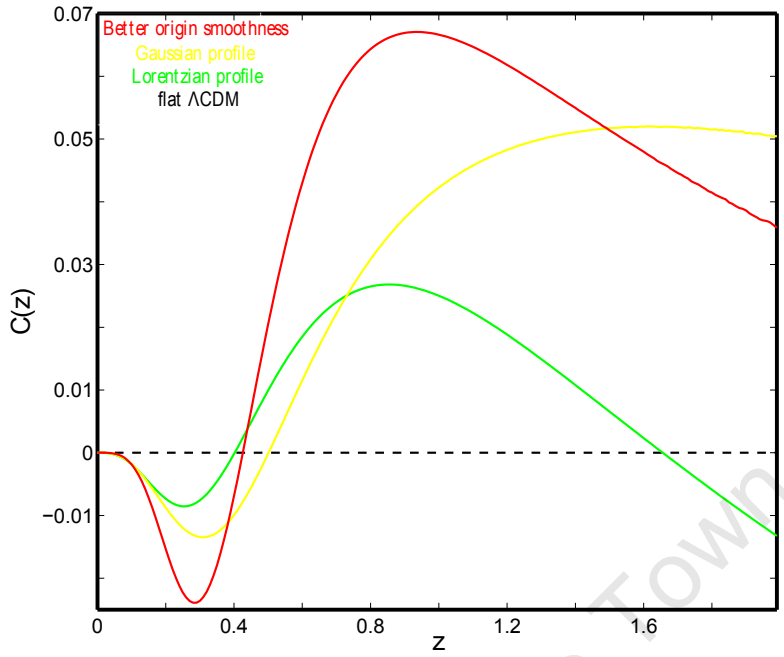

Figure 2.1: Figure shown the Copernican function $\mathcal{C}(z)$ for a few LTB cases. Modified from original figure courtesy of Sean February.

2.4 Alternative approaches in testing Copernican Principle

In addition to the key test just presented we present two other novel approaches to the problem. Future cosmological data will allow us to measure $w(z)$ (assuming FLRW and an appropriate parametrisation) to high accuracy [1]. With $w(z)$ known, one can make predictions for what will be observed with the Alcock-Paczynski (AP) test [2]. The AP test relies on the idea that a spherical object in real space will appear oblate or prolate in redshift space due to the fact that the radial size, $L_{\parallel}$ is determined by $\Delta z/H(z)$ while the transverse size, $L_{\perp}$ is determined by $d_A(z)$. By demanding that $L_{\perp} = L_{\parallel}$ one can determine cosmic parameters, in particular, $w(z)$.

The canonical AP test in modern cosmology is provided by the Baryon Acoustic Oscillations (BAO) which uses the excess signal at ~ 150Mpc in the two point correlation function as a standard ruler. By observing this in both the angular and radial directions BAO will provide both $d_A(z)$ and $H(z)$, and hence allow us to measure $w(z)$ to similar accuracy as SNIa [198].

If the CP is violated through significant radial inhomogeneity then clustering in real space will not be isotropic. Hence the assumption underlying the AP and BAO tests (that the "bump" in the two point correlation function is isotropic) will be invalid. If one incorrectly assumes isotropic clustering one will reconstruct a $w(z)$ that disagrees with that from SNIa or other measurements. Put another way this would appear to violate distance duality (the equivalence between luminosity and angular diameter distances) [17,

18]. Tantalisingly such a mismatch has actually been observed between current BAO and SNIa data at about the 2σ level [177].

Indeed there are at least three ways in which violation of the CP would deform standard BAO results. First, the sound horizon – the fundamental standard ruler of the BAO method – would be different in the $\parallel$ and $\perp$ directions (relative to the observer) and in general will differ from the standard FLRW value (~ 150Mpc today). Both of these will cause problems. Secondly, the subsequent expansion of the sound horizon in the $\parallel$ and $\perp$ directions will be governed by different Hubble rates $H_\parallel$ and $H_\perp$ (see Eq. (2.41)). Hence, even if the sound horizon were isotropic and equal to the standard FLRW value at decoupling, the subsequent evolution would cause biases in measured cosmology. Finally, redshift distortions which need to be subtracted [60, 110, 150, 235, 236] in order to apply the AP test, will be significantly more complicated to model and crucially will be correlated with the background expansion, unlike the FLRW case. To see this consider a galaxy moving in a gravitational potential, $\Phi = \Phi_\parallel + \delta\Phi$ which is the sum of the usual perturbative gravitational potential and the radial inhomogeneity of the LTB background. Since $\nabla_\perp \Phi_\parallel = 0$, the $\parallel$ velocity of the galaxy will be different from the FLRW case even if the $\delta\Phi$ contribution is identical in both cases. This will modify the Doppler shift contribution to the redshift of the galaxy and hence will modify the usual Kaiser and "Fingers of God" effects in a way that is strongly correlated with the precise nature of the radial inhomogeneity.

Each of these effects will cause a bias in the estimation of dark energy parameters obtained by assuming a FLRW background which will manifest as a mismatch with the parameters derived from the distance measurements via supernovae or lensing. It is also perhaps worth noting that the growth rates will be different in the $\parallel$ and $\perp$ directions.

A significantly more exotic test for the CP is provided by the realisation that the $d_L(z)$ relation need not be single-valued; see Figs 5-8 of [160]. The same redshift can correspond to more than one distance. Clearly in FLRW this is impossible and the occurance is related to the possibility of gravitational blueshifts/redshifts adding to the standard expansion redshift. Hence, object A which is further away than object B, may still have the same redshift if it lies at a suitably higher "potential energy" which compensates the difference in cosmic expansion. Hence, the volume as a function of redshift can exhibit pathological behaviour which would be visible in number counts or a large dispersion in SNIa distances around the same redshift providing a clear signal of violations of the CP.

Chapter 3

Standard cosmological perturbation theory

There are two approaches to the study of the cosmological perturbation theory. The first one is the metric approach which follows the familiar style from the perturbation theory used in other areas of physics. The second is the covariant approach of a 1+3 spacetime splitting similar to the ADM formalism [153]. The metric approach is used for most of the work in this thesis, but the covariant approach is also used at times.

In this chapter, we will first present a brief review of some ideas of the background FLRW model. Next we will give a brief overview of linear order perturbation using the metric approach. Lastly the covariant formalism is introduced which will be important in a later chapter.

3.1 The background flat Friedmann-Lemaître-Robertson-Walker model

Here we will use the flat FLRW model as our background model. When using FLRW model, it is automatically assumed that the CP is valid. Such an issue has been addressed in chapter 2 already.

In this and the next chapters, we assume a flat FLRW background model that will be introduced briefly in this section. Details of the FLRW model with arbitrary spatial curvature can be found in most of the textbooks in cosmology. See for example [57, 188].

3.1.1 The metric

The flat FLRW metric is given as:

$$ds^2 = g_{\mu\nu}dx^\mu dx^\nu = -a^2(\eta)d\eta^2 + a^2(\eta)\gamma_{ij}dx^i dx^j, \tag{3.1}$$

where again η is the conformal time and γ_{ij} is the metric of a three-space of constant curvature, which in our case is assumed to be flat. In this and the next chapters, we will use the notation $' \equiv \frac{\partial}{\partial\eta}$. Note that as mentioned earlier, the conformal Hubble parameter is just $\mathcal{H} = \frac{a'(\eta)}{a(\eta)}$.

The Christoffel symbols are

$$\Gamma^{\alpha}_{\beta\gamma} = \frac{1}{2} g^{\alpha\rho} \left(g_{\rho\gamma,\beta} + g_{\beta\rho,\gamma} - g_{\beta\gamma,\rho} \right), \tag{3.2}$$

where the various components for our metric can be found in Appendix A. Usually, the covariant differentiation with respect to $g_{\mu\nu}$ is denoted as $_{;\mu} \equiv \nabla_{\mu}$ and the covariant differentiation with respect to γ_{ij} is $\nabla_i \equiv |_i$. Since we only focus on flat FLRW here, we have $\nabla_i = \partial_i = {}_{,i}$.

Once we have the expressions for all the components of the Christoffel symbols, we can then derive the expressions for the Ricci tensor through

$$R_{\mu\nu} = \Gamma^{\alpha}_{\mu\nu,\alpha} - \Gamma^{\alpha}_{\nu\alpha,\mu} + \Gamma^{\alpha}_{\sigma\alpha}\Gamma^{\sigma}_{\mu\nu} - \Gamma^{\alpha}_{\sigma\nu}\Gamma^{\sigma}_{\mu\alpha}. \tag{3.3}$$

The various components of the Ricci tensor in our case are then

$$\begin{aligned} R_{00} &= -3\left[\frac{a''}{a} - \left(\frac{a'}{a}\right)^2\right], \\ R_{0i} &= 0, \\ R_{ij} &= \left[\frac{a''}{a} + \left(\frac{a'}{a}\right)^2\right]\gamma_{ij}. \end{aligned} \tag{3.4}$$

The Ricci scalar is a contraction of the Ricci tensor over its remaining indices

$$R = R^{\mu}_{\ \mu} = \frac{6a''}{a^3}. \tag{3.5}$$

3.1.2 The Einstein field equations

The standard form of the EFEs is

$$G_{\mu\nu} \equiv R_{\mu\nu} - \frac{1}{2} R g_{\mu\nu} = \kappa^2 T_{\mu\nu} - \Lambda g_{\mu\nu}, \tag{3.6}$$

where $G_{\mu\nu}$ is the Einstein tensor, $T_{\mu\nu}$ is the energy momentum tensor for the matter and $\kappa^2 = 8\pi G$. The contraction of the EFEs gives us

$$R = -\kappa^2 T + 4\Lambda, \tag{3.7}$$

where $T = T^{\mu}_{\mu}$. Substituting Eq. (3.7) into Eq. (3.6), we can rewrite the EFEs in its trace reversed form

$$R_{\mu\nu} = \kappa^2 \left(T_{\mu\nu} - \frac{1}{2} g_{\mu\nu} T \right) + \Lambda g_{\mu\nu}. \tag{3.8}$$

This form of the EFEs is preferable for us because it reduces the perturbative calculations for higher order, and therefore it is used at all orders.

Now we have introduced the EFEs which are crucial to us and we also have presented the left hand side of the EFEs, which shows us the geometry of our background. In the next subsection, we will look at what is at the right hand side of the EFEs - the energy momentum tensor of the background fluid.

3.1.3 The energy momentum tensor

We will consider the background matter to consist of a perfect fluid. The energy momentum tensor (EMT) for a perfect fluid can be written as

$$T_{\mu\nu} = (\rho + P)\, u_\mu u_\nu + P g_{\mu\nu}, \tag{3.9}$$

where ρ is the energy density, P is the isotropic pressure and u_μ is the four velocity of the fluid. It is well known that we can split any four vector into a temporal and spatial part. From the isotropy of our background, the spatial part should have no preferred direction and hence should be zero, but the temporal part can be non-zero.

For the metric shown in Eq. (3.1), the components of the four velocity are

$$u^\mu = \frac{1}{a}[1,\ \mathbf{0}],\ \text{and}\ u_\mu = a[-1,\ \mathbf{0}]. \tag{3.10}$$

The four velocity has to satisfy the normalisation condition $u^\mu u^\nu g_{\mu\nu} = -1$. Additionally, the EMT has an property, it is that it is covariantly conserved

$$\nabla^\mu T_{\mu\nu} = 0. \tag{3.11}$$

For our chosen background, this property implies the continuity (or energy conservation) equation

$$\rho' = -3\mathcal{H}\,(\rho + P)\,. \tag{3.12}$$

The accompanying momentum conservation equation (the Euler equation) vanishes due to spatial isotropy.

Using our EMT from Eq. (3.9) and equating the both sides of the EFEs, we obtain the Raychaudhuri equation and the Friedmann equation. They are given respectively

$$\mathcal{H}' = -\frac{\kappa^2 a^2}{6}\,(3P + \rho) + \frac{a^2 \Lambda}{3}, \tag{3.13}$$

$$\mathcal{H}^2 = \frac{\kappa^2 a^2}{3}\rho + \frac{a^2\Lambda}{3}, \tag{3.14}$$

where Λ represents the presence of the cosmological constant.

The universe went through several phases (eras) in its history due to various physical processes. We will discuss some of the eras that are of greatest interest to us below. We will consider the case when we have fluids with a linear equation of the state of the standard form $P = w\rho$.

Substituting $P = w\rho$, Eqs. (3.12) and (3.13) become

$$\begin{aligned} \rho' &= -3\mathcal{H}(1+w)\rho, \\ \mathcal{H}' &= -\frac{\kappa^2 a^2}{2}(1+w)\rho + \mathcal{H}^2. \end{aligned} \tag{3.15}$$

An expression for the energy density can be obtained from integrating the continuity equation

$$\rho = \rho_0 \left(\frac{a}{a_0}\right)^{-3(1+w)}. \tag{3.16}$$

The scale factor and the Hubble parameter are then given by

$$a = a_0 \left(\frac{\eta}{\eta_0}\right)^d, \; d = \frac{2}{1+3w}, \text{ and } \mathcal{H} = \frac{d}{\eta}, \tag{3.17}$$

where we have at $\eta = \eta_0$, $a = a_0$ and $\rho = \rho_0$.

Now we will look at the various eras, starting with the radiation era where $w = 1/3$. In this case, we have a fluid that describes particles that are travelling at or close to the speed of light such as the photons. The scale factor and the Hubble parameter have the form:

$$a = a_0 \left(\frac{\eta}{\eta_0}\right), \; \mathcal{H} = \frac{1}{\eta}, \text{ and } \frac{a''}{a} = 0. \tag{3.18}$$

This means that in a radiation dominated era, the scale factor grows linearly with respect to the conformal time η, i.e. $a \propto \eta$. The energy density of the fluid scales as $\rho \propto a^{-4}$. This comes from the fact that the volume expansion of the universe scales as a^{-3} and an additional a^{-1} factor comes from the redshifting of the particles frequency.

A fluid that describes a distribution of collisionless, non-relativistic particles which is pressure free, is called *dust*. An example is the cold dark matter (CDM). In the dust era, we have $w = 0$. The scale factor and the Hubble parameter have the form

$$a = a_0 \left(\frac{\eta}{\eta_0}\right)^2, \; \mathcal{H} = \frac{2}{\eta}, \text{ and } \frac{a''}{a} = \frac{2}{\eta^2}. \tag{3.19}$$

The energy density in this case scales as a^{-3} due to the volume expansion of the universe. This case describes a universe at late time and it is used, at times, by cosmologists to

describe our current universe when one does not consider the cosmological constant.

A more popular choice for our current universe is when we have the cosmological constant Λ. This is modelled by a fluid with $w = -1$. During this era, the scale factor and the Hubble parameter take the form

$$a = a_0 \left(\frac{\eta}{\eta_0}\right)^{-1}, \ \mathcal{H} = -\frac{1}{\eta}, \text{ and } \frac{a''}{a} = \frac{2}{\eta^2}. \tag{3.20}$$

The energy density scales as a constant. Here we have discussed three choices for w. Of course, other choices like $w = -1/3$ have been used by cosmologists too but the radiation, the dust and the cosmological constant cases are of most interest to us.

3.2 Linear cosmological perturbation theory

In this section, we will introduce some of the fundamental ideas of linear cosmological perturbation theory. We will focus on the physical aspects that are important toward our study in the higher order perturbation theory shown in chapter 4. More details on the cosmological perturbation theory can be found in the reviews [116, 159, 143].

3.2.1 Scalar-vector-tensor decomposition

In this subsection, we will briefly introduce scalar-vector-tensor decomposition that is commonly adopted in cosmological perturbation theory. For more detailed proofs of this type of decomposition, see [209, 116].

In linear perturbation theory, the metric degrees of freedom were first classified in 1946 by Lifshitz [128]. Lifshitz presented the scalar-vector-tensor decomposition of the perturbed four dimensional metric tensor $\delta^{(1)}g_{\mu\nu}$ based on a 1+3 (time + spatial) split of the components. It is useful to label the parts with names such as scalar, vector and tensor according to their respective transformation properties on the spatial hypersurface γ_{ij} (see also [12, 209]).

In the perturbed metric tensor expression only the scalar type of quantities can appear in the 00 component, whereas it is possible to have both scalar and vector quantities for the $0i$ component. A scalar perturbation can always be constructed from a scalar or its derivatives. We can further split a spatial one index quantity into a scalar part and a pure vector part. This decomposition is guaranteed by the Helmholtz's theorem since it shows that a vector field in Euclidean space can be decomposition into a curl-free (potential) part and a divergence free part. However, it is possible to find scalar, vector and tensor type of quantities for the ij component of the perturbed metric tensor. This is because we can split a two index quantity into a scalar, vector and pure tensor part.

As a result of this splitting, we have a set of decoupled equations of linear perturbation theory and hence making the properties of these perturbations at linear order easy to study as we will see later in this chapter. The splitting of the metric tensor component into scalar,

vector and tensor perturbations is also used for at second order higher order perturbation. However, as we go to higher order only the 'true' second or higher order perturbed quantities decouple, but the mixing between linear scalar, vector and tensor perturbations do not.

3.2.2 The perturbed metric

The full perturbed expression up to and including first order about the background FLRW metric is

$$\bar{g}_{\mu\nu} = g_{\mu\nu} + \delta^{(1)} g_{\mu\nu}, \tag{3.21}$$

where $\bar{g}_{\mu\nu}$ refers to the full quantity, and $g_{\mu\nu}$ and $\delta^{(1)} g_{\mu\nu}$ are the background and first order terms of the perturbed FLRW metric respectively. At each order, we will use this notation for the relevant quantities throughout the thesis unless stated otherwise.

Here we give the components of the metric tensor $\bar{g}_{\mu\nu}$ up to first order including the scalar, vector and tensor perturbations about a flat FLRW background:

$$\bar{g}_{00} = -a^2(\eta)\left[1 + 2\phi^{(1)}\right], \tag{3.22}$$

$$\bar{g}_{0i} = a^2(\eta)\left[\partial_i B^{(1)} - S_i^{(1)}\right], \tag{3.23}$$

and

$$\bar{g}_{ij} = a^2(\eta)\left[\left(1 - 2\psi^{(1)}\right)\gamma_{ij} + 2\partial_i\partial_j E^{(1)} + 2\partial_{(j} F_{i)}^{(1)} + h_{ij}^{(1)}\right]. \tag{3.24}$$

Here $S_i^{(1)}$ and $F_i^{(1)}$ are the two divergenceless vectors, i.e. $\partial^i S_i^{(1)} = 0$ and $\partial^i F_i^{(1)} = 0$. The four scalars are $B^{(1)}$, $E^{(1)}$, $\psi^{(1)}$ and $\phi^{(1)}$. The tensor $h_{ij}^{(1)}$ is divergenceless and traceless, i.e. $\partial^j h_{ij}^{(1)} = 0$ and $h_{\ i}^{(1)i} = 0$. All spatial indices of the perturbed quantities are raised and lowered with the flat three metric γ_{ij}. Following the usual covariant definition, we will denote the symmetric and anti-symmetric tensors as the following:

$$A_{(\mu\nu)} \equiv \frac{1}{2}\left(A_{\mu\nu} + A_{\nu\mu}\right),$$

$$A_{[\mu\nu]} \equiv \frac{1}{2}\left(A_{\mu\nu} - A_{\nu\mu}\right).$$

The contravariant form of the full non-linear metric up to first order is decomposed as

$$\bar{g}^{\mu\nu} = g^{\mu\nu} + \delta^{(1)} g^{\mu\nu}. \tag{3.25}$$

The contravariant metric can be obtained by requiring $\bar{g}_{\mu\nu}\bar{g}^{\nu\lambda} = \delta_\mu^{\ \lambda}$. If we impose this condition to first order, then it gives us the components of the contravariant metric up to first order:

$$\bar{g}^{00} = -a^{-2}(\eta)\left[1 - 2\phi^{(1)}\right], \tag{3.26}$$

$$\bar{g}^{0i} = a^{-2}(\eta)\left[\partial^i B^{(1)} - S^{(1)i}\right], \tag{3.27}$$

and

$$\bar{g}^{ij} = a^{-2}(\eta)\left[\left(1 + 2\psi^{(1)}\right)\gamma^{ij} - 2\partial^i\partial^j E^{(1)} - 2\partial^{(j}F^{(1)i)} - h^{(1)ij}\right]. \tag{3.28}$$

3.2.3 Coordinate transformation

In this subsection, we will consider the definition of the infinitesimal coordinate transformation (i.e. the gauge transformation) in the context of small perturbation of a homogeneous and isotropic background spacetime. We will also look at a few commonly used gauge choices in perturbation theory. More details can be found in [116, 159] and a mathematically more rigorous discussion on gauge transformation including second order can be found in [141].

We will use a hat notation to represent variables in the new coordinate system. The linear order coordinate transformation is of the form

$$x^\mu \to \hat{x}^\mu = x^\mu + \xi^\mu, \tag{3.29}$$

where ξ^μ is a four vector. We can split the four vector ξ^μ into a time component $\xi^0(\eta, x^i)$ and a three vector (spatial) component $\xi^i(\eta, x^i)$. The time component $\xi^0(\eta, x^i)$ determines the change in the time slicing. The spatial component $\xi^i(\eta, x^i)$ describes the change in the spatial coordinate. We can further split ξ^i into a divergence free part ξ^i_{DF} (i.e. $\xi^i_{DF|i} = 0$), and a gradient part $\xi^{|i}$. ξ^0 and ξ are the scalar like functions and the divergence free part will only contribute to the vector like perturbation. The coordinate transformation written in its split form is

$$\eta \to \hat{\eta} = \eta + \xi^0, \text{ and } x^i \to \hat{x}^i = x^i + \xi^{|i} + \xi^i_{DF}. \tag{3.30}$$

The metric perturbation under the change of coordinate is not invariant,

$$\bar{g}_{\mu\nu} \to \widehat{\bar{g}}_{\mu\nu} = \bar{g}_{\mu\nu} + \Delta\bar{g}_{\mu\nu} \tag{3.31}$$

We can calculate the line element of the perturbed metric from the total differentials of the gauge functions and the total differentials of Eq. (3.30),

$$\begin{aligned} d\xi^0 &= \xi^{0'}d\hat{\eta} + \xi^0_{|i}d\hat{x}^i, \\ d\xi &= \xi^{'}d\hat{\eta} + \xi^0_{|j}d\hat{x}^j, \\ d\xi^i_{DF} &= \xi^{i'}_{DF}d\hat{\eta} + \xi^i_{DF|j}d\hat{x}^j, \end{aligned} \tag{3.32}$$

and

$$\begin{aligned} d\eta &= d\hat{\eta} - \xi^{0\prime} d\hat{\eta} + \xi^{0}_{|i} d\hat{x}^i, \\ dx^i &= d\hat{x}^i - \left(\xi^{\prime|i} + \xi^{i\prime}_{DF}\right) d\hat{\eta} - \left(\xi^{|i}_{j} + \xi^{i}_{DFj}\right) d\hat{x}^j. \end{aligned} \tag{3.33}$$

Additionally, we also need the gauge transformation of the scale factor which is given below

$$a(\eta) = a(\hat{\eta}) - \xi^0 a'(\hat{\eta}). \tag{3.34}$$

This in turn gives us the gauge transformation properties of the four scalars in the perturbed metric. It is easy to verify that the four new scalar functions are given by

$$\begin{aligned} \hat{\phi}^{(1)} &= \phi^{(1)} - \frac{a'}{a}\xi^0 - \xi^{0\prime}, \\ \hat{\psi}^{(1)} &= \psi^{(1)} + \frac{a'}{a}\xi^0, \\ \hat{B}^{(1)} &= B^{(1)} + \xi^0 - \xi', \\ \hat{E}^{(1)} &= E^{(1)} - \xi. \end{aligned} \tag{3.35}$$

The gauge transformations of other scalar perturbations can be obtained in a similar way. For example, the transformed energy density is

$$\delta^{(1)}\hat{\rho} = \delta^{(1)}\rho - \xi^0 \rho'. \tag{3.36}$$

The velocity potential transforms as

$$\hat{v}_{(1)} = v_{(1)} + \xi'. \tag{3.37}$$

Note that it does not depend of the gauge function ξ^0 but depends on the scalar gauge function ξ associated withe the spatial coordinate choice. The velocity vector is a divergence free three vector, therefore it is only affected by ξ^i_{DF}:

$$\hat{v}^i_{(1)} = v^i_{(1)} + \xi^i_{DF}. \tag{3.38}$$

The most useful scalar quantities are those that are gauge invariant (invariant under gauge transformations). In the linear perturbation theory, the most popular gauge invariant quantities are the Bardeen potentials [1] [12] which can be obtained by carefully considering Eq. (3.35)

$$\begin{aligned} \Phi^{(1)} &\equiv \phi^{(1)} + \mathcal{H}\left(B^{(1)} - E^{(1)\prime}\right) + \left(B^{(1)} - E^{(1)\prime}\right)', \\ \Psi^{(1)} &\equiv \psi^{(1)} - \mathcal{H}\left(B^{(1)} - E^{(1)\prime}\right). \end{aligned} \tag{3.39}$$

[1] In Bardeen's notation, the two variables below are given as $\Phi^{(1)} \equiv \Phi_A Q^{(0)}$ and $\Psi^{(1)} \equiv -\Phi_H Q^{(0)}$.

Of course, any combination of gauge invariant quantities is again gauge invariant. We will take a more detailed look at the physical interpretations of the Bardeen potentials later.

The vector metric perturbations transform as

$$\begin{aligned}\hat{F}_i^{(1)} &= F_i^{(1)} - \xi_{DFi},\\ \hat{S}_i^{(1)} &= S_i^{(1)} + \xi'_{DFi}.\end{aligned} \tag{3.40}$$

It is obvious that we can construct a quantity from Eq. (3.40) that is gauge independent

$$\hat{F}_i^{(1)} = \hat{S}_i^{(1)} = S_i^{(1)} + F_i^{(1)\prime}. \tag{3.41}$$

Note that any tensor quantities are not affected by the gauge choice since they are automatically gauge invariant. Therefore, we have

$$\hat{h}_{ij} = h_{ij}.$$

3.2.4 The perturbed Ricci tensor

Next we introduce the perturbed connections and the Ricci tensor. The perturbed connection coefficients are give by

$$\bar{\Gamma}^{\alpha}_{\beta\gamma} = \Gamma^{\alpha}_{\beta\gamma} + \delta^{(1)}\Gamma^{\alpha}_{\beta\gamma} = \frac{1}{2}\bar{g}^{\alpha\rho}\left(\bar{g}_{\rho\gamma,\beta} + \bar{g}_{\beta\rho,\gamma} - \bar{g}_{\beta\gamma,\rho}\right). \tag{3.42}$$

At each order, Eq. (3.42) can be expanded to give the corresponding expression of the connection coefficients. For example, at first order after the expansion we obtain

$$\delta^{(1)}\Gamma^{\alpha}_{\beta\gamma} = \frac{1}{2}g^{\alpha\rho}\left(\delta^{(1)}g_{\rho\gamma,\beta} + \delta^{(1)}g_{\beta\rho,\gamma} - \delta^{(1)}g_{\beta\gamma,\rho}\right) + \frac{1}{2}\delta^{(1)}g^{\alpha\rho}\left(g_{\rho\gamma,\beta} + g_{\beta\rho,\gamma} - g_{\beta\gamma,\rho}\right). \tag{3.43}$$

Expression for the various connection coefficient components at first order are given in Appendix A.

Now we can calculate the various components of the first order Ricci tensor. The perturbed Ricci tensor can be similarly expanded as

$$\bar{R}_{\mu\nu} = R_{\mu\nu} + \delta^{(1)}R_{\mu\nu} = \bar{\Gamma}^{\alpha}_{\mu\nu,\alpha} - \bar{\Gamma}^{\alpha}_{\nu\alpha,\mu} + \bar{\Gamma}^{\alpha}_{\sigma\alpha}\bar{\Gamma}^{\sigma}_{\mu\nu} - \bar{\Gamma}^{\alpha}_{\sigma\nu}\bar{\Gamma}^{\sigma}_{\mu\alpha}. \tag{3.44}$$

At first order, it can be expanded to give

$$\delta^{(1)}R_{\mu\nu} = \delta^{(1)}\Gamma^{\alpha}_{\mu\nu,\alpha} - \delta^{(1)}\Gamma^{\alpha}_{\nu\alpha,\mu} + \Gamma^{\alpha}_{\sigma\alpha}\delta^{(1)}\Gamma^{\sigma}_{\mu\nu} + \delta^{(1)}\Gamma^{\alpha}_{\sigma\alpha}\Gamma^{\sigma}_{\mu\nu} - \Gamma^{\alpha}_{\sigma\nu}\delta^{(1)}\Gamma^{\sigma}_{\mu\alpha} - \delta^{(1)}\Gamma^{\alpha}_{\sigma\nu}\Gamma^{\sigma}_{\mu\alpha}. \tag{3.45}$$

The various components of the first order Ricci tensor are

$$\delta^{(1)}R_{00} = \nabla^2\left[B^{(1)\prime} + \mathcal{H}B^{(1)} - E^{(1)\prime\prime} - \mathcal{H}E^{(1)\prime} + \phi^{(1)}\right] + 3\psi^{(1)\prime\prime} + 3\mathcal{H}\left[\phi^{(1)\prime} + \psi^{(1)\prime}\right], \tag{3.46}$$

$$\delta^{(1)}R_{0i} = 2\partial_i\psi^{(1)\prime} + \left[\frac{a''}{a} + \mathcal{H}^2\right]\left(\partial_i B^{(1)} - S_i^{(1)}\right) + 2\mathcal{H}\partial_i\phi^{(1)} + \nabla^2\left(S_i^{(1)} + F_i^{(1)\prime}\right), \quad (3.47)$$

$$\begin{aligned}\delta^{(1)}R_{ij} = &\left[-\psi^{(1)\prime\prime} - 2\left(\frac{a''}{a} + \mathcal{H}^2\right)\left(\psi^{(1)} + \phi^{(1)}\right) + \nabla^2\left(\psi^{(1)} - \mathcal{H}B^{(1)} + \mathcal{H}E^{(1)\prime}\right)\right.\\ &\left.-5\mathcal{H}\psi^{(1)\prime} - \mathcal{H}\phi^{(1)\prime}\right]\gamma_{ij} + \partial_i\partial_j\left(\psi^{(1)} - \phi^{(1)} + 2\mathcal{H}E^{(1)\prime} + E^{(1)\prime\prime} - B^{(1)\prime}\right.\\ &\left.+2\left[\frac{a''}{a} + \mathcal{H}^2\right]E^{(1)} - 2\mathcal{H}B^{(1)}\right) + \partial_{(j}\left(S_{i)}^{(1)\prime} + F_{i)}^{(1)\prime\prime} + 2\mathcal{H}S_{i)}^{(1)} + 2\mathcal{H}F_{i)}^{(1)\prime}\right.\\ &\left.+2\left[\frac{a''}{a} + \mathcal{H}^2\right]F_{i)}^{(1)}\right) + \frac{1}{2}h_{ij}^{(1)\prime\prime} + \mathcal{H}h_{ij}^{(1)\prime} + \left(\frac{a''}{a} + \mathcal{H}^2\right)h_{ij}^{(1)} - \frac{1}{2}\nabla^2 h_{ij}^{(1)}.\end{aligned} \quad (3.48)$$

The first order Ricci scalar is

$$\begin{aligned}\delta^{(1)}R = \frac{1}{a(\eta)^2}&\left[-6\mathcal{H}\left(3\psi^{(1)\prime} + \phi^{(1)\prime}\right) - 6\psi^{(1)\prime\prime} + 2\nabla^2\left(2\psi^{(1)} - \phi^{(1)}\right) - 12\frac{a''}{a}\phi^{(1)\prime}\right.\\ &\left.-6\mathcal{H}\nabla^2\left(3B^{(1)} - E^{(1)\prime}\right) - 2\nabla^2\left(3B^{(1)\prime} - E^{(1)\prime\prime}\right)\right].\end{aligned} \quad (3.49)$$

3.2.5 The perturbed energy momentum tensor

In this subsection, we introduce the perturbed energy momentum tensor. It can be expanded in the familiar fashion up to first order as

$$\bar{T}_{\mu\nu} = T_{\mu\nu} + \delta^{(1)}T_{\mu\nu}. \quad (3.50)$$

Here, we shall consider an imperfect fluid at first order that includes anisotropic stresses and energy fluxes. Expressions necessary for a perfect fluid case can be obtained from the expressions derived here by eliminating the anisotropic stresses and energy fluxes.

The energy momentum tensor for an imperfect fluid is given by

$$\bar{T}_{\mu\nu} = \left(\bar{\rho} + \bar{P}\right)\bar{u}_\mu\bar{u}_\nu + \bar{P}\bar{g}_{\mu\nu} + \bar{q}_\mu\bar{u}_\nu + \bar{q}_\nu\bar{u}_\mu + \bar{\pi}_{\mu\nu}, \quad (3.51)$$

where $\bar{u}^\mu$ is the perturbed velocity, $\bar{\rho} = \rho + \delta^{(1)}\rho$ is the energy density perturbation, $\bar{P} = P + \delta^{(1)}P$ isotropic pressure, $\bar{q}_\mu = q_\mu + \delta^{(1)}q_\mu$ is the energy flux, and $\bar{\pi}_{\mu\nu} = \pi_{\mu\nu} + \delta^{(1)}\pi_{\mu\nu}$ is the anisotropic stress.

The perturbed four velocity up to first order is

$$\bar{u}^\mu = u^\mu + \delta^{(1)}u^\mu, \quad (3.52)$$

and it must satisfy the normalisation condition $\bar{u}^\mu\bar{u}^\nu\bar{g}_{\mu\nu} = -1$. The first order velocity three vector in its split form is then

$$\delta^{(1)}u^i = \partial^i v_{(1)} + v_{(1)}^i = \delta^{(1)}v^i, \quad (3.53)$$

where $\partial^i v_{(1)}$ is a scalar quantity and $v_{(1)}^i$ is considered as a pure vector quantity. The first

order velocity perturbation is

$$\delta^{(1)}u^{\mu} = \frac{1}{a}\left[-\phi^{(1)},\ \partial^{i}v_{(1)} + v^{i}_{(1)}\right], \tag{3.54}$$

and its covariant form is

$$\delta^{(1)}u_{\mu} = a\left[-\phi^{(1)},\ \partial_{i}B^{(1)} - S^{(1)}_{i} + \delta^{(1)}v_{i}\right], \tag{3.55}$$

where $\delta^{(1)}v_{i} = \partial_{i}v_{(1)} + v_{(1)i}$.

The energy flux and the anisotropic pressure only contain linear order quantities due to a perfect fluid background

$$\bar{q}_{\mu} = \delta^{(1)}q_{\mu},\ \text{and}\ \bar{\pi}_{\mu\nu} = \delta^{(1)}\pi_{\mu\nu}. \tag{3.56}$$

The energy flux must be orthogonal to the four velocity $\bar{u}^{\mu}$, i.e. $\bar{q}_{\mu}\bar{u}^{\mu} = 0$. Therefore, the first order energy flux is

$$\delta^{(1)}q_{\mu} = \left[0,\ \partial_{i}q_{(1)} + q_{(1)i}\right]. \tag{3.57}$$

The anisotropic pressure is traceless and must be orthogonal to the four velocity $\bar{u}^{\mu}$ with respect to each index,i.e. $\bar{g}^{\mu\nu}\bar{\pi}_{\mu\nu} = 0$ and $\bar{\pi}_{\mu\nu}\bar{u}^{\nu} = \bar{\pi}_{\mu\nu}\bar{u}^{\mu}\bar{u}^{\nu} = 0$. This shows us that the first order anisotropic pressure must obey the constraints: $\delta^{(1)}\pi_{00} = 0$, $\delta^{(1)}\pi_{0j} = 0$ and $\delta^{(1)}\pi^{k}_{\ k} = 0$. Note that the anisotropic pressure perturbation can be split into three parts: a scalar, vector and tensor part

$$\delta^{(1)}\pi_{ij} = \left(\partial_{i}\partial_{j} - \frac{1}{3}\nabla^{2}\gamma_{ij}\right)\Pi_{(1)} + \partial_{(j}\Pi_{(1)i)} + \Pi_{(1)ij}. \tag{3.58}$$

Now we have all the quantities needed in order to obtain expressions for various components of the energy momentum tensor. They are given below:

$$\delta^{(1)}T_{00} = a^{2}\delta^{(1)}\rho + 2a^{2}\phi^{(1)}\rho, \tag{3.59}$$

$$\delta^{(1)}T_{0j} = -a\left(\partial_{j}q_{(1)} + q_{(1)j}\right) - a^{2}\left(\rho + P\right)\left(\partial_{j}v_{(1)} + v_{(1)j}\right) - a^{2}\rho\left(\partial_{j}B^{(1)} - S^{(1)}_{j}\right), \tag{3.60}$$

$$\begin{aligned}\delta^{(1)}T_{ij} = {} & a^{2}\left(\delta^{(1)}P - 2P\psi^{(1)}\right)\gamma_{ij} + \left(\partial_{i}\partial_{j} - \frac{1}{3}\nabla^{2}\gamma_{ij}\right)\Pi_{(1)} + \partial_{(j}\Pi_{(1)i)} + \Pi_{(1)ij} \\ & + a^{2}P\left(2\partial_{i}\partial_{j}E^{(1)} + 2\partial_{(j}F^{(1)}_{i)} + h^{(1)}_{ij}\right).\end{aligned} \tag{3.61}$$

At each order, the energy momentum tensor is covariantly conserved $\bar{\nabla}^{\mu}\bar{T}_{\mu\nu} = 0$. Its time component gives rise to an conservation equations for the energy density perturbation such as

$$\delta^{(1)}\rho' = -3\mathcal{H}\left(\delta^{(1)}\rho + \delta^{(1)}P\right) + \left(\rho + P\right)\left[3\psi^{(1)\prime} - \nabla^{2}\left(v_{(1)} + E^{(1)\prime}\right)\right]. \tag{3.62}$$

However, the space component of $\bar{\nabla}^{\mu}\bar{T}_{\mu\nu}=0$ provides us with an expression

$$\begin{aligned}\partial_i\delta^{(1)}P=&-\left[(\rho+P)\left(\partial_i v_{(1)}+v_{(1)i}+\partial_i B^{(1)}-S_i^{(1)}\right)\right]'-\frac{1}{a}\left(\delta^{(1)}q_i'+3\mathcal{H}\delta^{(1)}q_i\right)\\&-(\rho+P)\left[\partial_i\phi^{(1)}+4\mathcal{H}\left(\partial_i v_{(1)}+v_{(1)i}+\partial_i B^{(1)}-S_i^{(1)}\right)\right]-\frac{1}{a^2}\partial_k\delta^{(1)}\pi^k{}_i.\end{aligned}\tag{3.63}$$

Note that the expression above contains a mixture of scalar and vector type of quantities. The scalar part should give us an evolution equation for the momentum, while the vector part should provide a momentum conservation equation.

3.2.6 First order Einstein field equations

In this subsection, we will present the EFE with only perfect fluid considered and with only scalar quantities considered at first order. We can expand the perturbed trace reversed EFEs

$$\bar{R}_{\mu\nu}=\kappa^2\left(\bar{T}_{\mu\nu}-\frac{1}{2}\bar{g}_{\mu\nu}\bar{T}\right)+\Lambda\bar{g}_{\mu\nu}\tag{3.64}$$

to obtain the first order EFEs

$$\delta^{(1)}R_{\mu\nu}=\kappa^2\left(\delta^{(1)}T_{\mu\nu}-\frac{1}{2}g_{\mu\nu}\delta^{(1)}T-\frac{1}{2}\delta^{(1)}g_{\mu\nu}T\right)+\Lambda\delta^{(1)}g_{\mu\nu}.\tag{3.65}$$

The 00 component gives us

$$\begin{aligned}&\nabla^2\left[B^{(1)\prime}+\mathcal{H}B^{(1)}\right]+\nabla^2\phi^{(1)}+3\psi^{(1)\prime\prime}+3\mathcal{H}\left[\phi^{(1)}+\psi^{(1)}\right]'-\nabla^2\left[E^{(1)\prime\prime}+\mathcal{H}E^{(1)\prime}\right]\\&=\kappa^2\left(a^2\rho\phi^{(1)}+\frac{1}{2}a^2\delta^{(1)}\rho+\frac{3}{2}a^2\delta^{(1)}P+3a^2P\phi^{(1)}\right)-2a^2\Lambda\phi^{(1)}.\end{aligned}\tag{3.66}$$

From the $0i$ component we can obtain an expression:

$$\begin{aligned}2\partial_i\psi^{(1)\prime}+\left[\frac{a''}{a}+\mathcal{H}^2\right]\partial_i B^{(1)}+2\mathcal{H}\partial_i\phi^{(1)}=\kappa^2\Bigg[&-a^2(\rho+P)\partial_i v_{(1)}-\frac{a^2}{2}\rho\partial_i B^{(1)}\\&-\frac{3}{2}a^2P\partial_i B^{(1)}\Bigg]+\Lambda a^2\partial_i B^{(1)},\end{aligned}\tag{3.67}$$

and from the ij component we can obtain

$$\begin{aligned}&\Bigg[-\psi^{(1)\prime\prime}-2\left[\frac{a''}{a}+\mathcal{H}^2\right]\left(\psi^{(1)}+\phi^{(1)}\right)+\nabla^2\psi^{(1)}+\mathcal{H}\nabla^2\left(E^{(1)\prime}-B^{(1)}\right)-\mathcal{H}\left(\phi^{(1)\prime}\right.\\&\left.+5\psi^{(1)\prime}\right)\Bigg]\gamma_{ij}-\partial_i\partial_j\left(\phi^{(1)}-\psi^{(1)}\right)+2\left[\frac{a''}{a}+\mathcal{H}^2\right]\partial_i\partial_j E^{(1)}-2\mathcal{H}\partial_i\partial_j\left(B^{(1)}-E^{(1)\prime}\right)\\&+\partial_i\partial_j\left(E^{(1)\prime\prime}-B^{(1)\prime}\right)=\kappa^2\left[\left(Pa^2\psi^{(1)}-\frac{a^2}{2}\delta^{(1)}P+\frac{a^2}{2}\delta^{(1)}\rho-\rho a^2\psi^{(1)}\right)\gamma_{ij}\right.\\&\left.+(\rho-P)a^2\partial_i\partial_j E^{(1)}\right]+2a^2\Lambda\left(-\psi^{(1)}\gamma_{ij}+\partial_i\partial_j E^{(1)}\right).\end{aligned}\tag{3.68}$$

We will calculate the second order EFEs in a similar manner in the next chapter.

3.2.7 Gauge choices

In subsection 3.2.3 we have looked at how one can perform gauge transformation for scalar, vector and tensor quantities and how to construct gauge invariant quantities. Now we will look at a few popular gauge choices used in the cosmological perturbation theory:

Longitudinal gauge: It is also known as the orthogonal zero shear gauge [12, 116] or the conformal Newtonian gauge [26, 139]. In this gauge choice, the two Bardeen potentials shown in Eq. (3.39) coincide with the two scalar metric perturbations. This is achieved by the condition $B^{(1)} = E^{(1)} = 0$. The two Bardeen potentials have the physical interpretation as the amplitude of the metric perturbation in the longitudinal coordinate system. This gauge can be extended to its more general form by considering the vector and tensor metric perturbations. The extended version of the longitudinal gauge is called the Poisson gauge [26, 38]. Additionally in the perfect fluid case, the two Bardeen potentials coincide, i.e. $\Phi^{(1)} = \Psi^{(1)}$. This means that there remains only one scalar metric variable which is a generalisation of the Newtonian gravitational potential.

Synchronous gauge: The synchronous gauge was used by Lifshitz in his work on FLRW perturbation [128]. It is defined through $\phi^{(1)} = 0$ and $B^{(1)} = 0$. However, it can be seen from Eq. (3.35) that this does not fix the coordinates completely. This residual coordinate freedom can leads to unphysical gauge modes appearing in the study of density perturbation. It has been shown that it is possible to remove this gauge freedom, see for example [41].

Spatially flat gauge: In this gauge, one works on spatial hypersurfaces which are not perturbed. This requires us to have $\psi^{(1)} = E^{(1)} = 0$. This gauge is also known as the uniform curvature gauge [102] or off-diagonal gauge [116].

3.3 Physical interpretations of metric perturbations in linear theory

In subsection 3.2.7 we have introduced a few common gauge choices used in the study of cosmological perturbation theory. In the next chapter, we will study the second order vector modes from linear scalar modes in the Poisson gauge (which is a generalisation of the longitudinal gauge) hence we will confine ourselves to consider scalar, vector and tensor modes in Poisson gauge at linear order in this section.

Before we look at metric perturbations, we will first introduce the power spectrum and its definition. We will look at scalar perturbations/Bardeen potentials at different eras. We will also briefly outline the matter transfer function that we use for our study of second order vector modes in dust era shown in chapter 4. Lastly, we will look at vector and tensor perturbations in linear theory.

3.3.1 The power spectrum

The power spectrum is useful for characterising the properties of a perturbed field. In flat space, we can expand an arbitrary field $f(\eta, \boldsymbol{x})$ in Fourier space:

$$f(\boldsymbol{x}, \eta) = \frac{1}{(2\pi)^{3/2}} \int d^3k \; f(\boldsymbol{k}, \eta) e^{i\boldsymbol{k}\cdot\boldsymbol{x}}.$$

We then define the dimensionless power spectrum $\mathcal{P}_f(k, \eta)$ in Fourier space to be

$$\langle f(\boldsymbol{k}_1, \eta) f^*(\boldsymbol{k}_2, \eta) \rangle \equiv \frac{2\pi^2}{k^3} \mathcal{P}_f(k, \eta) \delta^3 \left(\boldsymbol{k}_1 - \boldsymbol{k}_2\right), \tag{3.69}$$

where the angled brackets are the ensemble averages and $\delta^3(...)$ is the Dirac delta function in three space. We shall adopt this power spectrum definition throughout this thesis.

The power spectrum measures the amplitude of the fluctuations (the clumpiness) at a given scale k. For example, in structure formation if the power spectrum at a given scale k is large, then it means that there are lots of very under dense or over dense regions. However, if the power spectrum at a given scale k is small, then we have a smooth matter distribution [126].

We can also define an effective spectral index $n_s(k)$:

$$n_s(k) - 1 \equiv \frac{d \ln \mathcal{P}_f(k, \eta)}{d \ln k}. \tag{3.70}$$

This is used to describe the slope of the power spectrum. Note that a constant $n_s(k)$ corresponds to a power law form for the power spectrum, i.e. $\mathcal{P}_f(k, \eta) = A k^{n_s - 1}$ with some constant A. In the theory of linear density perturbation, the famous scale invariant Harrison-Zel'dovich power spectrum (proposed independently by Harrison [93] and Zel'dovich [238]) is of power law form with $n_s = 1$.

A popular alternative definition of the power spectrum is

$$P_f(k, \eta) = \frac{2\pi^2}{k^3} \mathcal{P}_f(k, \eta). \tag{3.71}$$

However this alternative power spectrum $P_f(k, \eta)$ is not dimensionless.

3.3.2 Scalar perturbations in linear theory

In the longitudinal gauge at first order and working with perfect fluid, the 00 component of the EFE from Eq. (3.66) gives

$$3\Phi^{(1)''} + 6\mathcal{H}\Phi^{(1)'} + \nabla^2 \Phi^{(1)} = \kappa^2 a^2 \left[(\rho + 3P)\Phi^{(1)} + \frac{1}{2} \left(\delta^{(1)}\rho + 3\delta^{(1)} P \right) \right] - 2a^2 \Lambda \Phi^{(1)}. \tag{3.72}$$

From the $0i$ and the ij components shown in Eqs. (3.67) and (3.68) we can obtain

$$2\partial_i\Phi^{(1)'} + 2\mathcal{H}\partial_i\Phi^{(1)} = \kappa^2 a^2 \left[-(\rho + P)\partial_i v_{(1)}\right], \tag{3.73}$$

and

$$-\Phi^{(1)''} - 6\mathcal{H}\Phi^{(1)'} - 4\left[\frac{a''}{a} + \mathcal{H}^2\right]\Phi^{(1)} + \nabla^2\Phi^{(1)} = \kappa^2 a^2\left[(P-\rho)\Phi^{(1)} + \frac{1}{2}\left(\delta^{(1)}\rho - \delta^{(1)}P\right)\right] - 2a^2\Lambda\Phi^{(1)} \tag{3.74}$$

respectively. Furthermore, the $0i$ component of the first order EFEs leads to an expression for $\partial_i v_{(1)}$ in terms of $\Phi^{(1)}$:

$$\partial_i v_{(1)} = -\frac{2}{\kappa^2 a^2 \rho(1+w)}\left[\partial_i\Phi^{(1)'} + \mathcal{H}\partial_i\Phi^{(1)}\right]. \tag{3.75}$$

We will assume that the first order matter perturbations are adiabatic, i.e., that pressure perturbations obey $\delta^{(1)}P = c_s^2\delta^{(1)}\rho$. The 00 and ij components give

$$\delta^{(1)}\rho = \frac{2}{\kappa^2 a^2}\left[\nabla^2\Phi^{(1)} - 3\mathcal{H}\left(\Phi^{(1)'} + \mathcal{H}\Phi^{(1)}\right)\right]. \tag{3.76}$$

Combining Eqs. (3.72) and (3.74) and simplifying using Eqs. (3.13) and (3.14), we obtain the first order equation of motion for the Bardeen potential in Fourier space [116]:

$$\Phi''(\boldsymbol{k},\eta) + 3\mathcal{H}(1+c_s^2)\Phi'(\boldsymbol{k},\eta) + \left[(1+w)\Lambda a^2 + k^2 w\right]\Phi(\boldsymbol{k},\eta) = 0. \tag{3.77}$$

Another important quantity is the density contrast, δ defined as $\delta = \delta^{(1)}\rho/\rho$. When the perturbation $\delta^{(1)}\rho$ is small, one can then use the well established linear perturbation to study its growth. However, if we have $\delta = \delta^{(1)}\rho/\rho \approx 1$, then the perturbation theory breaks down. It can easily be shown that in the Fourier space the density contrast is given as

$$\frac{\delta^{(1)}\rho}{\rho} = -\frac{2k^2}{3\mathcal{H}^2\Omega_m}\Phi(\boldsymbol{k},\eta) - \frac{2}{\mathcal{H}\Omega_m}\Phi'(\boldsymbol{k},\eta) - \frac{2}{\Omega_m}\Phi(\boldsymbol{k},\eta). \tag{3.78}$$

We can simplify Eq. (3.77) by rewriting it in terms of two new variables

$$u(\boldsymbol{k},\eta) = \frac{2\Phi(\boldsymbol{k},\eta)}{\kappa^2\sqrt{\rho_0(1+w)}}, \text{ and } \theta(\eta) = \frac{1}{a\sqrt{1+w}}. \tag{3.79}$$

These new variables eliminate the damping term [159]. The new equation of motion is

$$u''(\boldsymbol{k},\eta) + \left(c_s^2 k^2 - \frac{\theta''}{\theta}\right)u(\boldsymbol{k},\eta) = 0. \tag{3.80}$$

The solutions to this equation is a linear combinations of the n^{th} order Bessel functions of the first and second kind, i.e. $J_{(n)}(\zeta)$ and $Y_{(n)}(\zeta)$:

$$u(\boldsymbol{k},\eta) = A(\boldsymbol{k})\sqrt{k\eta}J_{(n)}(c_s k\eta) + B(\boldsymbol{k})Y_{(n)}(c_s k\eta), \tag{3.81}$$

where we have $n = 1/2 + 2/(1+3w)$. In the case of the radiation era with $c_s^2 = w = \frac{1}{3}$, it is now easy to obtain a general solution to Eq. (3.77)

$$\Phi_r(\boldsymbol{k},\eta) = \frac{A_r(\boldsymbol{k})}{(k\eta)^3}\left[\sin\left(\frac{k\eta}{\sqrt{3}}\right) - \frac{k\eta}{\sqrt{3}}\cos\left(\frac{k\eta}{\sqrt{3}}\right)\right] + \frac{B_r(\boldsymbol{k})}{(k\eta)^3}\left[\frac{k\eta}{\sqrt{3}}\sin\left(\frac{k\eta}{\sqrt{3}}\right) + \cos\left(\frac{k\eta}{\sqrt{3}}\right)\right]. \tag{3.82}$$

We shall ignore the decaying mode – that is terms with a $B_r(\boldsymbol{k})$ coefficient. It is clear that for the modes that are outside the Hubble radius ($k\eta \ll 1$) during the radiation era, we then have

$$\Phi_r(\boldsymbol{k},\eta) \approx \frac{1}{9\sqrt{3}}A_r(\boldsymbol{k}), \text{ and } \frac{\delta^{(1)}\rho}{\rho} \approx -2A_r(\boldsymbol{k}). \tag{3.83}$$

This means that we have a constant amplitude outside the Hubble radius for both the scalar potential and the density contrast. This is sometimes referred to as the perturbations being 'frozen' outside the Hubble radius. On the other hand, when the modes are inside the Hubble radius ($k\eta \gg 1$), the perturbation oscillating rapidly. This is to be expected because at small scales the pressure is working against the gravitational pull as the baryonic matter condenses together.

In the matter era but without Λ (we denote this with a subscript m), we have $w = c_s^2 = 0$. The general solution to Eq. (3.77) is

$$\Phi_m(\boldsymbol{k},\eta) = A_m(\boldsymbol{k}) + \frac{B_m(\boldsymbol{k})}{\eta^5}. \tag{3.84}$$

Ignoring the decaying mode, the scalar potential is constant at all scales and its time differentiation is zero, i.e. $\Phi_m'(\boldsymbol{k},\eta) = 0$. However, the density contrast is $\delta = -(2 + (k\eta)^2/6)A_m(\boldsymbol{k})$. From this we can see that when outside the Hubble radius ($k\eta \ll 1$) density contrast remains constant, i.e. $\delta \approx -2A_m(\boldsymbol{k})$. On the other hand, the density contrast is $\delta \approx -(k\eta)^2/6A_m(\boldsymbol{k})$ when inside the Hubble radius.

Assuming that the fluctuations are Gaussian, we may introduce Gaussian random variables, $\hat{E}$, with unit variance and the property

$$\langle \hat{E}^*(\boldsymbol{k}_1)\hat{E}(\boldsymbol{k}_2)\rangle = \delta^3(\boldsymbol{k}_1 - \boldsymbol{k}_2). \tag{3.85}$$

We can then separate the length and directional dependence of functions of $\boldsymbol{k}$ and write $\Phi(\boldsymbol{k},\eta) = \Phi(k,\eta)\hat{E}(\boldsymbol{k})$ hence $A_r(\boldsymbol{k}) = A_r(k)\hat{E}(\boldsymbol{k})$. Similar to the radiation case shown above, we can then write $A_m(\boldsymbol{k}) = A_m(k)\hat{E}(\boldsymbol{k})$ neglecting the decaying mode $B_m(\boldsymbol{k})/\eta^5$ for the matter era without a cosmological constant. However, in the presence of a cosmological

constant (we use d to denote this) the solution to the Bardeen equation Eq. (3.77) may be written as

$$\Phi_d(\boldsymbol{k},\eta) = A_d(k)g(\eta)\hat{E}(\boldsymbol{k}). \tag{3.86}$$

by approximating the time evolution with the growth suppression function $g(z)$. This function is given by

$$g(z) = \frac{5}{2}g_\infty\Omega_m(z)\left\{\Omega_m(z)^{4/7} - \Omega_\Lambda(z) + \left[1+\frac{1}{2}\Omega_m(z)\right]\left[1+\frac{1}{70}\Omega_\Lambda(z)\right]\right\}^{-1}, \tag{3.87}$$

where (assuming zero curvature)

$$\Omega_m(z) = \frac{\Omega_0(1+z)^3}{\Omega_\Lambda + \Omega_0(1+z)^3}, \text{ and } \Omega_\Lambda(z) = \frac{\Omega_\Lambda}{\Omega_\Lambda + \Omega_0(1+z)^3}. \tag{3.88}$$

Note however that $g(z)$ can easily be related to $g(\eta)$. The normalization factor g_∞ is chosen so that $g(0) = 1$. This approximation formula of the growth suppression follows from [121, 47].

The amplitude $A_d(k)$ [in Eq. (3.86)] today can be approximated by $A_d(k) = \tilde{A}_d(k)T(k)$, where $\tilde{A}_d(k)$ is the amplitude of perturbations and $T(k)$ is the transfer function. The fitting form used in our analysis for the transfer function will be introduced later.

The power spectrum for the first order scalar perturbation is defined by

$$\langle\Phi^*(\boldsymbol{k}_1,\eta)\Phi(\boldsymbol{k}_2,\eta)\rangle = \frac{2\pi^2}{k^3}\delta^3(\boldsymbol{k}_1-\boldsymbol{k}_2)\mathcal{P}_\Phi(k,\eta). \tag{3.89}$$

At early times during the radiation era the power spectrum becomes

$$\mathcal{P}_{\Phi_r}(k) \simeq A_r(k)^2\frac{k^3}{486\pi^2}. \tag{3.90}$$

Relating the Bardeen potential to the comoving curvature perturbation at early times gives us

$$A_r(k)^2 \approx \frac{216\pi^2}{k^3}\Delta^2_{\mathcal{R}}(k), \tag{3.91}$$

where $\Delta^2_{\mathcal{R}}$ is primordial power spectrum for the curvature perturbation $\mathcal{R}$. Current observations show $\Delta^2_{\mathcal{R}} \approx 2.41\times10^{-9}$ at a scale $k_{CMB} = 0.002\text{Mpc}^{-1}$, and $\Delta^2_{\mathcal{R}}$ is almost independent of wavenumber on these scales [117].

The overall amplitude of $\tilde{A}_d(k)$ can be found from the curvature perturbation [2]

$$\mathcal{R} = \Phi + \frac{2}{3(1+w)}\left(\Phi + \frac{\Phi'}{\mathcal{H}}\right), \tag{3.92}$$

[2]Note that it is denoted as ζ in [159]

which is constant for adiabatic perturbations on super-Hubble scales. This implies that at $\eta = \eta_{eq}$,

$$\mathcal{R}_r = \mathcal{R}_d, \tag{3.93}$$

for modes $k \ll k_{eq}$. This then results in a matching condition for the Bardeen potential on super-Hubble scales at matter-radiation equality (when the effects of the cosmological constant is insignificant):

$$\Phi_r = \frac{10}{9}\Phi_d. \tag{3.94}$$

Therefore, Eq. (3.94) gives us

$$\tilde{A}_d(k) = \frac{\sqrt{3}}{30 g_\infty} A_r(k) \approx \frac{3\sqrt{2}\pi\Delta_{\mathcal{R}}}{5 g_\infty k^{3/2}}, \tag{3.95}$$

assuming a scale-invariant initial spectrum.

Using the above results, we get an expression for the scalar power spectrum during the radiation era:

$$\mathcal{P}_{\Phi_r}(k) \simeq \frac{4}{9}\Delta^2_{\mathcal{R}}(k). \tag{3.96}$$

However, for the case of dust era with a cosmological constant the expression is

$$\mathcal{P}_{\Phi_d}(k) \simeq \left(\frac{3\Delta_{\mathcal{R}}}{5 g_\infty}\right)^2 T^2(k) g^2(\eta). \tag{3.97}$$

The matter transfer function

Here we will look at the matter transfer function mentioned earlier. A power spectrum of perturbation at present time (for example the scalar power spectrum as presented in Eq. (3.97)) results from the evolution of the primordial one. This evolution should take into account a variety of physical processes. These include, for example, the growth of structure under self gravitation, the effects of pressure on structure growth, the dissipation of perturbations; all of which are caused by the matter content of the universe and they can change the shape on the original power spectrum.

If we wish to relate the present time power spectrum to the primordial one, detailed discussions following matter perturbations starting from the time of horizon crossing through the radiation-matter transition to present day and encapsulating all physical effects during the evolution is required (see for example [173, 61]). However, such an approach is cumbersome since it requires one to solve the multispecies Boltzmann equations due to a mixture of CDM, baryons, neutrinos and photons exist in our universe.

Although numerical codes to solve the multispecies Boltzmann equations are publicly available (e.g. CMBfast and CAMB), however they are best used if one requires numerical results with high accuracy. Furthermore, having an analytic description for the matter transfer function even though it can be calculated using CMBfast or CAMB will provide us

with better understanding as to how behaviours one sees in matter transfer function can be matched to some physical effects. Therefore, much work has been done to develop accurate fitting formulae for the transfer functions for different mixtures of matter contents in the universe, see [71, 99, 13, 176] for example. Here we shall focus on the one that is used in our work on second order vector modes.

Throughout our studies of vector modes during dust era (see section 4.3), we have consistently used the matter transfer function from [71]. For this function, the universe is considered to be composed of photons, baryons, massless neutrinos and CDM. The total matter density today (defined in Eq. (2.7)) consists of baryons and CDM: $\Omega_m = \Omega_b + \Omega_c$, where Ω_b and Ω_c are the density of baryons and CDM today. The CMB temperature is written as $T_{\rm CMB} = 2.7\Theta_{2.7}$ K. We also use the definition $h \equiv H_0/(100\text{km s}^{-1}\text{Mpc}^{-1})$. It is assumed that the massless neutrinos contribute an energy density corresponding to three species at $(4/11)^{1/3}$ the temperature of the photons. It is worth noting that all the effects in the transfer function are set at early times. Late time effect such as the presence of a cosmological constant ($\Omega_\Lambda \neq 0$) is insignificant in this case.

Before we look at the transfer function itself, we will first look at the relevant length and time scales. The physical processes at work during the evolution of perturbation in a universe consists of baryons and CDM (such as in our case) involve three important length scales: the horizon size at the matter-radiation equality, the sound horizon scale at the time of recombination and the Silk damping scale at recombination. Complimenting these three length scales are two time scales: the time z_{eq} when radiation-matter equality occurs, and the time z_d, known as the drag epoch, when the baryons are released from the Compton drag of the photons (when the photon pressure can no longer prevent gravitational instability in the baryons).

Radiation-matter equality occurs approximately at [71]

$$z_{eq} = 2.5 \times 10^4 \Omega_m h^2 \Theta_{2.7}^{-4}. \tag{3.98}$$

This time scale marks the transition from a radiation dominated universe to a matter dominated universe. Therefore, this is the redshift where the density of the relativistic particles (photons and massless neutrinos) and the density of non-relativistic particles (CDM and baryons) equal. A numerically fitted formula for the drag epoch is [71]

$$z_d = 1291 \frac{(\Omega_m h^2)^{0.251}}{1 + 0.659(\Omega_m h^2)^{0.828}} \left[1 + b_1 (\Omega_m h^2)^{b_2}\right], \tag{3.99}$$

where it is defined that

$$b_1 = 0.313(\Omega_m h^2)^{-0.419} \left[1 + 0.607(\Omega_m h^2)^{0.74}\right], \text{ and } b_2 = 0.238(\Omega_m h^2)^{0.223}.$$

After this epoch, baryons fall into the CDM potential well and participate in gravitational

collapse.

The horizon scale at z_{eq} is [71]

$$k_{eq} \equiv (2\Omega_m H_0^2 z_{eq})^{1/2} = 7.46 \times 10^{-2} \Omega_m h^2 \Theta_{2.7}^{-2} \mathrm{Mpc}^{-1}. \tag{3.100}$$

The horizon at the drag epoch is defined as the comoving distance a wave can travel up to z_d:

$$\begin{aligned} s &= \int_0^{t(z_d)} c_s (1+z) dt \\ &= \frac{2}{3k_{eq}} \sqrt{\frac{6}{R_{eq}}} \ln \frac{\sqrt{1+R_d} + \sqrt{R_d + R_{eq}}}{1+\sqrt{R_{eq}}}, \end{aligned} \tag{3.101}$$

where $R_d \equiv R(z_d)$, $R_{eq} \equiv R(z_{eq})$ and $R(z)$ is the ratio of the baryon to photon momentum density

$$R(z) \equiv \frac{3\rho_b}{4\rho_\gamma} = 31.5 \Omega_b h^2 \Theta_{2.7}^{-4} (z/10^3)^{-1}. \tag{3.102}$$

The Silk damping effect is due to photon diffusion suppressing the baryon fluctuation [200]. This scale is well fitted by the approximation

$$k_{silk} = 1.6 (\Omega_b h^2)^{0.52} (\Omega_m h^2)^{0.73} \left[1 + (10.4 \Omega_m h^2)^{-0.95}\right] \mathrm{Mpc}^{-1}. \tag{3.103}$$

The matter transfer function $T(k)$ is formally defined as

$$T(k) \equiv \frac{\delta(k, z=0)}{\delta(k,z) \boldsymbol{D}(z)}, \tag{3.104}$$

where $\delta(k,z)$ is the density contrast for wavenumber k at redshift z, and $\boldsymbol{D}(z)$ is the large scale linear growth factor between redshift z and present. At large scale ($k \to 0$), by construction, we have $T \to 1$. However, the fitting formula of the transfer function is written as the density weighted average of two species (baryons and CDM):

$$T(k) = \frac{\Omega_b}{\Omega_m} T_b(k) + \frac{\Omega_c}{\Omega_m} T_c(k). \tag{3.105}$$

The growth of CDM is suppressed on scales below the sound horizon in the presence of baryons. Therefore, this suppression is introduced by interpolating between two solutions near sound horizon:

$$T_c(k) = f \hat{T}_0(k, 1, \beta_c) + (1-f) \hat{T}_0(k, \alpha_c, \beta_c), \tag{3.106}$$

where

$$f = \frac{1}{1 + (ks/5.4)^4}, \text{ and } \hat{T}_0(k, \alpha_c, \beta_c) = \frac{\ln(e + 1.8\beta_c q)}{\ln(e + 1.8\beta_c q) + Cq^2}, \tag{3.107}$$

with

$$C = \frac{14.2}{\alpha_c} + \frac{386}{1+69.9q^{1.08}},\ q = \left(\frac{k}{\mathrm{Mpc}^{-1}}\right)\Theta_{2.7}^2(\Omega_m h^2)^{-1} = \frac{k}{13.41k_{eq}}.$$

Furthermore, the parameters α_c and β_c take the form

$$\begin{aligned} \alpha_c &= a_1^{-\Omega_b/\Omega_m} a_2^{-(\Omega_b/\Omega_m)^3}, \\ a_1 &= (46.9\Omega_m h^2)^{0.67}\left[1+(32.1\Omega_m h^2)^{-0.532}\right], \\ a_2 &= (12.0\Omega_m h^2)^{0.424}\left[1+(45.0\Omega_m h^2)^{-0.582}\right], \end{aligned} \tag{3.108}$$

$$\begin{aligned} \beta_c^{-1} &= 1 + b_1\left[(\Omega_c/\Omega_m)^{b_2} - 1\right], \\ b_1 &= 0.944\left[1+(458\Omega_m h^2)^{-0.708}\right]^{-1}, \\ b_2 &= (0.395\Omega_m h^2)^{-0.0266}. \end{aligned} \tag{3.109}$$

However, the influence of the presence of baryon is by exhibiting a series of declining peaks (a series of oscillation with reduced amplitudes) due to acoustic oscillations in the transfer function where it departs from unity below the sound horizon. We can incorporate this by multiplying our expression with a declining oscillatory factor $j_0(x) \equiv (\sin x)/x$:

$$T_b(k) = \left[\frac{\hat{T}_0(k,1,1)}{1+(ks/5.2)^2} + \frac{\alpha_b}{1+(\beta_b/ks)^3}e^{-(k/k_{silk})^{1.4}}\right] j_0(k\tilde{s}). \tag{3.110}$$

Note that we have defined the quantity

$$\tilde{s}(k) = \frac{s}{[1+(\beta_{node}/ks)^3]^{1/3}},\ \text{and}\ \beta_b = 0.5 + \frac{\Omega_b}{\Omega_m} + \left(3 - 2\frac{\Omega_b}{\Omega_m}\right)\sqrt{(17.2\Omega_m h^2)^2+1},$$

with $\beta_{node} = 8.41(\Omega_m h^2)^{0.435}$.

The transfer function should contain a factor which describes suppression from the decay of potentials between the matter-radiation equality and drag scales, and an exponential Silk damping. As explained in [71] this is incorporated in the expression in the square bracket in Eq. (3.110) since it can trace the zero baryon CDM case above the sound horizon and then breaks to a constant multiplied by an exponential Silk damping factor. The Silk damping factor occurs only in the second term in the square bracket is because Silk damping effect can only happen on scales below sound horizon therefore only the second term has significant contribution.

Details on the development and performance testing of the fitting formula for the matter transfer function presented here have been compared with CMBfast and they are given in detail in [71] so we shall not present them here. The fitting formula for the transfer function shown in Eq. (3.105) works quite well for the parameter range $0.025 \leq \Omega_m h^2 \leq 0.25$ and $0 \leq \Omega_b/\Omega_m \leq 1$. A systematic effect which occurs when we have high baryon fraction with ranges like $0.7 < \Omega_b/\Omega_m < 0.9$. Within this baryon fraction range, the first valley is

systematically underestimated by $\sim 10\% - 15\%$ in amplitude.

3.3.3 Vector and tensor modes in linear theory

As illustrated in [19, 152], a scalar field cannot support vector modes at linear order. Here we will follow the presentation in [152] and show as to why this is the case.

The vector perturbations at linear order satisfy an evolution equation and a momentum constraint equation which can be found by calculating the ij and $0i$ parts of the EFEs respectively. The evolution equation takes the form of

$$\nabla^2 S_i^{(1)\prime} + 2\mathcal{H}\nabla^2 S_i^{(1)} = 0, \tag{3.111}$$

while the constraint equation takes the form

$$\frac{1}{2a^2}\nabla^2 S_i^{(1)} = -\kappa^2(\rho + P)\delta^{(1)}v_i. \tag{3.112}$$

As one can see from Eq. (3.111), there is no source in the vector evolution equation. If we solve Eq. (3.111), it then admits solutions proportional to $1/a^2$. The momentum constraint equation (Eq. (3.112)) relates the vector perturbation $S_i^{(1)}$ to the three velocity perturbation $\delta^{(1)}v_i$. If we take the universe to be sourced by a scalar field φ with a stress energy tensor of the form:

$$T_{\alpha\beta} = \varphi_{,\alpha}\varphi_{,\beta} - \frac{1}{2}g_{\alpha\beta}\varphi^{,\gamma}\varphi_{,\gamma} - g_{\alpha\beta}V(\varphi), \tag{3.113}$$

where $V(\varphi)$ is the associated scalar field potential. Following the expressions presented in [169], the correspondence of the scalar field stress energy tensor between the energy frame and the normal frame can be identified in such a way that the first order velocity perturbation $\delta^{(1)}v_i$ takes the form

$$\delta^{(1)}v_i = -\frac{1}{a\dot{\varphi}}\delta^{(1)}\varphi_{,i}. \tag{3.114}$$

It is important to note that the right hand side of Eq. (3.114) can be expressed as a gradient of a scalar and therefore first order velocity perturbation $\delta^{(1)}v_i$ does not have a pure vector part. Following this realisation together with Eq. (3.112) we can conclude that a scalar field does not support vector modes.

Next we shall consider the first order gauge invariant tensor perturbations which we have previously denoted as $h_{ij}^{(1)}$. Again here we have the perfect fluid background. It is possible to obtain an equation of motion for the tensor perturbation from Eqs. (3.48), (3.61), and (3.65). After Fourier decomposition we then have

$$h^{(1)\prime\prime}(\boldsymbol{k},\eta) + 2\mathcal{H}h^{(1)\prime}(\boldsymbol{k},\eta) + k^2 h^{(1)}(\boldsymbol{k},\eta) = 0. \tag{3.115}$$

We shall solve this equation in the same fashion as the scalar perturbation presented in Eq.

(3.77). If we define a new variable as

$$\upsilon(\boldsymbol{k},\eta) = ah^{(1)}(\boldsymbol{k},\eta), \tag{3.116}$$

then substituting into Eq. (3.115) we can then again eliminate the damping term. The tensor perturbation equation of motion in the new variable then becomes

$$\upsilon''(\boldsymbol{k},\eta) + \left(k^2 + \frac{2(1+3w)}{\eta(1+3w)^2}\right)\upsilon(\boldsymbol{k},\eta) = 0. \tag{3.117}$$

Again, the solutions to this equation is a linear combinations of the n^{th} order Bessel functions of the first and second kind, i.e. $J_{(n)}(\zeta)$ and $Y_{(n)}(\zeta)$,

$$\upsilon(\boldsymbol{k},\eta) = A(\boldsymbol{k})\sqrt{k\eta}J_{(n)}(k\eta) + B(\boldsymbol{k})Y_{(n)}(k\eta). \tag{3.118}$$

In the case of the radiation dominated era ($c_s^2 = w = 1/3$), the solutions are in the form of

$$h_r(\boldsymbol{k},\eta) = \frac{A(\boldsymbol{k})}{k\eta}\sin(k\eta) + \frac{B(\boldsymbol{k})}{k\eta}\cos(k\eta). \tag{3.119}$$

Furthermore, if we consider the dust era without cosmological constant ($c_s^2 = w = 0$ without Λ), we then have

$$h_m(\boldsymbol{k},\eta) = \frac{A(\boldsymbol{k})}{k^3\eta^3}\left[k\eta\cos(k\eta) - \sin(k\eta)\right] + \frac{B(\boldsymbol{k})}{k^3\eta^3}\left[k\eta\sin(k\eta) + \cos(k\eta)\right]. \tag{3.120}$$

3.4 The 1+3 covariant formalism

The covariant approach to general relativity and cosmology was first worked on by Heckman, Schücking and Raychaudhuri [95, 186] and it was further developed by [94, 72, 73, 69]. It has been reviewed by various authors, see for example [36, 74, 77, 222]. In this section, we give a brief overview of the 1+3 covariant formalism since we will use it in chapter 4 for our analysis on issues related to generation of vorticity at second order. We shall first start with the definition of some kinematical quantities in applying the covariant kinetic theory and the geometrical quantities. Next we present the decomposition of the energy momentum tensor. Lastly, we will present the covariant conservation/evolution equations and the covariant constrainte equations that are related to these kinematical or geometrical quantities. We shall see, in a later chapter, that the covariant method will be a great help when we try to clarify the issue of vorticity generation.

3.4.1 The four velocity vectors and notations

We will consider a general spacetime with a metric $g_{\alpha\beta}$. Also, a family of observers with worldlines tangent to the four velocity vector

$$u^{\alpha} = \frac{dx^{\alpha}}{d\tau} \tag{3.121}$$

is also introduced. Note that τ is the observers' proper time measured along the worldlines. This tells that the four velocity vector is timelike, i.e. $u_{\alpha}u^{\alpha} = -1$. We can then define two projection tensors $h_{\alpha\beta}$ and $U^{\alpha}_{\ \beta}$ where we have

$$h_{\alpha\beta} = g_{\alpha\beta} + u_{\alpha}u_{\beta}, \tag{3.122}$$

and

$$U^{\alpha}_{\ \beta} = -u^{\alpha}u_{\beta}. \tag{3.123}$$

Additionally, $h_{\alpha\beta}$ and U^{α}_{β} satisfy

$$h^{\alpha}_{\ \beta}h^{\beta}_{\ \gamma} = h^{\alpha}_{\ \gamma},\ h^{\alpha}_{\ \alpha} = 3,\ \text{and}\ h_{\alpha\beta}u^{\beta} = 0. \tag{3.124}$$

$$U^{\alpha}_{\ \beta}U^{\beta}_{\ \gamma} = U^{\alpha}_{\ \gamma},\ U^{\alpha}_{\ \alpha} = 1,\ \text{and}\ U_{\alpha\beta}u^{\beta} = u_{\alpha}. \tag{3.125}$$

This shows that $h_{\alpha\beta}$ projects orthogonal to the four velocity vector u^{α} into the observers' instantaneous rest spaces, while $U^{\alpha}_{\ \beta}$ projects parallel to the four velocity vector. Furthermore, the tensor $h_{\alpha\beta}$ allows for a unique decomposition of every spacetime quantity into its spacelike part.

The effective volume element for the rest spaces is also defined:

$$\epsilon_{\alpha\beta\gamma} = u^{\mu}\eta_{\mu\alpha\beta\gamma}. \tag{3.126}$$

It must satisfy the properties that

$$\epsilon_{\alpha\beta\gamma} = \epsilon_{[\alpha\beta\gamma]},\ \epsilon_{\alpha\beta\gamma}\epsilon^{\mu\nu\lambda} = 3!h^{\ \mu}_{[\alpha}h_{\beta}^{\ \nu}h^{\ \lambda}_{\gamma]},\ \text{and}\ \epsilon_{\alpha\beta\gamma}u^{\gamma} = 0. \tag{3.127}$$

And it is covariantly constant. The four dimensional volume element, $\eta_{\mu\alpha\beta\gamma}$, used in Eq. (3.126) must satisfy

$$\eta_{\mu\alpha\beta\gamma} = 2u_{[\mu}\epsilon_{\alpha]\beta\gamma} - 2\epsilon_{\mu\alpha[\beta}u_{\gamma]},\ \eta_{\mu\alpha\beta\gamma}\eta^{\nu\lambda\rho\phi} = -4!\delta^{\ \nu}_{[\mu}\delta_{\alpha}^{\ \lambda}\delta_{\beta}^{\ \rho}\delta^{\ \phi}_{\gamma]},\ \text{and}\ \eta^{0123} = [-\det(\mathrm{g}_{\alpha\beta})]^{-1/2}. \tag{3.128}$$

Next thing to consider is how the time and space derivatives are defined in the covariant approach.

The covariant time derivative along the comoving observers' worldlines, defined for any

tensor $T^{\alpha}_{\ \beta}$ is

$$\dot{T}^{\alpha}_{\ \beta} = u^{\gamma}\nabla_{\gamma}T^{\alpha}_{\ \beta}. \tag{3.129}$$

The fully orthogonally projected spatial covariant derivative for any tensor $T^{\alpha}_{\ \beta}$ is defined as

$$\tilde{\nabla}_{\gamma}T^{\alpha}_{\ \beta} = \mathrm{D}_{\gamma}T^{\alpha}_{\ \beta} = h^{\delta}_{\ \gamma}h^{\alpha}_{\ \mu}h^{\nu}_{\ \beta}\nabla_{\delta}T^{\mu}_{\ \nu}, \tag{3.130}$$

with total projection on all free indices. Note that the notation presented in the middle of the above equation is only used in the equations that will be used for the covariant discussions outside this chapter. We use a different notation here to distinguish their importance to us. Here, the tilde serves as a reminder that $\tilde{\nabla}_{\gamma}$ is a proper three dimensional derivative if u^{α} has zero vorticity [36]. Finally, we use angle brackets to denote orthogonal projections of vector quantities and the orthogonally projected symmetric trace-free part of tensors:

$$V^{\langle\alpha\rangle} = h^{\alpha}_{\ \beta}V^{\beta}, \tag{3.131}$$

and

$$T^{\langle\alpha\beta\rangle} = \left[h^{(\alpha}_{\ \mu}h^{\beta)}_{\ \nu} - \frac{1}{3}h^{\alpha\beta}h_{\mu\nu}\right]T^{\mu\nu}. \tag{3.132}$$

It is also possible to apply the angle brackets to denote the orthogonal projections of covariant time derivatives

$$\dot{V}^{\langle\alpha\rangle} = h^{\alpha}_{\ \beta}\dot{V}^{\beta}, \tag{3.133}$$

and

$$\dot{T}^{\langle\alpha\beta\rangle} = \left[h^{(\alpha}_{\ \mu}h^{\beta)}_{\ \nu} - \frac{1}{3}h^{\alpha\beta}h_{\mu\nu}\right]\dot{T}^{\mu\nu}. \tag{3.134}$$

3.4.2 Kinematical quantities

With the definition presented in the preceding subsection, we can now split the first covariant derivative of u^{α} into its irreducible parts, defined by their symmetry properties:

$$\begin{aligned}\nabla_{\mu}u_{\nu} &= -u_{\mu}\dot{u}_{\nu} + \tilde{\nabla}_{\mu}u_{\nu},\\ &= -u_{\mu}\dot{u}_{\nu} + \frac{1}{3}\Theta h_{\mu\nu} + \sigma_{\mu\nu} + \omega_{\mu\nu},\end{aligned} \tag{3.135}$$

where we have introduced a few new notations, and they are, in the order of appearance, the four acceleration vector $\dot{u}_{\mu}$, the volume expansion $\tilde{\nabla}_{\mu}u^{\mu}$, the expansion scalar Θ, the shear tensor $\sigma_{\mu\nu}$, and the vorticity tensor $\omega_{\mu\nu}$. By construction the four acceleration vector is

$$\dot{u}_{\mu} = u^{\nu}\nabla_{\nu}u_{\mu}. \tag{3.136}$$

It is simply the time rate of change of the four velocity vector u_μ. It represents a non-gravitational motion of the fluid flow. The expansion scalar is constructed to be

$$\Theta = \tilde{\nabla}_\mu u^\mu, \tag{3.137}$$

which describes the volume rate of expansion (or contraction) of the fluid. In the case of Robertson-Walker metric, it reduces to a representative length scale in cosmology - the Hubble parameter in proper time, i.e. $\Theta = 3\frac{da/dt}{a}$. The shear is the trace free symmetric tensor defined as

$$\sigma_{\mu\nu} = \tilde{\nabla}_{\langle\mu} u_{\nu\rangle}, \tag{3.138}$$

which satisfies the properties that

$$\sigma_{\mu\nu} = \sigma_{(\mu\nu)},\ \sigma_{\mu\nu}u^\nu = 0,\ \text{and}\ \sigma^\mu{}_\mu = 0. \tag{3.139}$$

It is used in describing the rate of distortion of the fluid, while the vorticity tensor

$$\omega_{\mu\nu} = \tilde{\nabla}_{[\mu} u_{\nu]} \tag{3.140}$$

is used in describing the change of orientation (the rotation) of the fluid with respect to a non-rotating frame. The vorticity tensor has the properties

$$\omega_{\mu\nu}u^\nu = 0 \text{ and } \omega_{\mu\nu} = \omega_{[\mu\nu]}. \tag{3.141}$$

One defines the vorticity vector from vorticity tensor as

$$\omega^\mu = \frac{1}{2}\epsilon^{\mu\nu\alpha}\omega_{\nu\alpha}, \tag{3.142}$$

with easy reverse construction as

$$\omega^{\mu\nu} = \epsilon^{\mu\nu\gamma}\omega_\gamma. \tag{3.143}$$

Following [222], we shall also use the sign convensions such that $\vec{\omega} = -\vec{\nabla}\times\vec{v}/2$ in the Newtonian limit. This choice of sign convensions, however, will lead to the opposite signs in the vorticity tensor $\omega_{\mu\nu}$ and the volume element $\epsilon_{\alpha\beta\gamma}$ when compared with related expressions shown in [77].

3.4.3 The geometrical quantities

We now face the quantities that describe the geometrical properties of the spacetime. The Riemann tensor $R_{\alpha\beta\gamma\mu}$ provides information on the curvature of spacetime and it is defined as

$$\left(\nabla_\alpha\nabla_\beta - \nabla_\beta\nabla_\alpha\right)u_\gamma = R_{\alpha\beta\gamma\mu}u^\mu. \tag{3.144}$$

Additionally, the Riemann tensor has the following properties

$$R_{\alpha\beta\gamma\mu} = R_{[\alpha\beta][\gamma\mu]} = R_{\gamma\mu\alpha\beta}, \text{ and } R_{\alpha[\beta\gamma\mu]} = 0.$$

The Ricci tensor is the trace contracted over the first and third indices of the Riemann tensor, i.e., $R_{\alpha\gamma} = R^{\beta}{}_{\alpha\beta\gamma}$. The Riemann tensor has 20 independent components and the Ricci tensor has only 10. The Weyl curvature tensor $C_{\alpha\beta\gamma\mu}$ contains the remaining independent components. The Weyl curvature tensor represents the free gravitational field, allowing for gravitational action at a distance (for example tidal forces and gravitational waves) [77]. It is defined as

$$C_{\alpha\beta\gamma\mu} = R_{\alpha\beta\gamma\mu} - \left(g_{\alpha[\gamma}R_{\mu]\beta} - g_{\beta[\gamma}R_{\mu]\alpha}\right) + \frac{1}{3}g_{\alpha[\gamma}g_{\mu]\beta}R, \tag{3.145}$$

where R is the Ricci scalar. It can also influence the motion of matter and radiation. A splitting relative to u^{α} of the Weyl tensor is possible. This will give us an 'electric' part and a 'magnetic' part. The electric part of the Weyl tensor is defined according to

$$E_{\alpha\gamma} = C_{\alpha\beta\gamma\mu}u^{\beta}u^{\mu}. \tag{3.146}$$

It must satisfies

$$E_{\alpha\gamma} = E_{(\alpha\gamma)}, \; E^{\alpha}{}_{\alpha} = 0, \; E_{\alpha\gamma}u^{\gamma} = 0.$$

The magnetic part of the Weyl tensor is defined by

$$H_{\alpha\gamma} = \frac{1}{2}\epsilon_{\alpha\mu\nu}C^{\mu\nu}{}_{\gamma\beta}u^{\beta} = \frac{1}{2}\eta_{\alpha\mu}{}^{\lambda\nu}C_{\lambda\nu\gamma\beta}u^{\mu}u^{\beta}, \tag{3.147}$$

with additional conditions that

$$H_{\alpha\gamma} = H_{(\alpha\gamma)}, \; H^{\alpha}{}_{\alpha} = 0, \; H_{\alpha\gamma}u^{\gamma} = 0.$$

Now we can introduce the Bianchi identities for the Riemann tensor

$$\nabla_{[\delta}R_{\alpha\beta]\gamma\mu} = 0. \tag{3.148}$$

With the Weyl tensor introduced in Eq. (3.145), we can rewrite the above equation as

$$\nabla^{\mu}C_{\alpha\beta\gamma\mu} = \nabla_{[\beta}R_{\alpha]\gamma} + \frac{1}{6}g_{\gamma[\beta}\nabla_{\alpha]}R. \tag{3.149}$$

The twice contracted Bianchi identities can be obtained from contracting Eq. (3.149) and by EFEs they imply the conservation equations.

3.4.4 The energy momentum tensor

The general energy momentum tensor can be decomposed relative to the four velocity vector as

$$T_{\alpha\beta} = \rho u_\alpha u_\beta + P h_{\alpha\beta} + 2q_{(\alpha}u_{\beta)} + \pi_{\alpha\beta}. \tag{3.150}$$

The relativistic energy density relative to u^α is defined as

$$\rho = T_{\alpha\beta}u^\alpha u^\beta. \tag{3.151}$$

The isotropic pressure of the fluid

$$P = \frac{1}{3}h^{\alpha\beta}T_{\alpha\beta}. \tag{3.152}$$

The energy flux relative to u^α which is also the relativistic momentum density

$$q_\alpha = -h^\gamma{}_\alpha T_{\gamma\mu}u^\mu, \tag{3.153}$$

which must satisfy $q_\alpha u^\alpha = 0$. The trace free anisotropic pressure (stress) is

$$\pi_{\alpha\beta} = T_{\langle\alpha\beta\rangle} = h^\mu{}_{\langle\alpha}h^\nu{}_{\beta\rangle}T_{\mu\nu}, \tag{3.154}$$

and it must satisfy $\pi^\alpha{}_\alpha = 0$, $\pi_{\alpha\beta} = \pi_{(\alpha\beta)}$, and $\pi_{\alpha\beta}u^\alpha = 0$.

3.4.5 Covariant conservation equations

In this subsection, the covariant conservation/evolution equations are presented using the covariant formalism developed in the preceding subsections. The energy and momentum conservation equations, the Raychaudhuri equation, the shear and vorticity evolution equations, and finally the electric and magnetic Weyl evolution equations are shown here. The covariant constraint equations can be found in the next subsection.

In our current notation, the energy conservation equation is

$$\dot{\rho} = -\Theta(\rho + P) - 2\dot{u}_\alpha q^\alpha - \mathrm{D}_\alpha \mathrm{q}^\alpha - \sigma^\alpha{}_\beta \pi^\beta{}_\alpha. \tag{3.155}$$

The momentum conservation equation is

$$h_\mu{}^\nu \dot{q}_\nu + \frac{4}{3}\Theta q_\mu + (\rho + P)\dot{u}_\mu + \mathrm{D}_\mu P + \mathrm{D}^\nu \pi_{\mu\nu} + \sigma_{\mu\nu}q^\nu - \epsilon_{\mu\nu\gamma}\omega^\nu q^\gamma - \pi_{\mu\nu}\dot{u}^\nu = 0. \tag{3.156}$$

The Raychaudhuri equation is

$$\dot{\Theta} - \tilde{\nabla}_\alpha \dot{u}^\alpha = -\frac{1}{3}\Theta^2 - \frac{1}{2}(\rho + 3P) + \dot{u}_\alpha \dot{u}^\alpha - 2\sigma^2 + 2\omega^2 + \Lambda, \tag{3.157}$$

which is the basic equation of gravitational attraction. Here we have included the cosmo-

logical constant Λ and it shows a repulsive nature should it be positive.

The shear evolution equation is

$$\dot{\sigma}^{\langle\alpha\beta\rangle} - \tilde{\nabla}^{\langle\alpha}\dot{u}^{\beta\rangle} = -\frac{2}{3}\Theta\sigma^{\alpha\beta} + \dot{u}^{\langle\alpha}\dot{u}^{\beta\rangle} - \sigma^{\langle\alpha}{}_{\mu}\sigma^{\beta\rangle\mu} - \omega^{\langle\alpha}\omega^{\beta\rangle} - E^{\alpha\beta} + \frac{1}{2}\pi^{\alpha\beta}. \tag{3.158}$$

If we have a perfect fluid, the anisotropic pressure source term $\pi^{\alpha\beta}$ vanishes. This demonstrate how the shear can be induced from the electric Weyl tensor. The propagation equation the vorticity vector obeys allows for full nonlinearity

$$h_{\mu}{}^{\nu}\dot{\omega}_{\nu} = -\frac{2}{3}\Theta\omega_{\mu} - \frac{1}{2}\mathrm{curl}\,\dot{u}_{\mu} + \sigma_{\mu\nu}\omega^{\nu}. \tag{3.159}$$

The covariant spatial curl is defined by $\mathrm{curl}\,n_{\mu} = \epsilon_{\mu\nu\gamma}\mathrm{D}^{\nu}n^{\gamma}$, where D_{μ} is the spatially projected covariant derivative as mentioned earlier.

The electric Weyl evolution equation is just that

$$\begin{aligned}\dot{E}_{\langle\alpha\beta\rangle} - \mathrm{curlH}_{\alpha\beta} = &-\frac{1}{2}\dot{\pi}_{\alpha\beta} - \frac{1}{2}\tilde{\nabla}_{\langle\alpha}q_{\beta\rangle} - \frac{1}{2}(\rho+P)\sigma_{\alpha\beta} - \Theta\left(E_{\alpha\beta} + \frac{1}{6}\pi_{\alpha\beta}\right)\\ &+ 3\sigma_{\langle\alpha}{}^{\mu}E_{\beta\rangle\mu} - \frac{1}{2}\sigma_{\langle\alpha}{}^{\mu}\pi_{\beta\rangle\mu} - \dot{u}_{\langle\alpha}q_{\beta\rangle} + 2\epsilon_{\mu\nu\langle\alpha}\dot{u}^{\mu}H_{\beta\rangle}{}^{\nu}\\ &- \epsilon_{\mu\nu\langle\alpha}\omega^{\mu}E_{\beta\rangle}{}^{\nu} - \frac{1}{2}\epsilon_{\mu\nu\langle\alpha}\omega^{\mu}\pi_{\beta\rangle}{}^{\nu},\end{aligned} \tag{3.160}$$

and the magnetic Weyl evolution equation is

$$\begin{aligned}\dot{H}_{\langle\alpha\beta\rangle} + \mathrm{curlE}_{\alpha\beta} = &\frac{1}{2}\mathrm{curl}\pi_{\alpha\beta} + 3\sigma_{\langle\alpha}{}^{\mu}\mathrm{H}_{\beta\rangle\mu} - \frac{3}{2}\omega_{\langle\alpha}\mathrm{q}_{\beta\rangle} - 2\epsilon_{\mu\nu\langle\alpha}\dot{\mathrm{u}}^{\mu}\mathrm{E}_{\beta\rangle}{}^{\nu}\\ &+ \frac{1}{2}\epsilon_{\mu\nu\langle\alpha}q^{\nu}\sigma_{\beta\rangle}{}^{\mu} - \epsilon_{\mu\nu\langle\alpha}\omega^{\mu}H_{\beta\rangle}{}^{\nu} - \Theta H_{\alpha\beta}.\end{aligned} \tag{3.161}$$

3.4.6 Covariant constraint equations

In this subsection, we shall present various constraint equations. First we will look at the shear divergence equation

$$\tilde{\nabla}^{\gamma}\sigma_{\alpha\gamma} = \frac{2}{3}\tilde{\nabla}_{\alpha}\Theta + \epsilon_{\alpha\gamma\mu}\tilde{\nabla}^{\gamma}\omega^{\mu} + 2\epsilon_{\alpha\gamma\mu}\dot{u}^{\gamma}\omega^{\mu} - q_{\alpha}. \tag{3.162}$$

This equation shows us that in the case of non-perfect fluid how the flux q_{α} can be related to the spatial inhomogeneity of the expansion. Next we should introduce the vorticity divergence identity

$$\tilde{\nabla}_{\alpha}\omega^{\alpha} = \dot{u}_{\alpha}\omega^{\alpha}. \tag{3.163}$$

The magnetic equation is introduced below

$$H_{\alpha\gamma} = \mathrm{curl}\sigma_{\alpha\gamma} + 2\dot{\mathrm{u}}_{\langle\alpha}\omega_{\gamma\rangle} + \tilde{\nabla}_{\langle\alpha}\omega_{\gamma\rangle}. \tag{3.164}$$

It gives the relationship between the magnetic Weyl curvature and the distortion of the vorticity and the curl of the shear. The electric and magnetic Weyl divergence equations are what we look at next. We will present the electric Weyl divergence equation first

$$\tilde{\nabla}^{\gamma}E_{\alpha\gamma}=\frac{1}{3}\tilde{\nabla}_{\alpha}\rho-\frac{1}{2}\tilde{\nabla}^{\gamma}\pi_{\alpha\gamma}-\frac{1}{3}\Theta q_{\alpha}+\frac{1}{2}\sigma_{\alpha\gamma}q^{\gamma}-3\omega^{\gamma}H_{\alpha\gamma}+\epsilon_{\alpha\gamma\mu}\sigma^{\gamma}{}_{\nu}H^{\nu\mu}-\frac{3}{2}\epsilon_{\alpha\gamma\mu}\omega^{\gamma}q^{\mu}, \quad (3.165)$$

and the magnetic Weyl divergence equation is

$$\tilde{\nabla}^{\gamma}H_{\alpha\gamma}=(\rho+P)\omega_{\alpha}+3\omega^{\gamma}E_{\alpha\gamma}-\frac{1}{2}\omega^{\gamma}\pi_{\alpha\gamma}-\frac{1}{2}\epsilon_{\alpha\gamma\mu}\tilde{\nabla}^{\gamma}q^{\mu}-\frac{1}{2}\epsilon_{\alpha\gamma\mu}\sigma^{\gamma}{}_{\nu}\pi^{\mu\nu}-\epsilon_{\alpha\gamma\mu}\sigma^{\gamma}{}_{\nu}E^{\mu\nu}. \quad (3.166)$$

In this chapter, we have introduced some basic concepts in standard cosmological perturbation theory. We will turn our attention to the detailed investigation of second order vector modes from coupled linear scalar modes in next chapter.

Chapter 4

The cosmological background of vector modes

In chapter 1, it was pointed out that scalar field cannot support linear vector modes, therefore vector perturbations at linear order are considered to be insignificant. On the contrary to the naive expectation that second order vector modes would be the same as in the linear case, it has also been mentioned that it is possible to generate second order vector modes from coupled linear scalar modes as in the case of generating second order tensor modes.

Some authors have studied issues related to second order vector modes. One of these includes, for example, generation of second order vector modes from coupled linear scalar modes but in a collapsing universe scenario [152]. However, a detailed investigation of the generation mechanism that produces second order vector modes from coupled linear scalar modes in the standard (inflationary) scenario has not been done before and this is the focus of current chapter. As emphasised in chapter 1, it is both timely and important to better understand these vector modes since they are likely to play a more prominent role in cosmology in the near future due to their contributions to the CMB (in particular the B-mode polarization in the CMB).

In this chapter, we will first present all the algebraic expressions that have been calculated from the metric which only includes linear order scalar modes and second order vector modes in Poisson gauge. These expressions include, for example, the components of perturbed Ricci and energy momentum tensors and the components of EFEs. All the expressions presented in this chapter are derived from scratch as an independent check of the solutions that were presented in [6]. Generation of second order vector modes from two interacting scalar modes during the radiation era by assuming a two delta function form for the scalar power spectrum and the power spectrum of vector modes from power-law scalar modes are studied here.

For the second part of this chapter, the argument as to why there shall be no vorticity

generation in the fluid at second order via the covariant approach is presented. Investigation of the second order vector modes power spectrum today by density perturbation and the energy density of the vector part of the shear at second order are also shown here. Note that all the numerical results presented in this chapter were obtained from using Maple 11.

4.1 The second order vector modes from linear scalars

For this section we are considering a perfect fluid for the flat FLRW background and its linear perturbation. As mentioned before, we have linear constant equation of state, $c_s^2 = w$ and we assume that the first order matter perturbations are adiabatic ($\delta^{(1)}P = c_s^2\delta^{(1)}\rho$). Furthermore, we will adopt the Poisson gauge and this leaves us with the Bardeen potential $\Phi^{(1)}$ at first order and the second order vector mode, $S_i^{(2)}$, in the metric.

4.1.1 The metric

Similar to the linear order, the full perturbed expression up to and including second order about the background FLRW metric is

$$\bar{g}_{\mu\nu} = g_{\mu\nu} + \delta^{(1)}g_{\mu\nu} + \delta^{(2)}g_{\mu\nu}, \tag{4.1}$$

The perturbed metric in the case we are considering has components:

$$\bar{g}_{00} = -a^2\left(1 + 2\Phi^{(1)}\right), \quad \bar{g}_{0i} = -\frac{1}{2}a^2 S_i^{(2)}, \quad \bar{g}_{ij} = a^2\left(1 - 2\Phi^{(1)}\right)\gamma_{ij}, \tag{4.2}$$

where $\Phi^{(1)}$ is the first order Bardeen potential. $S_i^{(2)}$ describes the gauge-invariant [152, 143] second order vector modes, so that $\partial^i S_i^{(2)} = 0$. Note that we will use the conformal time again in this chapter. At second order, the contravariant form of our perturbed metric is

$$\delta^{(2)}g^{00} = -4a^{-2}\left(\Phi^{(1)}\right)^2, \ \delta^{(2)}g^{0i} = -\frac{1}{2}a^{-2}S^{(2)i}, \ \delta^{(2)}g^{ij} = 4a^{-2}\left(\Phi^{(1)}\right)^2\gamma^{ij}. \tag{4.3}$$

where the background and linear components have been introduced before.

The second order connection coefficients can be calculated from

$$\begin{aligned}\delta^{(2)}\Gamma^{\alpha}_{\beta\gamma} = {} & \frac{1}{2}g^{\alpha\rho}\left(\delta^{(2)}g_{\rho\gamma,\beta} + \delta^{(2)}g_{\beta\rho,\gamma} - \delta^{(2)}g_{\beta\gamma,\rho}\right) + \frac{1}{2}\delta^{(2)}g^{\alpha\rho}\left(g_{\rho\gamma,\beta} + g_{\beta\rho,\gamma} - g_{\beta\gamma,\rho}\right) \\ & + \frac{1}{2}\delta^{(1)}g^{\alpha\rho}\left(\delta^{(1)}g_{\rho\gamma,\beta} + \delta^{(1)}g_{\beta\rho,\gamma} - \delta^{(1)}g_{\beta\gamma,\rho}\right),\end{aligned} \tag{4.4}$$

where the various components are given in Appendix A. The second order Ricci tensor can be obtained from

$$\begin{aligned}\delta^{(2)}R_{\mu\nu} = {} & \delta^{(2)}\Gamma^{\alpha}_{\mu\nu,\alpha} - \delta^{(2)}\Gamma^{\alpha}_{\nu\alpha,\mu} + \Gamma^{\alpha}_{\sigma\alpha}\delta^{(2)}\Gamma^{\sigma}_{\mu\nu} + \delta^{(1)}\Gamma^{\alpha}_{\sigma\alpha}\delta^{(1)}\Gamma^{\sigma}_{\mu\nu} + \delta^{(2)}\Gamma^{\alpha}_{\sigma\alpha}\Gamma^{\sigma}_{\mu\nu} \\ & - \Gamma^{\alpha}_{\sigma\nu}\delta^{(2)}\Gamma^{\sigma}_{\mu\alpha} - \delta^{(1)}\Gamma^{\alpha}_{\sigma\nu}\delta^{(1)}\Gamma^{\sigma}_{\mu\alpha} - \delta^{(2)}\Gamma^{\alpha}_{\sigma\nu}\Gamma^{\sigma}_{\mu\alpha}.\end{aligned} \tag{4.5}$$

It can be split into two parts where one part contains only the pure second order terms and another part contains quadratic scalar terms:

$$\delta^{(2)}R_{\mu\nu} = \delta^{(2)}R^{\mathcal{V}}_{\mu\nu} + \delta^{(2)}R^{(S,S)}_{\mu\nu}. \tag{4.6}$$

The various Ricci tensor components are

$$\delta^{(2)}R_{00} = 6\Phi^{(1)}\Phi^{(1)\prime\prime} - 2\partial^m\Phi^{(1)}\partial_m\Phi^{(1)} + 2\Phi^{(1)}\nabla^2\Phi^{(1)}, \tag{4.7}$$

$$\delta^{(2)}R_{0i} = \frac{1}{4}\nabla^2 S_i^{(2)} - \frac{1}{2}\left[\frac{a''}{a} + \mathcal{H}^2\right]S_i^{(2)} + 4\Phi^{(1)}\left[\partial_i\Phi^{(1)\prime} - \mathcal{H}\partial_i\Phi^{(1)}\right] + 2\Phi^{(1)\prime}\partial_i\Phi^{(1)}. \tag{4.8}$$

Note that in the expression of $\delta^{(2)}R_{00}$ there is no pure second order vector modes, but there contains only quadratic scalar terms. As for $\delta^{(2)}R_{ij}$, we can write down the diagonal (di) and non-diagonal (nd) terms separately

$$\begin{aligned}\delta^{(2)^{(di)}}R_{ij} = \Big\{&16\mathcal{H}\Phi^{(1)\prime}\Phi^{(1)} + 2\Phi^{(1)}\Phi^{(1)\prime\prime} + 8\left[\frac{a''}{a} + \mathcal{H}^2\right]\left(\Phi^{(1)}\right)^2 + 2\Phi^{(1)}\nabla^2\Phi^{(1)} \\ &+2\left(\Phi^{(1)\prime}\right)^2 + 2\partial^m\Phi^{(1)}\partial_m\Phi^{(1)}\Big\}\gamma_{ij},\end{aligned} \tag{4.9}$$

$$\delta^{(2)^{(nd)}}R_{ij} = \frac{1}{2}\partial_{(i}S_{j)}^{(2)\prime} + \mathcal{H}\partial_{(i}S_{j)}^{(2)} + 4\Phi^{(1)}\partial_i\partial_j\Phi^{(1)} + 2\partial_i\Phi^{(1)}\partial_j\Phi^{(1)}. \tag{4.10}$$

One thing worth mentioning here is that Eqs. (4.7), (4.8), (4.9) and (4.10) are expressions obtained directly from algebraic calculation from our metric shown Eq. (4.2).

4.1.2 The perturbed energy momentum tensor

As for the EMT, we also only consider the perfect fluid case at each order, i.e. the energy flux $\bar{q}_\mu = 0$, the anisotropic stress $\bar{\pi}_{\mu\nu} = 0$. Similar to linear expansion, the EMT can be expanded up to second order as

$$\bar{T}_{\mu\nu} = T_{\mu\nu} + \delta^{(1)}T_{\mu\nu} + \delta^{(2)}T_{\mu\nu} = (\bar{\rho} + \bar{P})\bar{u}^\mu\bar{u}^\nu + \bar{P}\bar{g}_{\mu\nu}. \tag{4.11}$$

The perturbed four velocity up to second order is

$$\bar{u}^\mu = u^\mu + \delta^{(1)}u^\mu + \delta^{(2)}u^\mu, \tag{4.12}$$

and again it must satisfy the normalisation condition $\bar{u}^\mu\bar{u}^\nu\bar{g}_{\mu\nu} = -1$. Note that the components of background four velocity is given in Eq. (3.10). After adopting the Poisson gauge, at first order the four velocity takes the form

$$\delta^{(1)}u^\mu = \frac{1}{a}\left[-\Phi^{(1)},\ \partial^i v_{(1)}\right],\ \delta^{(1)}u_\mu = a\left[-\Phi^{(1)},\ \partial_i v_{(1)}\right]. \tag{4.13}$$

Again we have only scalar quantities in Eq. (4.13) since it shows the components of four velocity at linear order. Components of second order four velocity can be calculated using the normalisation condition $\bar{u}^\mu \bar{u}^\nu \bar{g}_{\mu\nu} = -1$ and the resulting expressions are shown below:

$$\begin{aligned}\delta^{(2)}u^\mu &= \frac{1}{2a}\left[3\left(\Phi^{(1)}\right)^2 + \partial^m v_{(1)}\partial_m v_{(1)}, v^i_{(2)}\right] \\ \delta^{(2)}u_\mu &= a\left[\frac{1}{2}\left(\Phi^{(1)}\right)^2 - \frac{1}{2}\partial^m v_{(1)}\partial_m v_{(1)}, \frac{1}{2}v_{(2)i} - 2\Phi^{(1)}\partial_i v_{(1)} - \frac{1}{2}S^{(2)}_i\right].\end{aligned} \tag{4.14}$$

Therefore, at second order our resulting EMT components are given as

$$\delta^{(2)}T_{00} = a^2(\rho + P)\partial^m v_{(1)}\partial_m v_{(1)} + 2a^2\Phi^{(1)}\delta^{(1)}\rho, \tag{4.15}$$

$$\begin{aligned}\delta^{(2)}T_{0i} = &-a^2\left(\rho + P\right)\left[\frac{1}{2}v_{(2)i} - \Phi^{(1)}\partial_i v_{(1)}\right] + \frac{a^2}{2}\rho S^{(2)}_i \\ &- a^2\left(\delta^{(1)}\rho + \delta^{(1)}P\right)\partial_i v_{(1)},\end{aligned} \tag{4.16}$$

$$\delta^{(2)}T_{ij} = a^2(\rho + P)\partial_i v_{(1)}\partial_j v_{(1)} - 2a^2\delta^{(1)}P\Phi^{(1)}\gamma_{ij}. \tag{4.17}$$

From the energy momentum tensor, we then can obtain at each order the expressions for $\bar{T} = \bar{T}^\mu_{\ \mu}$, where we have, at zeroth and first order

$$T = 3P - \rho, \text{and } \delta^{(1)}T = -\delta^{(1)}\rho + 3\delta^{(1)}P,$$

respectively. Note that from our way of setting up the EMT, we have $\delta^{(2)}T = 0$ at second order.

The perturbed energy and momentum conservation equations are given by

$$\bar{\nabla}^\mu \bar{T}_{\mu\nu} = 0. \tag{4.18}$$

The time component of the above conservation equations should provide us with an evolution equation for the perturbed energy density. However, since we consider only vector quantities at second order, $\bar{\nabla}^\mu \bar{T}_{\mu 0} = 0$ does not provide us with a correct expression at second order since we do not include any pure second order scalar perturbations. Whereas the momentum conservation equation has the form

$$\left\{v_{(2)i} - S^{(2)}_i\right\}' + \mathcal{H}\left(1 - 3w\right)\left\{v_{(2)i} - S^{(2)}_i\right\} = M_i, \tag{4.19}$$

where the source term M_i is as follows (where we have kept the assumption that w is

constant):

$$
\begin{aligned}
9\mathcal{H}^4\Omega_m^2(\eta)(1+w)M_i = {} & 6\mathcal{H}^3\left[12w+\Omega_m(\eta)(5+3w)\right]\left\{\Phi^{(1)}\partial_i\Phi^{(1)\prime}\right\}^V + 4w\left\{\nabla^2\Phi^{(1)}\nabla^2\partial_i\Phi^{(1)}\right\}^V \\
& - 4\mathcal{H}\left(7-12w+\frac{2}{1+w}\right)\left\{\mathcal{H}\partial_i\Phi^{(1)}\nabla^2\Phi^{(1)}+\partial_i\Phi^{(1)\prime}\nabla^2\Phi^{(1)}\right\}^V \\
& - 24\mathcal{H}w\left\{\Phi^{(1)\prime}\nabla^2\partial_i\Phi^{(1)}\right\}^V - 36\mathcal{H}^2w\left(2+\Omega_m(\eta)\right)\left\{\Phi^{(1)}\nabla^2\partial_i\Phi^{(1)}\right\}^V \\
& + \frac{8w}{1+w}\left\{\mathcal{H}\nabla^2\Phi^{(1)\prime}\partial_i\Phi^{(1)}+\nabla^2\Phi^{(1)\prime}\partial_i\Phi^{(1)\prime}\right\}^V \\
& + 6\mathcal{H}^3\left[12w+2\Omega_m(\eta)(3w-2)\right]\left\{\Phi^{(1)\prime}\partial_i\Phi^{(1)}\right\}^V \\
& + \frac{8\mathcal{H}}{1+w}\left\{\left[\partial^k\Phi^{(1)}\partial_k\partial_i\Phi^{(1)}\right]'\right\}^V .
\end{aligned}
\tag{4.20}
$$

Note that from Eq. (3.14) and the definition $\Omega_\Lambda(\eta) = \frac{a^2\Lambda}{3\mathcal{H}^2(\eta)}$, we can obtain $\kappa^2a^2\rho = 3\mathcal{H}^2(\eta)\Omega_m(\eta)$.

One thing worth noting is that here we use V to denote schematically the vector part of the quadratic source term since on the left hand side of Eq. (4.19) both $v_{(2)i}$ and $S_i^{(2)}$ are vector quantities. This type of representation will be frequently used throughout this thesis.

4.1.3 Einstein field equations at second order

When we perturb the trace reversed EFEs as shown in Eq. (3.64), we then expand it up to second order. At second order, the trace reversed EFEs can be calculated from

$$
\delta^{(2)}R_{\mu\nu} = \kappa^2\left(\delta^{(2)}T_{\mu\nu} - \frac{1}{2}g_{\mu\nu}\delta^{(2)}T - \frac{1}{2}\delta^{(1)}g_{\mu\nu}\delta^{(1)}T - \frac{1}{2}\delta^{(2)}g_{\mu\nu}T\right) + \Lambda\delta^{(2)}g_{\mu\nu}. \tag{4.21}
$$

It can be seen from Eqs. (4.7) and (4.15) that direct algebraic calculation of 00 component of EFEs at second order yields only scalar quantities from our set up. Since we are interested in vector quantities at second order, we shall ignore it and not present it here. However, the $0i$ and the ij components are to be

$$
\begin{aligned}
& \frac{1}{4}\nabla^2S_i^{(2)} - \frac{1}{2}\left[\frac{a''}{a}+\mathcal{H}^2\right]S_i^{(2)} + 4\left[\Phi^{(1)}\partial_i\Phi^{(1)\prime}\right]^V + 2\left[\Phi^{(1)\prime}\partial_i\Phi^{(1)}\right]^V - 4\mathcal{H}\left[\Phi^{(1)}\partial_i\Phi^{(1)}\right]^V \\
& = -\frac{\kappa^2a^2}{2}\left(\rho+P\right)\left[v_{(2)i}-\frac{1}{2}S_i^{(2)}\right] + \left(\frac{\kappa^2a^2P}{2}-\frac{\Lambda a^2}{2}\right)S_i^{(2)} + \kappa^2a^2\left(\rho+P\right)\left[\Phi^{(1)}\partial_iv_{(1)}\right]^V \\
& - \kappa^2a^2\left[\left(\delta^{(1)}\rho+\delta^{(1)}P\right)\partial_iv_{(1)}\right]^V ,
\end{aligned}
\tag{4.22}
$$

and

$$\begin{aligned}\frac{1}{2}\partial_{(i}S^{(2)'}_{j)} + \mathcal{H}\partial_{(i}S^{(2)}_{j)} + 4\left[\Phi^{(1)}\partial_i\partial_j\Phi^{(1)}\right]^V + 2\left[\partial_i\Phi^{(1)}\partial_j\Phi^{(1)}\right]^V \\ = \kappa^2 a^2(\rho + P)\left[\partial_i v_{(1)}\partial_j v_{(1)}\right]^V.\end{aligned} \tag{4.23}$$

Note that in Eq. (4.23), terms multiplied by γ_{ij} are not presented since they are really scalar quantities which we are not interested in. This can be easily verified from the fact that when we apply the projection operator to terms multiplied by γ_{ij}, one will obtain factors such as $k^i\gamma_{ij}e^j(\boldsymbol{k})$ which gives us 0. Also, Eqs. (4.22) and (4.23) corresponds to the components of EFEs for the case we are considering here.

4.1.4 The vector mode evolution and constraint equations

If we substitute Eqs. (3.75) and (3.76) into Eq. (4.22) and rearrange it, we can obtain a constraint equation for vector modes $S_{(2)i}$ from the $0i$ component of the EFEs

$$\begin{aligned}6\mathcal{H}^2\Omega_m(\eta)(1+w)\left[v_{(2)_i} - S_{(2)i}\right] = -\nabla^2 S_{(2)i} + 8\left[\frac{2}{3\mathcal{H}^2\Omega_m(\eta)}\nabla^2\Phi^{(1)}\partial_i\left(\Phi^{(1)'} + \mathcal{H}\Phi^{(1)}\right)\right. \\ \left. + 2\Phi^{(1)'}\partial_i\Phi^{(1)}\right]^V.\end{aligned} \tag{4.24}$$

We can get an evolution equation for $S_{(2)i}$ from the ij component of the EFEs Eq. (4.23). Below is what we arrived at after substituting Eq. (3.76)

$$\partial_{(i}S'_{(2)j)} + 2\mathcal{H}\partial_{(i}S_{(2)j)} = a\partial_{(i}\Gamma_{j)}, \tag{4.25}$$

where the source term is

$$\begin{aligned}a\partial_{(i}\Gamma_{j)} = \frac{8}{3\mathcal{H}^2\Omega_m(\eta)(1+w)}\left\{\partial_i\Phi^{(1)'}\partial_j\Phi^{(1)'} + 2\mathcal{H}\partial_{(i}\Phi^{(1)}\partial_{j)}\Phi^{(1)'}\right\}^V \\ + 4\left[1 + \frac{2}{3\Omega_m(\eta)(1+w)}\right]\left\{\partial_i\Phi^{(1)}\partial_j\Phi^{(1)}\right\}^V,\end{aligned} \tag{4.26}$$

where we have used the fact that $\left\{\Phi^{(1)}\partial_i\partial_j\Phi^{(1)}\right\}^V = -\left\{\partial_i\Phi^{(1)}\partial_j\Phi^{(1)}\right\}^V$. This can be realised from the fact that the vector component of a scalar quantity is zero:

$$\left[\partial_i\partial_j\left(\Phi^{(1)^2}\right)\right]^V = 2\left[\partial_i\Phi^{(1)}\partial_j\Phi^{(1)} + \Phi^{(1)}\partial_i\partial_j\Phi^{(1)}\right]^V = 0. \tag{4.27}$$

4.1.5 The shear and vorticity in perturbative approach

Vector perturbations typically produce vorticity and a transverse shear in the fluid four-velocity Eq. (4.14). In order to compute them, we need to use the covariant definitions

shown in Eqs. (3.138) and (3.140):

$$\bar{\omega}_{\mu\nu} = \delta^{(1)}\omega_{\mu\nu} + \delta^{(2)}\omega_{\mu\nu} = \bar{h}^{\alpha}_{[\mu}\bar{h}^{\beta}_{\nu]}\bar{u}_{\alpha;\beta}, \tag{4.28}$$

$$\bar{\sigma}_{\mu\nu} = \delta^{(1)}\sigma_{\mu\nu} + \delta^{(2)}\sigma_{\mu\nu} = \left\{\bar{h}^{\alpha}_{(\mu}\bar{h}^{\beta}_{\nu)} - \frac{1}{3}\bar{h}_{\mu\nu}\bar{h}^{\alpha\beta}\right\}\bar{u}_{\alpha;\beta}, \tag{4.29}$$

where again $\bar{h}_{\mu\nu} = \bar{g}_{\mu\nu} + \bar{u}_{\mu}\bar{u}_{\nu}$ is the projector into the instantaneous fluid rest space. Note that the components of the projection tensor are shown in Appendix A. Here, $\omega_{\mu\nu}$ and $\sigma_{\mu\nu}$ must satisfy conditions shown in Eqs. (3.139) and (3.141). The vorticity is a purely vector quantity.

At first order, there is only scalar shear:

$$\delta^{(1)}\omega_{ij} = 0, \tag{4.30}$$

$$\delta^{(1)}\sigma_{ij} = a\left(\partial_i\partial_j - \frac{1}{3}\gamma_{ij}\nabla^2\right)v_{(1)}. \tag{4.31}$$

The second order vorticity is given by Eqs. (4.14) and (4.28):

$$\delta^{(2)}\omega_{ij} = \frac{a}{2}\left\{\partial_{[j}v_{(2)i]} - \partial_{[j}S_{(2)i]} + 6\partial_{[i}\Phi^{(1)}\partial_{j]}v_{(1)} + 2\partial_{[i}v'_{(1)}\partial_{j]}v_{(1)}\right\}, \tag{4.32}$$

which is in agreement with the expression in [147]. Using Eqs. (3.75) and (4.24) we can rewrite Eq. (4.32) as

$$\begin{aligned}\delta^{(2)}\omega_{ij} =& \frac{a}{12(1+w)\mathcal{H}^2\Omega_m(\eta)}\left\{\nabla^2\partial_{[i}S_{(2)j]}\right. \\ &\left. -\frac{16}{3(1+w)\mathcal{H}^2\Omega_m(\eta)}\nabla^2\partial_{[i}\Phi^{(1)}\,\partial_{j]}\left(\Phi^{(1)\prime} + \mathcal{H}\Phi^{(1)}\right)\right\}.\end{aligned} \tag{4.33}$$

The vector part of the second order shear $\sigma_{(2)i}$ is defined via

$$\delta^{(2)}\sigma_{ij} = a\partial_{(i}\sigma_{(2)j)},\ \partial_i\sigma^i_{(2)} = 0. \tag{4.34}$$

An expression for the second order vector shear follows from Eq. (4.29) is given as

$$\delta^{(2)}\sigma_{ij} = \frac{a}{2}\partial_{(i}v_{(2)j)} + a\left\{\partial_{(i}v_{(1)}\partial_{j)}\left[\Phi^{(1)} + v'_{(1)}\right]\right\}^{V} = a\partial_{(i}\sigma_{(2)j)}. \tag{4.35}$$

Again using Eqs. (3.75) and (4.24) we can rewrite Eq. (4.35) as the following

$$\begin{aligned} a\partial_{(i}\sigma_{(2)j)} = \frac{a}{2}\partial_{(i}\left\{S_{(2)j)} - \frac{1}{6\mathcal{H}^2\Omega_m(\eta)(1+w)}\nabla^2 S_{(2)j)}\right\} \\ - \frac{2a}{9\mathcal{H}^4\Omega_m^2(\eta)(1+w)^2}\Big\{\mathcal{H}^3\left[2+3(2-\Omega_m(\eta))(1+w)\right]\partial_i\Phi^{(1)}\partial_j\Phi^{(1)} \\ + 2\mathcal{H}(4+3w)\partial_i\Phi^{(1)\prime}\partial_j\Phi^{(1)\prime} + 2\mathcal{H}^2\left[1+3(1+\Omega_m(\eta))(1+w)\right]\left(\partial_i\Phi^{(1)}\partial_j\Phi^{(1)}\right)' \\ - (1+2w)\nabla^2\partial_{(i}\Phi^{(1)}\partial_{j)}(\Phi^{(1)\prime}+\mathcal{H}\Phi^{(1)})\Big\}^V. \end{aligned} \tag{4.36}$$

4.1.6 Extraction of pure vector quantities

From Eq. (B.16) we have defined the Fourier transform of the vector perturbation. We have also introduced the vector projection operator in real space, $\mathcal{V}_l^{ij}(\boldsymbol{x},\boldsymbol{x}')$. Although the expression can be found in Eq. (B.40), we shall present it here again:

$$\mathcal{V}_l^{ij}(\boldsymbol{x},\boldsymbol{x}') = -\frac{2i}{(2\pi)^3}\int d^3k'\ k'^{-2}k'^i\left[e_l(\boldsymbol{k}')e^j(\boldsymbol{k}')+\tilde{e}_l(\boldsymbol{k}')\tilde{e}^j(\boldsymbol{k}')\right]\int d^3x'\ e^{i\boldsymbol{k}'\cdot(\boldsymbol{x}-\boldsymbol{x}')}.$$

What the above projection operator does is extracting pure vector quantity from a two index object that could have a possible mixture of scalar, vector and tensor parts. The equivalent of the operator $\mathcal{V}_l^{ij}(\boldsymbol{x},\boldsymbol{x}')$ in pure index notations instead of integral notation will be present below.

If we have a two index object X_{ij} such that it is of the form

$$X_{ij} = \partial_{(i}S_{j)} + \partial_i\partial_j\Phi, \tag{4.37}$$

then we can obtain an expression for Φ by applying $\partial^i\partial^j$ to both sides of Eq. (4.37) where we have

$$\Phi = \partial^{-4}\partial^i\partial^j X_{ij}. \tag{4.38}$$

If we apply ∂^i only to both sides of Eq. (4.37) and isolate S_j on one side we obtain

$$S_j = 2\partial^{-2}\partial^i X_{ij} - 2\partial_j\Phi. \tag{4.39}$$

Substituting Eq. (4.38) into Eq. (4.39) and collecting terms, we then have

$$S_j = \left\{2\partial^{-2}\partial^i\delta_j^k - 2\partial_j\partial^{-4}\partial^i\partial^k\right\}X_{ik}. \tag{4.40}$$

The projection operator $\mathcal{V}_l^{ij}(\boldsymbol{x},\boldsymbol{x}')$ essentially corresponds to the operation shown in the curly brackets in Eq. (4.40).

4.1.7 Second order vector modes in Fourier space

Now we have looked at the equivalent of $\mathcal{V}_l^{ij}(\boldsymbol{x},\boldsymbol{x}')$ in a pure index notation form, let us turn our attention back to these projection operators presented in Appendix B and use them for our calculation since the integral form suits our need the most when we need to calculate the power spectra later. Note that for the expressions in Fourier space, we drop the order sub- or super-scripts since it should be obvious from the real space for whence they come from.

The vector projection operator in Fourier space, $\hat{\mathcal{V}}(\boldsymbol{k},\boldsymbol{x})$, is presented in Eq. (B.45)). However, we will present it here again in order to make it easier to follow our calculation.

$$\hat{\mathcal{V}}^{ij}(\boldsymbol{k},\boldsymbol{x}) = -\frac{1}{(2\pi)^{3/2}}\frac{2i}{k^2}\int d^3x\ k^i e^j(\boldsymbol{k}) e^{-i\boldsymbol{k}\cdot\boldsymbol{x}}.$$

Applying $\mathcal{V}_l^{ij}(\boldsymbol{x},\boldsymbol{x}')$ to both sides of Eq. (4.25), we then have a representation for extracting pure vector components in real space:

$$\mathcal{V}_l^{ij}(\boldsymbol{x},\boldsymbol{x}')\left[\partial_{(i}S'_{(2)j)} + 2\mathcal{H}\partial_{(i}S_{(2)j)}\right](\boldsymbol{x}',\eta) = \mathcal{V}_l^{ij}(\boldsymbol{x},\boldsymbol{x}')\left[a\partial_{(i}\Gamma_{j)}\right](\boldsymbol{x}',\eta). \tag{4.41}$$

Should we wish to perform the equivalent operation in Fourier space, we then have

$$\hat{\mathcal{V}}^{ij}(\boldsymbol{k},\boldsymbol{x})\left[\partial_{(i}S'_{(2)j)} + 2\mathcal{H}\partial_{(i}S_{(2)j)}\right](\boldsymbol{x},\eta) = \hat{\mathcal{V}}^{ij}(\boldsymbol{k},\boldsymbol{x})\left[a\partial_{(i}\Gamma_{j)}\right](\boldsymbol{x},\eta). \tag{4.42}$$

Let us look at how exactly the operation shown in Eq. (4.42) can be calculated in more detail. For a term on the left hand side of Eq. (4.42), we have

$$\begin{aligned}\hat{\mathcal{V}}^{ij}(\boldsymbol{k},\boldsymbol{x})\left[\partial_{(i}S_{(2)j)}\right](\boldsymbol{x},\eta) &= \frac{2}{k^2(2\pi)^3}\int d^3k' S(\boldsymbol{k}',\eta)\left[e_j(\boldsymbol{k}')k'_i + e_i(\boldsymbol{k}')k'_j\right] \\ &\quad\times\int d^3x\ e^{i(\boldsymbol{k}'-\boldsymbol{k})\cdot\boldsymbol{x}}\ k^i e^j(\boldsymbol{k}) \\ &= \frac{2}{k^2}S(\boldsymbol{k},\eta)\left[e_j(\boldsymbol{k})k_i + e_i(\boldsymbol{k})k_j\right]k^i e^j(\boldsymbol{k}) \\ &= 2S(\boldsymbol{k},\eta).\end{aligned} \tag{4.43}$$

Similar approach for the term $\partial_{(i}S_{(2)j)}$. As for the terms on the right hand side of Eq. (4.42), we have

$$\begin{aligned}\hat{\mathcal{V}}^{ij}(\boldsymbol{k},\boldsymbol{x})\left[\partial_i\Phi^{(1)}\partial_j\Phi^{(1)}\right](\boldsymbol{x},\eta) &= \frac{1}{(2\pi)^3}\frac{2i}{k^2}\frac{1}{(2\pi)^{3/2}}\int d^3k'\Phi(\boldsymbol{k}',\eta)k'_i\int d^3\tilde{k}\Phi(\tilde{\boldsymbol{k}},\eta)\tilde{k}_j \\ &\quad\times\int d^3x\ e^{i[\tilde{\boldsymbol{k}}-(\boldsymbol{k}-\boldsymbol{k}')]}k^i e^j(\boldsymbol{k}) \\ &= \frac{-2i}{k^2}\frac{1}{(2\pi)^{3/2}}\int d^3k'\Phi(\boldsymbol{k}',\eta)\Phi(\boldsymbol{k}-\boldsymbol{k}',\eta)k'_i k'_j k^i e^j(\boldsymbol{k}).\end{aligned} \tag{4.44}$$

Again, the calculation is very similar for the terms $\partial_{(i}\Phi^{(1)}\partial_{j)}\Phi^{(1)'}$ and $\partial_i\Phi^{(1)'}\partial_j\Phi^{(1)'}$. After collecting all the terms, for either polarisation the evolution equation in Fourier space for the vector mode becomes

$$S'\left(\boldsymbol{k},\eta\right)+2\mathcal{H}S\left(\boldsymbol{k},\eta\right)=a\Gamma(\boldsymbol{k},\eta), \tag{4.45}$$

where the source term $a\Gamma(\boldsymbol{k},\eta)$ is an appropriate convolution over the quadratic first order quantities,

$$\begin{aligned} a\Gamma(\boldsymbol{k},\eta)=-\frac{8i}{(2\pi)^{3/2}}\frac{k^i e^j(\boldsymbol{k})}{k^2}\int d^3k'\left(k'_i k'_j\right)\Bigg[\left(1+\frac{2}{3\Omega_m(\eta)(1+w)}\right)\Phi(\boldsymbol{k}',\eta)\Phi(\boldsymbol{k}-\boldsymbol{k}',\eta) \\ +\frac{2}{3(1+w)\Omega_m(\eta)\mathcal{H}^2(\eta)}\Phi'(\boldsymbol{k}-\boldsymbol{k}',\eta)\Big(\Phi'(\boldsymbol{k}',\eta)+2\mathcal{H}\Phi(\boldsymbol{k}',\eta)\Big)\Bigg]. \end{aligned} \tag{4.46}$$

The general solution for $S\left(\boldsymbol{k},\eta\right)$ can be written as

$$S\left(\boldsymbol{k},\eta\right)=\frac{1}{a^2(\eta)}\int_{\eta_0}^{\eta}d\tilde{\eta}\;a^3(\tilde{\eta})\Gamma\left(\boldsymbol{k},\tilde{\eta}\right). \tag{4.47}$$

This can easily be obtained by multiplying a^2 to both sides of Eq. (4.45).

Similar to what we have done here, we can also apply $\mathcal{V}_l^{ij}(\boldsymbol{x},\boldsymbol{x}')$ in Eq. (B.45) to Eq. (4.36) in order to extract the divergenceless vector $\sigma_{(2)i}$ from $\partial_{(i}\sigma_{(2)j)}$. Then $\sigma_{(2)m}(\boldsymbol{x},\eta)=\mathcal{V}_m^{ij}(\boldsymbol{x},\boldsymbol{x}')\partial_{(i}\sigma_{(2)j)}(\boldsymbol{x}',\eta)$, which will be given in more detail later.

4.2 Vector modes in the radiation era

Before we can study the behaviour of the second order vector modes induced from linear scalars, we need to calculate its power spectrum. We shall define the vector mode power spectrum in the same fashion as given in Eq. (3.69)

$$\left\langle S^*\left(\boldsymbol{k}_1,\eta\right)S\left(\boldsymbol{k}_2,\eta\right)\right\rangle=\frac{2\pi^2}{k^3}\delta^3\left(\boldsymbol{k}_1-\boldsymbol{k}_2\right)\mathcal{P}_{\mathcal{V}}(k,\eta). \tag{4.48}$$

Setting $\Omega_m = 1$ and $w = 1/3$ (since we are considering radiation era) in Eq. (4.47) then substituting it into Eq. (4.48), we find

$$\begin{aligned}\langle S^*\left(\boldsymbol{k}_1,\eta\right) S\left(\boldsymbol{k}_2,\eta\right)\rangle &= \frac{1}{a^4(\eta)}\int_{\eta_0}^{\eta} d\tilde{\eta}_2 \int_{\eta_0}^{\eta} d\tilde{\eta}_1\ a^3(\tilde{\eta}_1)a^3(\tilde{\eta}_2)\left\langle \Gamma^*\left(\boldsymbol{k}_1,\tilde{\eta}_1\right)\Gamma\left(\boldsymbol{k}_2,\tilde{\eta}_2\right)\right\rangle \\ &= \frac{16}{(2\pi)^3 a^4(\eta)}\frac{\left[{k_1}^m e^n(\boldsymbol{k}_1)\right]\left[{k_2}^i e^j(\boldsymbol{k}_2)\right]}{k_1^2 k_2^2}\int_{\eta_0}^{\eta} d\tilde{\eta}_2 \int_{\eta_0}^{\eta} d\tilde{\eta}_1\ a^2(\tilde{\eta}_1)a^2(\tilde{\eta}_2) \\ &\times \int d^3k_1' \int d^3k_2'\ \left(k_{1m}' k_{1n}'\right)\left(k_{2i}' k_{2j}'\right)\Xi\left(k_1', |\boldsymbol{k}_1 - \boldsymbol{k}_1'|, \tilde{\eta}_1\right) \\ &\times \Xi\left(k_2', |\boldsymbol{k}_2 - \boldsymbol{k}_2'|, \tilde{\eta}_2\right)\left\langle \hat{E}^*(\boldsymbol{k}_1')\hat{E}^*(\boldsymbol{k}_1 - \boldsymbol{k}_1')\hat{E}(\boldsymbol{k}_2')\hat{E}(\boldsymbol{k}_2 - \boldsymbol{k}_2')\right\rangle,\end{aligned} \tag{4.49}$$

where

$$\Xi\left(\mathcal{K}_1,\mathcal{K}_2,\eta\right) = 3\Phi(\mathcal{K}_1,\eta)\Phi(\mathcal{K}_2,\eta) + \frac{1}{\mathcal{H}^2(\eta)}\Phi'(\mathcal{K}_2,\eta)\Big(\Phi'(\mathcal{K}_1,\eta) + 2\mathcal{H}\Phi(\mathcal{K}_1,\eta)\Big). \tag{4.50}$$

Wick's theorem tells us that

$$\begin{aligned}\left\langle \hat{E}^*(\boldsymbol{k}_1')\hat{E}^*(\boldsymbol{k}_1 - \boldsymbol{k}_1')\hat{E}(\boldsymbol{k}_2')\hat{E}(\boldsymbol{k}_2 - \boldsymbol{k}_2')\right\rangle &= \left\langle \hat{E}^*(\boldsymbol{k}_1')\hat{E}^*(\boldsymbol{k}_1 - \boldsymbol{k}_1')\right\rangle\left\langle \hat{E}(\boldsymbol{k}_2')\hat{E}(\boldsymbol{k}_2 - \boldsymbol{k}_2')\right\rangle \\ &+ \left\langle \hat{E}^*(\boldsymbol{k}_1')\hat{E}(\boldsymbol{k}_2')\right\rangle\left\langle \hat{E}^*(\boldsymbol{k}_1 - \boldsymbol{k}_1')\hat{E}(\boldsymbol{k}_2 - \boldsymbol{k}_2')\right\rangle \\ &+ \left\langle \hat{E}^*(\boldsymbol{k}_1')\hat{E}(\boldsymbol{k}_2 - \boldsymbol{k}_2')\right\rangle\left\langle \hat{E}^*(\boldsymbol{k}_1 - \boldsymbol{k}_1')\hat{E}(\boldsymbol{k}_2')\right\rangle.\end{aligned} \tag{4.51}$$

Note that the Wick's theorem and its proof can be found in [66]. This then implies that we can rewrite Eq. (4.49) as

$$\begin{aligned}\langle S^*\left(\boldsymbol{k}_1,\eta\right) S\left(\boldsymbol{k}_2,\eta\right)\rangle &= \frac{16}{(2\pi)^3 a^4(\eta)}\frac{\left[{k_1}^m e^n(\boldsymbol{k}_1)\right]\left[{k_2}^i e^j(\boldsymbol{k}_2)\right]}{k_1^2 k_2^2}\int_{\eta_0}^{\eta} d\tilde{\eta}_2 \int_{\eta_0}^{\eta} d\tilde{\eta}_1\ a^2(\tilde{\eta}_1)a^2(\tilde{\eta}_2) \\ &\times \int d^3k_1' \int d^3k_2'\ \left(k_{1m}' k_{1n}'\right)\left(k_{2i}' k_{2j}'\right)\Xi\left(k_1', |\boldsymbol{k}_1 - \boldsymbol{k}_1'|, \tilde{\eta}_1\right) \\ &\times \Xi\left(k_2', |\boldsymbol{k}_2 - \boldsymbol{k}_2'|, \tilde{\eta}_2\right)\left[\delta^3\left(\boldsymbol{k}_1' - \boldsymbol{k}_2'\right)\delta^3\left(\boldsymbol{k}_1 - \boldsymbol{k}_1' - \boldsymbol{k}_2 + \boldsymbol{k}_2'\right)\right. \\ &\left.+\delta^3\left(\boldsymbol{k}_1' - \boldsymbol{k}_2 + \boldsymbol{k}_2'\right)\delta^3\left(\boldsymbol{k}_1 - \boldsymbol{k}_1' - \boldsymbol{k}_2'\right)\right].\end{aligned} \tag{4.52}$$

After further simplifying and collecting terms, the power spectrum of the induced vector mode is

$$\begin{aligned}\mathcal{P}_{\mathcal{V}}\left(k,\eta\right) &= \frac{1}{k\pi^5 a^4(\eta)}\int_{\eta_0}^{\eta} d\tilde{\eta}_2 \int_{\eta_0}^{\eta} d\tilde{\eta}_1\ a^2(\tilde{\eta}_1)a^2(\tilde{\eta}_2)\int d^3k'\left(k^a k_a'\right)\left[e^b(\boldsymbol{k})k_b'\right]\left[e^j(\boldsymbol{k})k_j'\right] \\ &\times \Xi\left(k', |\boldsymbol{k} - \boldsymbol{k}'|, \tilde{\eta}_1\right)\left[\left(k^i k_i'\right)\Xi\left(k', |\boldsymbol{k} - \boldsymbol{k}'|, \tilde{\eta}_2\right) + \left(k^i k_i' - k^2\right)\Xi\left(|\boldsymbol{k} - \boldsymbol{k}'|, k', \tilde{\eta}_2\right)\right].\end{aligned} \tag{4.53}$$

Next, we let θ be the angle between the two modes $\boldsymbol{k}$ and $\boldsymbol{k}'$ and rewrite the mode $\boldsymbol{k}'$ with mode $\boldsymbol{k}$ unit basis vectors $e(\boldsymbol{k})$, $\bar{e}(\boldsymbol{k})$ and $\hat{k}$, we then have

$$k^{'a} = \kappa_1 e^a + \kappa_2 \bar{e}^a + \kappa_3 \hat{k}^a, \tag{4.54}$$

and

$$k_i = |\boldsymbol{k}|\hat{k}_i. \tag{4.55}$$

We can rewrite everything in terms of the spherical coordinate and therefore the coefficients in Eq. (4.54) are

$$\kappa_1 = |\boldsymbol{k}'|\sin\theta\cos\phi\ ,\ \kappa_2 = |\boldsymbol{k}'|\sin\theta\sin\phi\ ,\ \kappa_3 = |\boldsymbol{k}'|\cos\theta. \tag{4.56}$$

We can now express terms such as $k^a k'_a$ and $k'_b e^b(\boldsymbol{k})$ in terms of the new bases to be

$$k^a k'_a = |\boldsymbol{k}|\hat{k}^a\left(\kappa_1 e_a + \kappa_2 \bar{e}_a + \kappa_3 \hat{k}_a\right) = |\boldsymbol{k}||\boldsymbol{k}'|\cos\theta = k^i k'_i. \tag{4.57}$$

$$k'_b e^b(\boldsymbol{k}) = e^b(\boldsymbol{k})\left(\kappa_1 e_b + \kappa_2 \bar{e}_b + \kappa_3 \hat{k}_b\right) = |\boldsymbol{k}'|\sin\theta\cos\phi = k'_j e^j(\boldsymbol{k}). \tag{4.58}$$

Therefore, we have

$$\left(k^a k'_a\right)\left(k'_b e^b(\boldsymbol{k})\right)\left(k'_j e^j(\boldsymbol{k})\right) = |\boldsymbol{k}||\boldsymbol{k}'|\cos\theta|\boldsymbol{k}'|^2\sin^2\theta\cos^2\phi, \tag{4.59}$$

and

$$d^3k' = k^{'2}dk'd(\cos\theta)d\phi. \tag{4.60}$$

Changing the notations such that $|\boldsymbol{k}'| = k'$ and $|\boldsymbol{k}| = k$, Eq. (4.53) can be written in terms of the spherical coordinate as

$$\begin{aligned}\mathcal{P}_{\mathcal{V}}(k,\eta) = \frac{1}{k\pi^5 a^4(\eta)}\int_{\eta_0}^{\eta} d\tilde{\eta}_2 \int_{\eta_0}^{\eta} d\tilde{\eta}_1\ a^2(\tilde{\eta}_1)a^2(\tilde{\eta}_2)\int_0^{\infty} dk' k^{'2}\int_{-1}^{1} d(\cos\theta)\\ \times\int_0^{2\pi} d\phi\left[kk^{'3}\cos\theta\sin^2\theta\cos^2\phi\right]\Xi\left(k',|\boldsymbol{k}-\boldsymbol{k}'|,\tilde{\eta}_1\right)\\ \times\left\{\left(kk'\cos\theta\right)\Xi\left(k',|\boldsymbol{k}-\boldsymbol{k}'|,\tilde{\eta}_2\right)+\left(kk'\cos\theta-k^2\right)\Xi\left(|\boldsymbol{k}-\boldsymbol{k}'|,k',\tilde{\eta}_2\right)\right\}.\end{aligned} \tag{4.61}$$

Note that here we have used $\int_0^{2\pi} d\phi\ \cos^2\phi = \pi$.

In order to compute the integrals over Fourier space, we first introduce the dimensionless variables u and v, where

$$v = \frac{k'}{k} \text{ and } u = \sqrt{1+v^2-2v\cos\theta}. \tag{4.62}$$

From here we can also derive the expressions that

$$d(\cos\theta) = -\frac{u}{v}du, \text{ and } \cos\theta = -\frac{1}{2}\left(\frac{1}{v}\right)\left[u^2 - 1 - v^2\right]. \tag{4.63}$$

We can also easily work out, from the expression for $\cos\theta$ that

$$\begin{aligned}\cos\theta\sin^2\theta &= -\frac{1}{2}\left(\frac{k}{k'}\right)\left[u^2 - 1 - \left(\frac{k'}{k}\right)^2\right] + \frac{1}{8}\left(\frac{k}{k'}\right)^3\left[u^2 - 1 - \left(\frac{k'}{k}\right)^2\right]^3 \\ &= \frac{1}{8}\frac{1}{v^3}\left[u^2 - 1 - v^2\right]\left[\left(u^2 - 1 - v^2\right)^2 - 4v^2\right],\end{aligned} \tag{4.64}$$

and

$$kk'\cos\theta = -\frac{1}{2}k^2\left[u^2 - 1 - v^2\right],\ kk'\cos\theta - k^2 = -\frac{1}{2}k^2\left[u^2 + 1 - v^2\right]. \tag{4.65}$$

Collecting terms and simplifying the expressions, the power spectrum then becomes

$$\begin{aligned}\mathcal{P}_{\mathcal{V}}(k,\eta) = \frac{k^8}{16\pi^4 a^4(\eta)}\int_{\eta_0}^{\eta} d\tilde{\eta}_2 \int_{\eta_0}^{\eta} d\tilde{\eta}_1\ a^2(\tilde{\eta}_1)a^2(\tilde{\eta}_2)\int_0^{\infty} dv\ \int_{|v-1|}^{v+1} du\ (uv) \\ \times \left(v^2 + 1 - u^2\right)\left[(u^2 - 1 - v^2)^2 - 4v^2\right]\Xi\left(kv, ku, \tilde{\eta}_1\right) \\ \times \left\{(u^2 - 1 - v^2)\Xi\left(kv, ku, \tilde{\eta}_2\right) + (u^2 + 1 - v^2)\Xi\left(ku, kv, \tilde{\eta}_2\right)\right\}.\end{aligned} \tag{4.66}$$

The power spectrum can now be calculated once the power spectra (initial conditions) for the scalar modes are chosen.

4.2.1 Vector mode power spectra

We shall now investigate the power spectrum of the induced vector modes during the radiation era. After substituting for the first order solution for Φ for the radiation era from Eq. (3.82) (but ignoring the decaying mode) and Eq. (3.90), the power spectrum then becomes

$$\mathcal{P}_{\mathcal{V}}(k,\eta) = \left(\frac{243}{2(k\eta)^2}\right)^2 \int_0^{\infty} dv \int_{|v-1|}^{v+1} du\ \mathcal{P}_{\Phi}(ku)\mathcal{P}_{\Phi}(kv)\mathcal{F}(u,v,x), \tag{4.67}$$

where

$$\begin{aligned}\mathcal{F}(u,v,x) = \frac{1}{(uv)^8}\left(v^2 + 1 - u^2\right)\left[(u^2 - 1 - v^2)^2 - 4v^2\right] \\ \times \int_{x_0}^{x} d\tilde{x}_1\ \mathcal{I}_1(\tilde{x}_1)\left[(u^2 - 1 - v^2)\int_{x_0}^{x} d\tilde{x}_2\ \mathcal{I}_1(\tilde{x}_2) + (u^2 + 1 - v^2)\int_{x_0}^{x} d\tilde{x}_2\ \mathcal{I}_2(\tilde{x}_2)\right],\end{aligned} \tag{4.68}$$

and x is another dimensionless variable defined as $x = k\eta$, and $x_0 = k\eta_0$. We have defined the functions

$$\mathcal{I}_j(x) = \sum_{m=1}^{5}\sum_{n=1}^{4} \sin\left(\alpha_n x + \phi_n\right) \frac{M^j_{nm}}{x^{m-1}}, \tag{4.69}$$

with the coefficients α_n, ϕ_n and M^j_{nm} defined as

$$\phi_n = \frac{\pi}{2}\begin{pmatrix} \mathbf{1} \\ \mathbf{0} \end{pmatrix} \text{ and } \alpha_n = \frac{1}{\sqrt{3}}\begin{pmatrix} -u\mathbf{1} + \upsilon\boldsymbol{b} \\ u\mathbf{1} + \upsilon\boldsymbol{a} \end{pmatrix}, \tag{4.70}$$

$$M^1_{nm} = \begin{pmatrix} \frac{u^2\upsilon^2}{18}\boldsymbol{b} & \mathbf{0} & (\frac{1}{6}u^2 + \frac{1}{2}\upsilon^2)\boldsymbol{a} + u\upsilon\mathbf{1} & \mathbf{0} & 3\boldsymbol{b} \\ \mathbf{0} & \frac{u^2\upsilon}{6\sqrt{3}}\mathbf{1} + \frac{u\upsilon^2}{2\sqrt{3}}\boldsymbol{a} & \mathbf{0} & -\sqrt{3}\upsilon\mathbf{1} + \sqrt{3}u\boldsymbol{b} & \mathbf{0} \end{pmatrix}, \tag{4.71}$$

$$M^2_{nm} = \begin{pmatrix} \frac{u^2\upsilon^2}{18}\boldsymbol{b} & \mathbf{0} & (\frac{1}{2}u^2 + \frac{1}{6}\upsilon^2)\boldsymbol{a} + u\upsilon\mathbf{1} & \mathbf{0} & 3\boldsymbol{b} \\ \mathbf{0} & \frac{u^2\upsilon}{2\sqrt{3}}\mathbf{1} + \frac{u\upsilon^2}{6\sqrt{3}}\boldsymbol{a} & \mathbf{0} & -\sqrt{3}\upsilon\mathbf{1} + \sqrt{3}u\boldsymbol{b} & \mathbf{0} \end{pmatrix}. \tag{4.72}$$

Here we have defined the matricies $\mathbf{1}$, $\mathbf{0}$, $\boldsymbol{a}$ and $\boldsymbol{b}$ as

$$\mathbf{1} = \begin{pmatrix} 1 \\ 1 \end{pmatrix},\ \mathbf{0} = \begin{pmatrix} 0 \\ 0 \end{pmatrix},\ \boldsymbol{a} = \begin{pmatrix} 1 \\ -1 \end{pmatrix},\ \boldsymbol{b} = \begin{pmatrix} -1 \\ 1 \end{pmatrix}. \tag{4.73}$$

As we have four integrals to carry out it is useful to calculate them analytically where possible. This is not particularly simple, however it is possible to do so for the x integrals in Eq. (4.68) by analytically expanding the integrals over the functions $\mathcal{I}_j$ by parts up to Si and Ci functions (the sin and cos integral functions) to get

$$\begin{aligned}\int_{x_0}^{x} d\tilde{x}\ \mathcal{I}_j(\tilde{x}) = \sum_{m=1}^{5}\sum_{n=1}^{4} M^j_{nm}\Bigg\{&\left[\sum_{k=1}^{m-3}\frac{(m-k-3)!}{(m-2)!}{\alpha_n}^k \sin\left(\alpha_n\tilde{x} + \phi_n + \frac{k+2}{2}\pi\right)\tilde{x}^{(2+k-m)}\right]_{x_0}^{x} \\ &-\frac{{\alpha_n}^{(m-2)}}{(m-2)!}\left[\mathrm{Si}\left(\alpha_n\tilde{x}\right)\cos\left(\phi_n + \frac{m}{2}\pi\right) + \mathrm{Ci}\left(\alpha_n\tilde{x}\right)\sin\left(\phi_n + \frac{m}{2}\pi\right)\right]_{x_0}^{x}\Bigg\}.\end{aligned} \tag{4.74}$$

For the radiation era we assume that all modes are well outside the horizon when the interaction begins and therefore can set $x_0 = 0$.

Case I: Interaction of scalar modes

Before calculating the power spectrum for the case of power law scalar modes, it is useful and important to investigate how the vector modes are generated from individual scalar modes. Previously, it has been shown that a single scalar mode with an isotropic distribution of wavevectors, i.e. at a single comoving scale (a single wavelength) but with all possible angles, will induce second order gravitational waves [7]. This is not the case with vector modes: *scalar modes of differing wavelengths need to interact to generate vector modes.*

To investigate the generation of vector modes from scalars in more details, we choose then a scalar power spectrum of the form of two delta functions:

$$\mathcal{P}_\Phi(k) = \frac{4}{9}\mathcal{A}^2\Delta^2_{\mathcal{R}}(k_{CMB})\left\{\delta[\ln(k_1/k)] + \delta[\ln(k_2/k)]\right\}, \tag{4.75}$$

where $\mathcal{A}$ is the mean amplitude of each wavenumber, k_i, relative to the observed amplitude of the primordial power spectrum, $\Delta^2_{\mathcal{R}}(k_{CMB})$, at wavenumber $k_{CMB} \gg k_i$. We assume for simplicity that they both have the same amplitude. Substituting the input scalar power spectrum of the form (4.75) into (4.67) and carrying out the u and v integrals, we then find that the vector power spectra becomes, in terms of $v_i = k_i/k$,

$$\mathcal{P}_\mathcal{V}(k,\eta) = 26244\mathcal{A}^4\Delta^4_{\mathcal{R}}\frac{k_1k_2}{x^4k^2}\left[\mathcal{F}(v_1,v_2,x) + \mathcal{F}(v_2,v_1,x)\right] \tag{4.76}$$

provided $v_1 + 1 > v_2 > |v_1 - 1|$, and is zero otherwise. Therefore modes are induced for all wavenumbers k such that $k_1 + k_2 > k > |k_1 - k_2|$, and are scattered into angles such that $u_1 = v_2$, and $u_2 = v_1$ (a further requirement from carrying out the integration). In the case where only one input mode is present, for example $v_2 = v_1$, this inequality becomes $k_1 > k/2$ while we also have $v_1 = u_1$, as in [7]. From Eq. (4.68) with $u = v$, however, we see that $\mathcal{F}$ vanishes in this case. Therefore, we can see that vector modes cannot be induced by a single scalar degree of freedom. The physical reason for this is because vector modes are associated with rotational degrees of freedom. A consequence of $k_1 = k_2$ is that $\theta_1 = \pm\theta_2$, i.e., the input modes only have momentum along the same axis in Fourier space. Consequently, there is no angular momentum generated, and hence no vectors.

Provided that $k_1 \neq k_2$, we can have vectors induced over the appropriate range of wavelengths. Closely separated scalar modes will produce a much broader spectrum of vector modes while modes of vastly differing wavelengths will produce a very narrow range of vectors, with wavenumbers close to the largest input wavenumber. Note that as the generated wavenumbers are restricted from above and below, we can't expect any noise on large scales, as is the case for gravitational waves. This is also evidenced by the fact that one input mode can't produce any vectors – there would be nothing to set the long wavelength cutoff in that case. Having discussed the properties of Eq. (4.76) analytically, we next shall look at the numerical output for the case of $v_2 = 1$ with various v_1 values.

In Fig. 4.1 we show the induced vector modes as a function of x with $v_2 = 1$, i.e. the evolution of modes of wavenumber $k = k_2$. By setting $v_2 = 1$ we require that $0 < v_1 < 2$ and we will look at $v_1 = 1.5,\ 10^{-1}, 10^{-3}, 10^{-5}$ to be specific.

While the generated mode is outside the Hubble radius, there is power law growth with $\mathcal{P}_\mathcal{V} \sim \eta^2$ (since we are looking at fixed k values). When the scalar mode k_2 enters the Hubble radius, the principle generation of vector modes stops shortly thereafter, and the induced modes start to decay as η^{-4}. This continues until the longer wavelength mode enters the Hubble radius at $k_1\eta = 1 \Rightarrow x \sim 1/v_1$. This then generates a further burst of

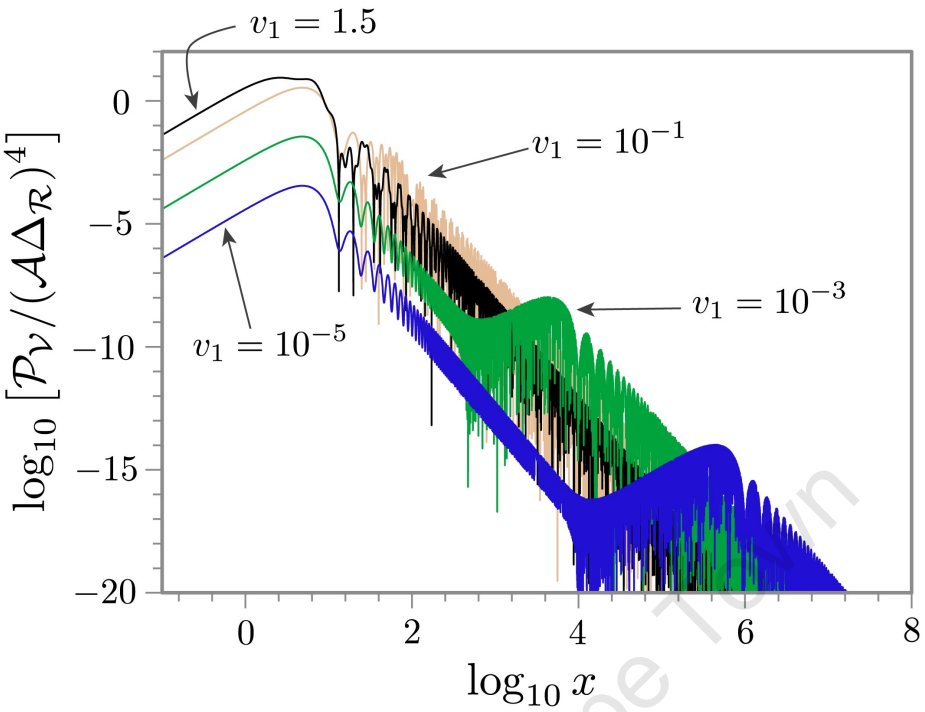

Figure 4.1: The power spectrum of vector modes induced by two interacting scalar modes. Although maximum power is generated in the scenario $k_1/k_2 \sim 1$ shortly after the Hubble radius is crossed, at late times scalar interactions with vastly differing wavelengths produce more power once the long wavelength mode enters the Hubble radius.

vector modes, which we can see by progressively more pronounced knees, as $v_1 \to 0$, in the curves at late times. For the case when $v_1 = 1.5$, on the other hand, we see some confusion as the modes enter the horizon more-or-less together, before decaying as normal.

Thus we see that vector modes are most efficiently generated when at least one of the scalar modes is entering its Hubble radius while another scalar mode exists to help seed the vector mode. We have also explained why we have knees at later times in the evolution of the generated vector modes, since two interacting scalars enter the Hubble radius at different times. The power generated into vectors as each mode enters depends on the relative ratio k_1/k_2. Scalar modes of similar wavelength generate more overall power, because they are entering the Hubble radius at the same time. However, modes that are widely separated in wavenumber don't generate as much overall power but produce more pronounced knees instead.

Case II: Power law scalar modes

With the discussion provided in the preceding case, we have gained some insights into the generation mechanism of vector modes from scalars. Let us now investigate the power spectrum of vector modes from power-law scalar modes. To do this, we assume that the

input power spectrum is:

$$\mathcal{P}_\Phi(k) = \frac{4}{9}\Delta^2_{\mathcal{R}} \left(\frac{k}{k_{CMB}}\right)^{n_s-1}, \tag{4.77}$$

where the index n_s tells us the tilt of the spectrum relative to scale invariance, $n_s = 1$, and $k_{CMB} = 0.002\text{Mpc}^{-1}$ is a pivot scale for the power spectrum [117]. The induced vector modes are then given by

$$\mathcal{P}_\mathcal{V}(k,\eta) = \frac{729\Delta^4_{\mathcal{R}}}{(k\eta)^4}\left(\frac{k}{k_{CMB}}\right)^{2(n_s-1)} \mathcal{F}_{n_s}(x), \tag{4.78}$$

where $\mathcal{F}_{n_s}(x)$ is defined as

$$\mathcal{F}_{n_s}(x) = \int_0^\infty dv \int_{|v-1|}^{v+1} du\ (uv)^{n_s-1}\mathcal{F}(u,v,x). \tag{4.79}$$

We integrate this numerically, and show the results in Fig. 4.2 for the case $n_s = 1$.

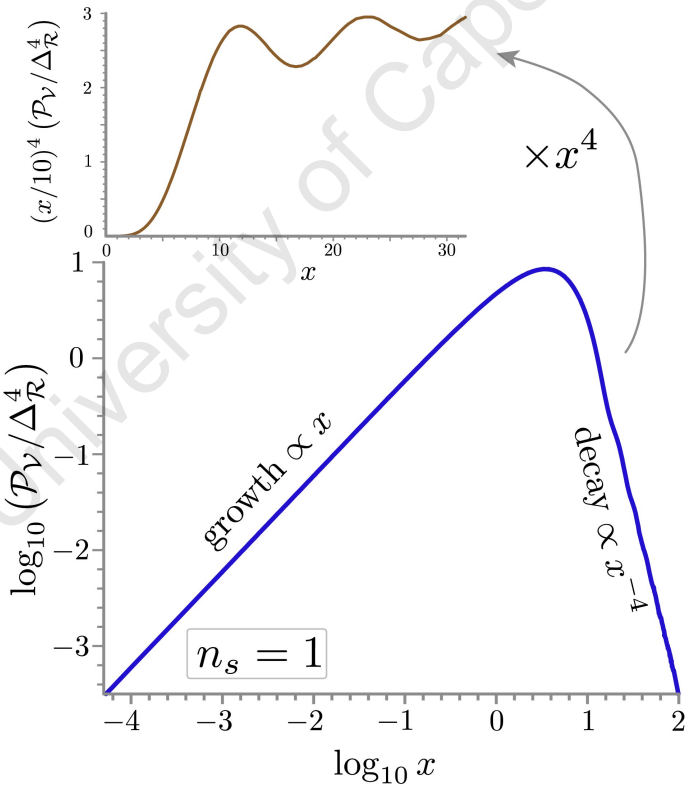

Figure 4.2: The power spectrum of vector modes induced by scale invariant scalar modes. Scalar modes outside the Hubble radius interact to give power law growth until the modes enter the Hubble radius. Thereafter the modes decay as normal vectors, with some gentle oscillatory features.

In Fig. 4.2 we can see that the tilt of the scalar power spectrum tends to affect the amplitude of second-order modes on large scales at the level of a few percent [7, 155]. Viewing x as time for constant k, we see that the modes grow as η, peak when inside the Hubble radius and decay as η^{-4}. While the modes are decaying there are faint oscillations as shown in the top panel of the Figure. Fig. 4.2 can also be interpreted as the power spectrum at fixed time, it grows as k when outside the Hubble radius, it peaks at a scale smaller than the Hubble radius (i.e. it peaks at a larger wavenumber k) and decays as k^{-4}.

It is worth mentioning that we have taken the upper limit of the k' integral to be infinity. In reality there is a cutoff from the end of inflation, at $\eta = \eta_*$, corresponding to modes which are inside the Hubble radius at that time, $k_* = 1/\eta_*$, so giving a finite upper limit to the v-integral, $v_* = k_*/k$ (although this is on very small scales in reality). This causes a break from linear scaling in x in the power spectrum for $x \lesssim 1/v_*$, and we may analytically find the leading behaviour of Eq. (4.67) is $\mathcal{P}_\mathcal{V} \sim \frac{32}{15} v_* x^2$. Why is this the case?

In the interacting delta function case we saw that modes are efficiently produced – and grow like x^2 – when both modes are outside the Hubble radius; once one is inside and the other outside there is effectively no generation of vectors. In power-law case, however, the modes which are generating vectors are those outside the Hubble radius, providing an effective cutoff to the v-integral of $v \sim 1/x$, so giving us growth $\propto x$ when $v_* \gg 1/x$. When we have the cutoff v_* on the other hand, for early times when $\eta < 1/k_*$, all relevant modes are outside the Hubble radius, and interact coherently giving us growth $\propto \eta^2$. For $\eta > 1/k_*$, modes which have entered the Hubble radius no longer contribute to the generation of modes outside the Hubble radius giving weaker growth $\propto x$. Of course, we are not in a position here to analyse times before inflation ends, but this helps us understand why we have the x scaling behaviour we do.

4.3 Vector modes in the dust era

In this section, we investigate the spectrum of vector modes today which is generated at second order by density perturbations. We have shown in subsection 4.1.5 the expressions we recovered independently via the perturbative approach. In this section we use a covariant and fully nonlinear approach, which is more direct and transparent than a perturbative approach in order to clarify and extend previous results, and explain carefully why no vorticity is generated in the fluid at second order in our case. We will also discuss how one can interpret physically the vector part of the shear. After which, we will show that the result we arrived at about vorticity provides us with a simpler way to present the solution to the vector mode evolution Eq. (4.25) (and hence a simpler expression for the vector shear). We will then use these new expressions to study the vector modes and the vector shear in the dust era.

4.3.1 Vorticity and shear in covariant approach

The vorticity tensor of a fluid with four-velocity u^μ defines the vorticity vector as shown in Eq. (3.142). The vorticity vector obeys the propagation equation Eq. (3.159) as introduced in an earlier chapter. In order to evaluate the curl of the acceleration, $\mathrm{curl}\dot{u}^\mu$, in Eq. (3.159), we need the momentum conservation equation Eq. (3.156) and the energy conservation equation Eq. (3.155). In general, Eq. (3.156) shows that the curl of acceleration can introduce source terms for vorticity in Eq. (3.159). In the case of a perfect fluid, we have $q_\mu = 0 = \pi_{\mu\nu}$. Taken this into account, Eq. (3.156) now looks like

$$(\rho + P)\dot{u}_\mu + \mathrm{D}_\mu \mathrm{P} = 0. \tag{4.80}$$

where as Eq. (3.155) now looks like

$$\dot{\rho} = -\Theta(\rho + P). \tag{4.81}$$

We can also use the relation (see e.g. [222])

$$\mathrm{D}_\mu P = c_s^2 \mathrm{D}_\mu \rho, \tag{4.82}$$

where c_s is the adiabatic sound speed. Taking curl of Eq. (4.80) then using the exact identity [222]

$$\mathrm{curl}\,\mathrm{D}_\mu f = -2\dot{f}\omega_\mu\,, \tag{4.83}$$

we then get

$$(\rho + P)\mathrm{curl}\,\dot{u}_\mu = 2\dot{P}\,\omega_\mu + \epsilon_{\mu\nu\gamma}\dot{u}^\nu \mathrm{D}^\gamma(\rho + P). \tag{4.84}$$

Using Eq. (4.80) again, we find that the second term is proportional to $\epsilon_{\mu\nu\gamma}\mathrm{D}^\nu P \mathrm{D}^\gamma \rho$, which vanishes, since $\mathrm{D}_\mu P$ is parallel to $\mathrm{D}_\mu \rho$ for a perfect fluid. Using Eq. (4.81) and collecting results, we arrive at the fully nonlinear vorticity propagation equation for a perfect fluid:

$$h_\mu{}^\nu \dot{\omega}_\nu + \left(\frac{2}{3} - c_s^2\right)\Theta\omega_\mu - \sigma_{\mu\nu}\omega^\nu = 0\,. \tag{4.85}$$

Note that the last term on the left is at least third order since the non-zero vorticity and shear are at least second and first order respectively. This equation shows that there is no source for vorticity, so that vorticity cannot be generated in a perfect fluid, at any perturbative order.

In particular, *there is no generation of vorticity at non-linear order by first order scalar perturbations, in the case of adiabatic perfect fluid,* and thus

$$\delta^{(2)}\omega_{ij} = 0\,. \tag{4.86}$$

If there is primordial vorticity, then it must be introduced as an initial condition. Any primordial vorticity will simply redshift away as the universe expands, according to Eq. (4.85), and will be entirely unaffected by the growth of density perturbations. Effectively, the density perturbations generate metric vector perturbations, and the fluid velocity adjusts so as to maintain zero vorticity. This is similar to what happens with the Harrison mechanism for magnetogenesis, where the vector modes generated at first order by defects cannot induce vorticity in the plasma [98]. For more than one perfect fluid, vorticity non-generation applies separately to each fluid, as long as there is no momentum exchange between the fluids. This is the case for example with CDM and baryons, which interact only gravitationally.

The vector part of the shear may be interpreted as a rotational quantity, even though the vorticity of the fluid is zero. The vector shear is

$$\sigma_{\mu\nu} = \mathrm{D}_{\langle\mu}\sigma_{\nu\rangle} \equiv \left\{ h^{\alpha}_{(\mu}h^{\beta}_{\nu)} - \frac{1}{3}h_{\mu\nu}h^{\alpha\beta} \right\} \mathrm{D}_{\alpha}\sigma_{\beta},\ \mathrm{D}_{\mu}\sigma^{\mu} = 0. \tag{4.87}$$

By boosting from the fluid rest frame to a different frame,

$$\tilde{u}^{\mu} = u^{\mu} + v^{\mu}, \tag{4.88}$$

where v_{μ} is some 'peculiar' velocity with $v_{\mu}u^{\mu} = 0$ and v_{μ} remains constant up to first order, the vorticity and shear become [222]

$$\tilde{\omega}_{\mu} = -\frac{1}{2}\mathrm{curl}v_{\mu},\ \tilde{\sigma}_{\mu} = \sigma_{\mu} + v_{\mu}. \tag{4.89}$$

If we choose the frame by $v_{\mu} = -\sigma_{\mu}$, the vector part of the shear $\tilde{\sigma}_{\mu}$ is zero, but the vorticity $\tilde{\omega}_{\mu}$ no longer vanishes. This shows the essentially rotational nature of the fluid vector shear, even though the vorticity of the fluid is zero. Note that it is not possible to boost away the scalar or tensor part of the shear in this way.

We have now presented our arguments on concluding to the result that there shall be no vorticity generation via covariant approach. Returning to the perturbative analysis, we can now use Eqs. (4.86), (4.25) and (4.33) to determine the vector metric perturbation $S^{i}_{(2)}$, which will be shown in the next two subsections.

4.3.2 More on vector mode equations

Having made the statement that $\delta^{(2)}\omega_{ij} = 0$ in the previous subsection, Eq. (4.33) implies that

$$\nabla^2 S_{(2)i} = \frac{16}{3\mathcal{H}^2\Omega_m(\eta)(1+w)} \left\{ \nabla^2\Phi^{(1)}\partial_i \left(\Phi^{(1)\prime} + \mathcal{H}\Phi^{(1)} \right) \right\}^{V}. \tag{4.90}$$

This directly recovers the solution that can be obtained via a Fourier space projection of the second order ij component of the EFEs Eq. (4.25). Here, however, I shall demonstrate that Eq. (4.90) does indeed satisfy Eq. (4.25) in the real space for any constant equation

of state w since this is not as obvious as it seems. For the purpose of expressing ourselves clearly, we shall present Eq. (4.90) in the simplified form of $\nabla^2 S_{(2)i} = A(\eta)\Big\{\nabla^2\Phi^{(1)}\partial_i F_\Phi\Big\}^V$. It can then be verified that $A'(\eta) = \mathcal{H}(1+3w)A(\eta)$ and $F'_\Phi = -\mathcal{H}(2+3w)F_\Phi + w\nabla^2\Phi^{(1)} + 3/2\mathcal{H}^2\Omega_m(\eta)(1+w)\Phi^{(1)}$.

Applying $\epsilon^{imk}\partial_m\partial^j$ to both sides of Eq. (4.25) we have

$$\epsilon^{imk}\Big[\frac{1}{2}\partial_m\nabla^2 S'_{(2)k} + \mathcal{H}\partial_m\nabla^2 S_{(2)k}\Big] = \frac{a}{2}\epsilon^{imk}\Big[\partial_m\nabla^2\Gamma_k\Big]. \tag{4.91}$$

Note that from the simplified form of Eq. (4.90) we obtain

$$\epsilon^{imk}\partial_m\nabla^2 S_{(2)k} = A(\eta)\epsilon^{imk}\partial_m\nabla^2\Phi^{(1)}\partial_k F_\Phi,$$

and

$$\begin{aligned}\epsilon^{imk}\partial_m\nabla^2 S'_k = {} & A'(\eta)\epsilon^{imk}\partial_m\nabla^2\Phi^{(1)}\partial_k F_\Phi \\ & + A(\eta)\epsilon^{imk}\Big[\partial_m\nabla^2\Phi^{(1)'}\partial_k F_\Phi + \partial_m\nabla^2\Phi^{(1)}\partial_k F'_\Phi\Big],\end{aligned}$$

where we have used the fact that $\epsilon^{imk}\partial_m\partial_k F_\Phi = 0$. Substituting the expressions for $A'(\eta)$ and F'_Φ and collecting the terms together for the left hand side (lhs) of Eq. (4.91), we arrive at

$$\begin{aligned}\text{lhs} \Rightarrow \frac{A(\eta)}{2}\epsilon^{imk}\Bigg[& \frac{3\mathcal{H}^2\Omega_m(\eta)(1+w)}{2}\partial_m\nabla^2\Phi^{(1)}\partial_k\Phi^{(1)} + \mathcal{H}\partial_m\nabla^2\Phi^{(1)}\partial_k F_\Phi \\ & + \partial_m\nabla^2\Phi^{(1)'}\partial_k F_\Phi\Bigg].\end{aligned} \tag{4.92}$$

As for the right hand side (rhs) of Eq. (4.91), it can be shown that it has the terms

$$\begin{aligned}\text{rhs} \Rightarrow \epsilon^{imk}\Bigg\{ & 4\Bigg[1 + \frac{2}{3\Omega_m(\eta)(1+w)}\Bigg]\partial_k\Phi^{(1)}\partial_m\nabla^2\Phi^{(1)} + \frac{8}{3\mathcal{H}^2\Omega_m(\eta)(1+w)}\Big[\partial_k\Phi^{(1)'} \\ & \times\partial_m\nabla^2\Phi^{(1)'} + \mathcal{H}\Big(\partial^j\partial_k\Phi^{(1)}\partial_m\partial_j\Phi^{(1)}\Big)' + \mathcal{H}\Big(\partial_k\Phi^{(1)}\partial_m\nabla^2\Phi^{(1)}\Big)'\Big]\Bigg\},\end{aligned} \tag{4.93}$$

where we have used the fact that a symmetric quantity vanishes if we apply ϵ^{imk} to it. Now even in the form of Eq. (4.92) it is not difficult to see that it is identical to the terms on the right hand side. This can best be viewed if we identify the terms with the same order of $\mathcal{H}$ together.

4.3.3 Vector metric perturbations

Since we have shown that Eq. (4.90) provides us with a solution to Eq. (4.25), we shall use Eq. (4.90) for our analysis from here on since its expression is simpler. Eq. (4.90) gives a

solution in Fourier space

$$S(\boldsymbol{k},\eta) = \frac{16i}{3\Omega_m(\eta)(2\pi)^{3/2}}\frac{e^j(\boldsymbol{k})}{k^2}\int d^3k'\ |\boldsymbol{k}-\boldsymbol{k}'|^2 k'_j \mathcal{B}(\boldsymbol{k}-\boldsymbol{k}',\boldsymbol{k}',\eta), \tag{4.94}$$

where

$$\mathcal{B}(\mathcal{K}_1,\mathcal{K}_2,\eta) = \mathcal{H}^{-2}\Phi(\mathcal{K}_1,\eta)\left[\Phi'(\mathcal{K}_2,\eta)+\mathcal{H}\Phi(\mathcal{K}_2,\eta)\right]. \tag{4.95}$$

Defining the power spectrum as in Eq. (4.48) we find, using Wick's theorem,

$$\begin{aligned}\mathcal{P}_S(k,\eta) = {}& \frac{16}{9k\Omega_m^2(\eta)\pi^5}\int d^3k'|\boldsymbol{k}-\boldsymbol{k}'|^2\left[k'_j e^j(\boldsymbol{k})\right]\left[k'_m e^m(\boldsymbol{k})\right]\mathcal{B}(|\boldsymbol{k}-\boldsymbol{k}'|,k',\eta)\\ &\times\left\{|\boldsymbol{k}-\boldsymbol{k}'|^2\mathcal{B}(|\boldsymbol{k}-\boldsymbol{k}'|,k',\eta)-(k')^2\mathcal{B}(k',|\boldsymbol{k}-\boldsymbol{k}'|,\eta)\right\}.\end{aligned} \tag{4.96}$$

Note however that in this subsection, we use the notation $\mathcal{P}_S$ to represent the vector mode power spectrum in order to have better distinction between the two eras. Eq. (4.96) may be simplified when the first order power spectrum Eq. (3.97) is substituted in to give

$$\mathcal{P}_S(k) = \left(\frac{2\Delta_{\mathcal{R}}}{5g_\infty}\right)^4\left(\frac{3g\left[g'+\mathcal{H}g\right]}{\Omega_m(\eta)\mathcal{H}^2}\right)^2 k^2\,\Pi(u^2), \tag{4.97}$$

where

$$\Pi(\xi) = \int_0^\infty dv\ \int_{|v-1|}^{v+1} du\ \xi\ (uv)^{-2}(u^2-v^2)\left[4v^2-(1+v^2-u^2)^2\right]\left[T(kv)T(ku)\right]^2, \tag{4.98}$$

and as before $v = k'/k$, $u = \sqrt{1+v^2-2v\cos\theta}$ and $\cos\theta = \boldsymbol{k}'\cdot\boldsymbol{k}/(k'k)$. This resulting second order vector power spectrum $\mathcal{P}_S$ using WMAP5 best fit parameters is shown in Fig. 4.3. This may be compared with the power spectrum in Eq. (4.78), which is computed from scalar modes in the radiation era ($w = 1/3$), assuming a power law form for the scalar spectrum. Here we have found $\mathcal{P}_S$ today, and we have calculated $\mathcal{P}_{\Phi_d}$ directly from the first order solutions, using the transfer function to relate back to the primordial perturbations and the growth suppression factor to take account of Λ in the background. Detailed discussions on linear scalar modes, the transfer function and the growth suppression factor used here have been presented in chapter 3.

In Fig. 4.3 we compare the power spectrum of the vectors with that of the Newtonian potential. For comparison we also show the power spectrum of the two gauge-invariant density perturbations introduced in [12]. In the Poisson gauge, they are just $\delta = \frac{\delta^{(1)}\rho}{\rho}$ and $\Delta = \delta - 3\mathcal{H}v^{(1)}$. The amplitude of the vectors decays on small scales, $k > k_{eq} \approx 0.009\,\mathrm{Mpc}^{-1}$ (obtained using Eq. (3.100)), in contrast to the density perturbation, which is growing, but in line with Φ. For WMAP5 data [117]

$$\mathcal{P}_S \approx 6.5\times10^{-5}\mathcal{P}_{\Phi_d} \quad \text{for} \quad k \gtrsim k_{silk} \approx 0.09\,\mathrm{Mpc}^{-1}, \tag{4.99}$$

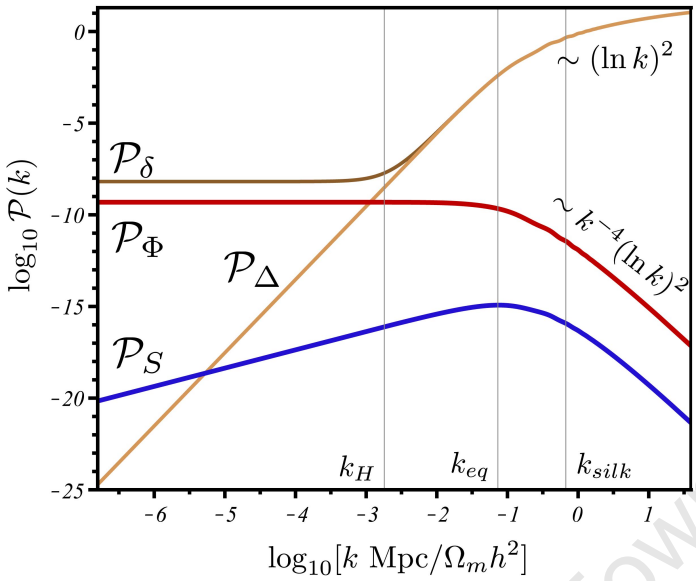

Figure 4.3: The power spectrum today of metric vector modes generated at second order by density perturbations, $\mathcal{P}_S$, together with the power spectra of first-order quantities: the density contrast $\delta = \delta^{(1)}\rho/\rho$ and comoving density perturbation $\Delta = \delta - 3\mathcal{H}v^{(1)}$, and Φ (using best-fit WMAP5 parameters [117]: $\Omega_m h^2 = 0.1326, 100\Omega_b h^2 = 2.273, h = 0.719$). k_H represents the Hubble scale.

so that the amplitude of the metric vector modes is nearly 1% that of the metric scalar modes on small scales. Note that the value for k_{silk} is obtained using expression from Eq. (3.103) For zero baryons we find that

$$\mathcal{P}_S \approx z_{eq}^{-1}(5.49\Omega_m h^2 - 0.13)^{2.33}\mathcal{P}_{\Phi_d} \sim (\ln k)^2/k^4 \text{ for } \mathrm{k} \gtrsim \mathrm{k_{silk}} \approx 0.09\,\mathrm{Mpc}^{-1}, \qquad (4.100)$$

where z_{eq} can be expressed as in Eq. (3.98). On large scales $\mathcal{P}_S$ scales like k, with a peak in the spectrum around the equality scale. This is analogous to the peak in the induced gravitational wave background on similar scales [22]. In Fig. 4.4 we also show that including baryons induces oscillations in the vector power spectrum (bottom panel). They are washed out in comparison to those present in the scalars which inherited this oscillating feature from the transfer function (top panel) mostly, but are still very prominent.

The overall shape of the $S_{(2)i}$ spectrum may be understood from the generation of vectors during the radiation era introduced earlier in this chapter. Vector modes grow outside the Hubble radius as $a^{1/2}$ only through the interaction of scalar modes which are larger than the Hubble radius. Inside the Hubble radius, vector modes decay, slightly less rapidly than a^{-2}, when fluctuations in the radiation fluid no longer support vectors. At the end of the radiation era, vector modes with $k < k_{eq}$ have acquired a tilt because modes are more aggressively produced by scalars which are close to the Hubble radius – very long wavelength modes interact only weakly. After equality, all vector modes grow at the same

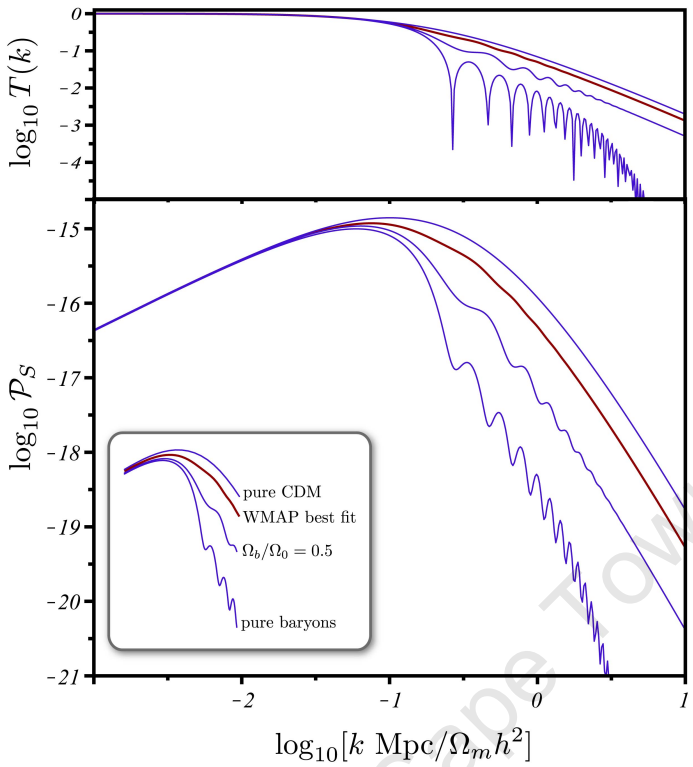

Figure 4.4: The power spectrum today of metric vector modes generated at second order by density perturbations. We show how increasing the baryon fraction decreases the power in the vectors above k_{eq}. The baryon oscillations are washed out to some extent in the vectors as can be seen by comparing $\mathcal{P}_S$ with the first-order transfer function in the top panel.

rate, so that those which entered the Hubble radius before equality are suppressed.

4.3.4 Vector shear

As mentioned earlier, in order to extract the divergenceless vector shear, $\sigma_{(2)i}$, from $\partial_{(i}\sigma_{(2)j)}$, we need to use the operator $\mathcal{V}_m^{ij}(\boldsymbol{x}, \boldsymbol{x}')$ given in Eq. (B.40):

$$\sigma_{(2)m}(\boldsymbol{x}, \eta) = \mathcal{V}_m^{ij}(\boldsymbol{x}, \boldsymbol{x}')\partial_{(i}\sigma_{(2)j)}(\boldsymbol{x}', \eta). \tag{4.101}$$

From Eqs. (4.90), (4.36) and (B.45), we can derive second order vector shear in Fourier space

$$\begin{aligned}\sigma(\boldsymbol{k}, \eta) = \frac{-2ai}{3\Omega_m(\eta)(2\pi)^{3/2}}\frac{e^j(\boldsymbol{k})}{k^2}\int d^3k' k'_j\Big\{ &\left(k^2 - 6(k'_i k^i) - 4|\boldsymbol{k} - \boldsymbol{k}'|^2\right)\mathcal{B}(\boldsymbol{k} - \boldsymbol{k}', \boldsymbol{k}', \eta) \\ &+ \frac{2}{3\Omega_m(\eta)}\left(k^2 - 2k'_i k^i\right)\left[\mathcal{C}(\boldsymbol{k}', \boldsymbol{k} - \boldsymbol{k}', \eta) + \left(1 - \frac{3\Omega_m(\eta)}{2}\right)\mathcal{B}(\boldsymbol{k}', \boldsymbol{k} - \boldsymbol{k}', \eta)\right]\Big\},\end{aligned} \tag{4.102}$$

where the expression for $\mathcal{B}(\mathcal{K}_1, \mathcal{K}_2, \eta)$ can be found in Eq. (4.95) and

$$\mathcal{C}(\mathcal{K}_1, \mathcal{K}_2, \eta) = \frac{1}{\mathcal{H}^3}\Phi'(\mathcal{K}_1, \eta)\left[\Phi'(\mathcal{K}_2, \eta) + \mathcal{H}\Phi(\mathcal{K}_2, \eta)\right]. \tag{4.103}$$

The power spectrum is defined as in Eq. (4.48). By Eq. (4.102) and Wick's theorem, we obtain

$$\begin{aligned}\mathcal{P}_{\sigma_V}(k,\eta) = \left(\frac{\Delta_{\mathcal{R}}}{g_\infty}\right)^4 \left[\frac{3ka(g'+\mathcal{H}g)}{50\Omega_m(\eta)\mathcal{H}^2}\right]^2 \Big\{ &- 2g^2\Pi(2+u^2+3v^2) - \frac{8}{3\mathcal{H}\Omega_m(\eta)}g \\ &\times \left[g' + \left(1 - \frac{3\Omega_m(\eta)}{2}\right)\mathcal{H}g\right]\Pi(1+2v^2) + \frac{8}{9\mathcal{H}^2\Omega_m^2(\eta)} \\ &\times \left[g' + \left(1 - \frac{3\Omega_m(\eta)}{2}\right)\mathcal{H}g\right]^2 \Pi(u^2 - v^2)\Big\},\end{aligned} \tag{4.104}$$

where g is given by Eq. (3.87) and $\Pi(\xi)$ by Eq. (4.98). The resulting power spectrum has a similar shape to $\mathcal{P}_S$, since $\sigma_{(2)i} = S_{(2)i}/2 +$small corrections as can be seen from Eq. (4.36). See Fig. 4.5 for the resulting vector shear power spectrum, $\mathcal{P}_{\sigma_V}$.

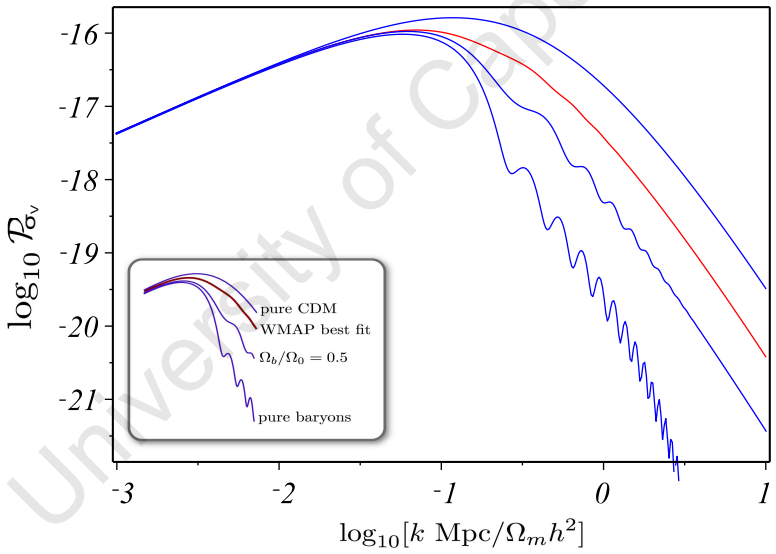

Figure 4.5: The power spectrum today of second order vector shear generated by density perturbations. We show as in the vector mode case how increasing the baryon fraction decreases the power in the vector shear above k_{eq}. The resulting power spectrum has a similar shape to $\mathcal{P}_S$.

It is also useful to compare the first order scalar and second order vector contributions to the shear energy density. We define the dimensionless shear density

$$\Omega_\sigma = \frac{a^2}{6\mathcal{H}^2}\sigma_{\mu\nu}\sigma^{\mu\nu}. \tag{4.105}$$

The scalar and vector contributions to shear are given by $\sigma = v_{(1)}$ [from Eq. (4.31)] and

$\sigma_{(2)i}$ [from Eq. (4.36)] respectively. They define scalar power $\mathcal{P}_{\sigma_S}$ and vector power $\mathcal{P}_{\sigma_V}$, which then define the spatial averages of Ω_{σ_S} and Ω_{σ_V} via

$$\frac{d\langle\Omega_{\sigma_S}\rangle}{d\ln k} = \frac{a^2k^4}{6\mathcal{H}^2}\,\mathcal{P}_{\sigma_S}, \tag{4.106}$$

and

$$\frac{d\langle\Omega_{\sigma_V}\rangle}{d\ln k} = \frac{a^2k^2}{12\mathcal{H}^2}\,\mathcal{P}_{\sigma_V}, \tag{4.107}$$

respectively. Note that there are in reality two polarisations implicit in $\mathcal{P}_{\sigma_V}$ shown in Eq. (4.107), however in an unpolarized background the two contributions are equal.

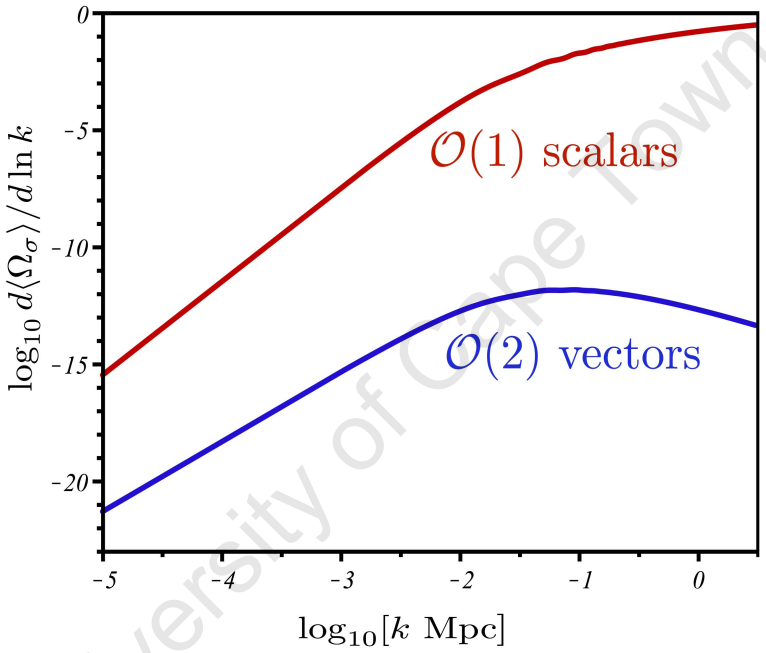

Figure 4.6: The energy densities of the first order scalar and second order vector shear per logarithmic k interval. Figure plotted using WMAP5 best fit parameters.

The quantities in Eqs. (4.106) and (4.107) are shown in Fig. 4.6. As $k \to 0$, $d\langle\Omega_{\sigma_V}\rangle/d\ln k \sim k^3$ and $d\langle\Omega_{\sigma_S}\rangle/d\ln k \sim k^4$. This shows that the second order vector shear is much smaller than the linear scalar shear – except on very large scales (for very small k values). However, this feature in the Poisson gauge will not lead to any growing physical effect, since both quantities are decaying on large scales. In Fig. 4.7 we present a figure with only the scalar shear energy density plotted, however with different baryon fraction. We include a case where there is only CDM as its matter content, a case with WMAP5 best fit parameter, a case with only baryon as its matter content and a case where CDM and baryon are equally proportioned. Similar to what we have seen before for the transfer function cases, more rapid oscillation appears in the curves with higher percentage of baryon fraction. In accompanying to the scalar case, we also present the vector shear energy density with different

baryon fraction in Fig. 4.8. Again, for the vector curves the oscillatory feature is less pronounced when compared with the scalar ones.

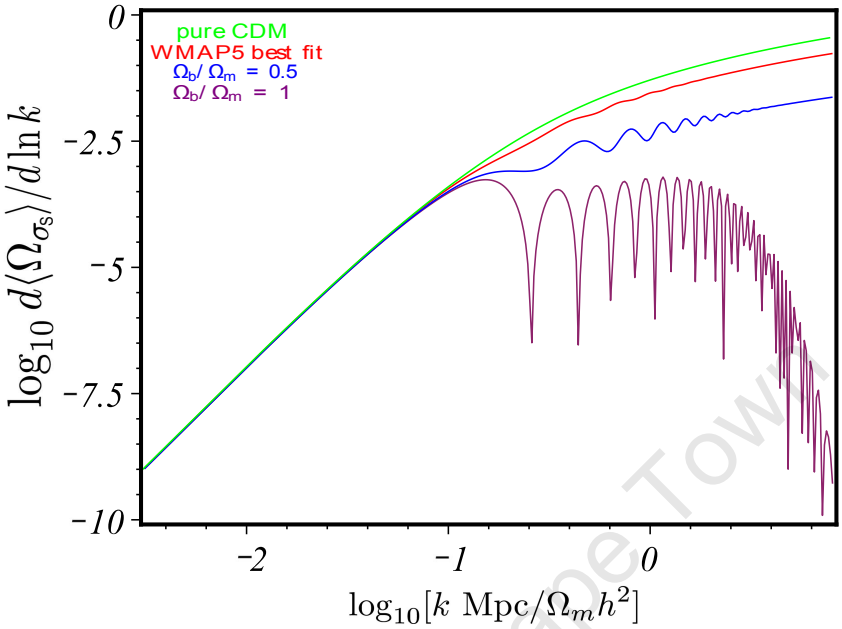

Figure 4.7: The energy densities of the first order scalar shear per logarithmic k interval. We plotted the cases: pure CDM, WMAP5 best fit parameter, pure baryon and $\Omega_b/\Omega_m = 1/2$.

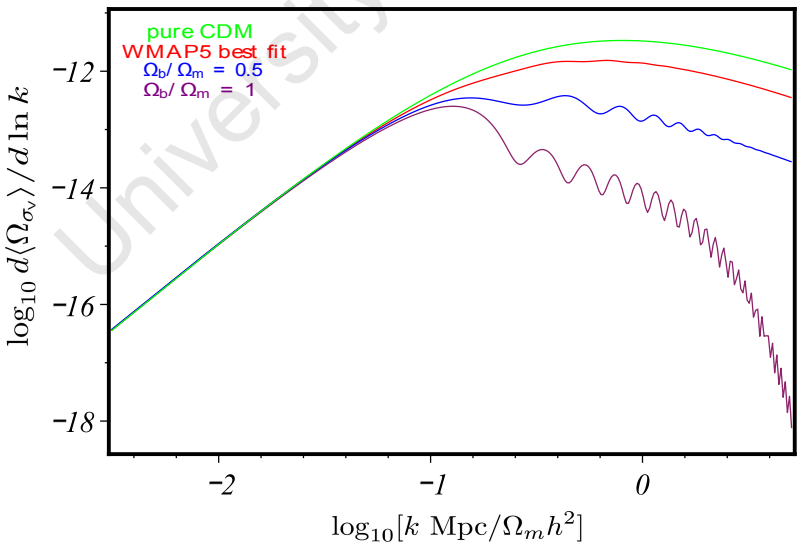

Figure 4.8: The energy densities of the second order vector shear per logarithmic k interval. We plotted the cases: pure CDM, WMAP5 best fit parameter, pure baryon and $\Omega_b/\Omega_m = 1/2$. When compared with the scalar shear energy density, the oscillation is washed out.

One can also obtain $\langle\Omega_{\sigma_S}\rangle$ and $\langle\Omega_{\sigma_V}\rangle$ up to a given scale k from the energy densities

shown in Eqs. (4.106) and (4.107):

$$\langle \Omega_{\sigma_S} \rangle(k) = \frac{a^2}{6\mathcal{H}^2} \int_0^k d\ln k' k'^4 \mathcal{P}_{\sigma_S}(k'), \tag{4.108}$$

$$\langle \Omega_{\sigma_V} \rangle(k) = \frac{a^2}{12\mathcal{H}^2} \int_0^k d\ln k' k'^2 \mathcal{P}_{\sigma_V}(k'). \tag{4.109}$$

Again, there are two polarizations implicit in $\mathcal{P}_{\sigma_V}$. The ratio between the two scalar functions, $\frac{d\langle\Omega_{\sigma_S}\rangle}{d\ln k}$ and $\langle \Omega_{\sigma_S} \rangle(k)$, and the two vector functions, $\frac{d\langle\Omega_{\sigma_V}\rangle}{d\ln k}$ and $\langle \Omega_{\sigma_V} \rangle(k)$ per logarithmic bin are plotted in Fig. 4.9. Note however that we use $\frac{d\ln\langle\Omega_{\sigma}\rangle}{d\ln k}$ to denote the ratio function. From Fig. 4.9 we can see that on large scales the ratio function for both the scalars and the vectors remain constant. However, the ratio beginning to decrease as we approach the equality scale k_{eq}. Again, we can observe the baryon oscillations being washed out to some extent in the vectors as this can be seen in Fig. 4.9 when the scalar ratio curve is showing some oscillatory feature whereas it is barely visible in the vector ratio curve. As a point of interest, in Figs. 4.10 and 4.11 we present the ratio function between the energy density per logarithmic bin and the energy density up to a given scale k for both the linear scalars and second order vector cases with different baryon fractions. As expected, the curves with most baryon fraction have a sharper drop off and a more visible oscillation.

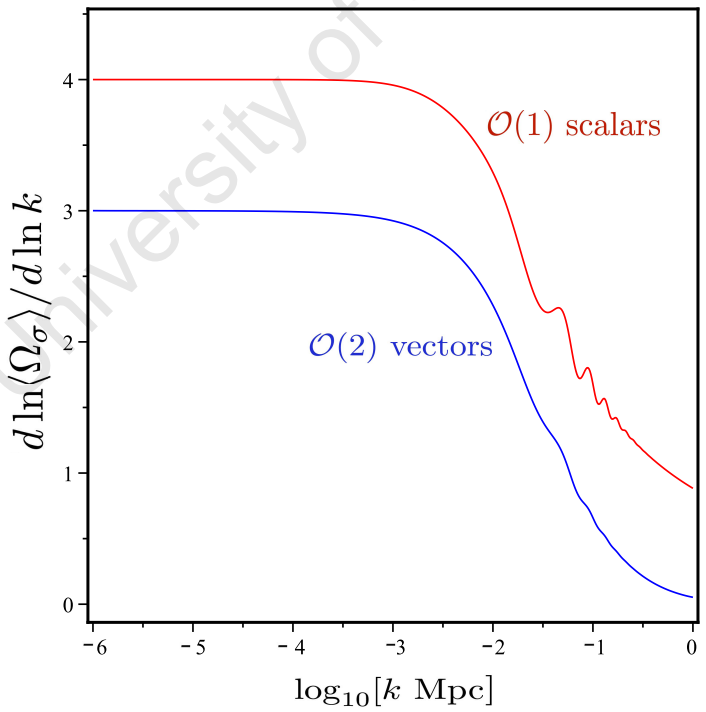

Figure 4.9: The ratio between the energy density per logarithmic bin and the energy density up to a given scale k. Figure plotted using WMAP5 best fit parameters.

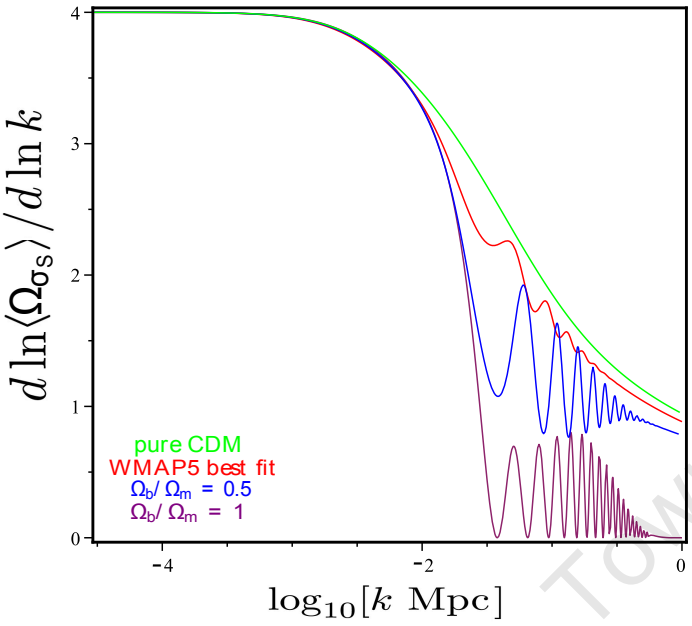

Figure 4.10: The ratio between the scalar energy density per logarithmic bin and the scalar energy density up to a given scale k for different baryon fraction. In the figure we show curves with pure CDM, WMAP5 best fit parameter, 50% baryon out of total mass density and pure baryon cases.

It is also interesting to look at the spectral index for the scalar shear energy density (denoted as $\mathrm{n}_{\sigma_\mathrm{S}}(\mathrm{k})$) and vector shear energy density (denoted as $\mathrm{n}_{\sigma_\mathrm{V}}(\mathrm{k})$) by using Eqs. (4.106) and (4.107) to define

$$\frac{d\langle\Omega_{\sigma_S}\rangle}{d\ln k} \propto k^{\mathrm{n}_{\sigma_\mathrm{S}}(\mathrm{k})}, \text{ and } \frac{d\langle\Omega_{\sigma_V}\rangle}{d\ln k} \propto k^{\mathrm{n}_{\sigma_\mathrm{V}}(\mathrm{k})}, \tag{4.110}$$

Measures of the two spectral index are plotted in Fig. 4.12. As mentioned in subsection 3.3.1, the spectral index is used to describe the slope of the power spectrum. If we look at the curves shown in Fig. 4.6 and bear in mind the definition for an effective spectral index shown in Eq. (3.70), then we can see that Fig. 4.12 roughly matches the slope of the curves in Fig. 4.6. As $k \to 0$, the scalars do roughly scale as k^4 and the vectors roughly scale as k^3. Since the slope for the scalars in Fig. 4.6 is always positive, we only get positive values for $\mathrm{n}_{\sigma_\mathrm{S}}(\mathrm{k})$ in Fig. 4.12. However, there is a turn over of the slope for the vectors in Fig. 4.6, therefore we obtain negative values for $\mathrm{n}_{\sigma_\mathrm{V}}(\mathrm{k})$ in Fig. 4.12. Note also that should we take the extra -1 in Eq. (3.70) into consideration (and some more scaling is needed when the exact form is considered), $\mathrm{n}_{\sigma_\mathrm{V}}(\mathrm{k})$ crosses over to negative value approximately at where we expect to find the turning point in the vector curve shown in Fig. 4.6. And once again, the scalars show more oscillatory feature in Fig. 4.12 than the vectors.

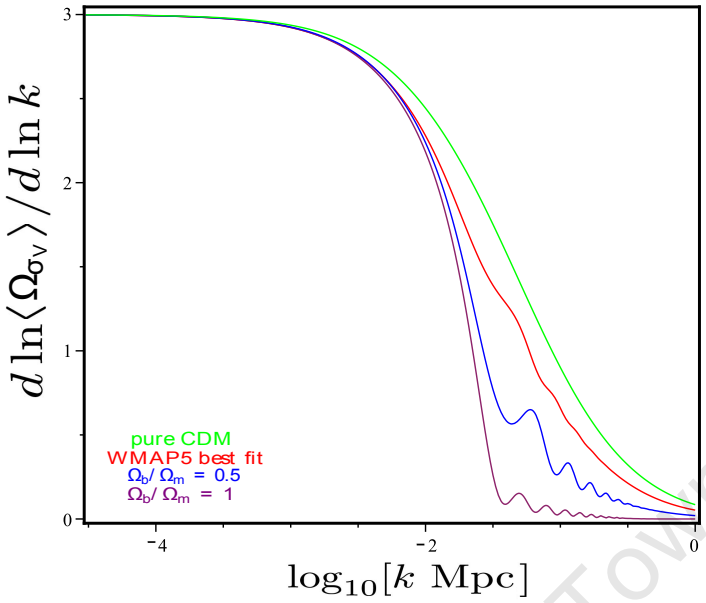

Figure 4.11: The ratio between the vector energy density per logarithmic bin and the vector energy density up to a given scale k for different baryon fraction. In the figure we show curves with pure CDM, WMAP5 best fit parameter, 50% baryon out of total mass density and pure baryon cases.

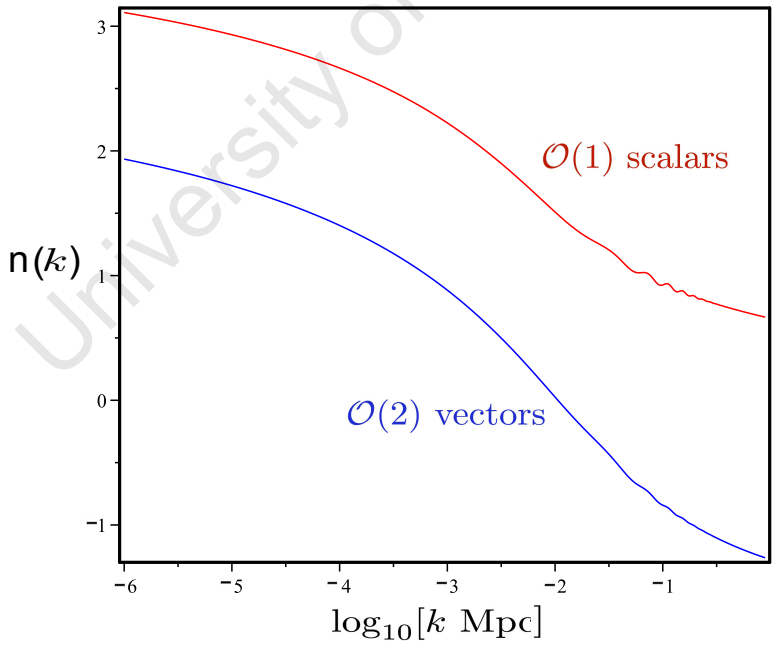

Figure 4.12: The spectral index of the scalar and vector shear energy densities: we define $\frac{d\langle\Omega_\sigma\rangle}{d\ln k} \propto k^{\mathrm{n}_\sigma(\mathrm{k})}$ for each case. Figure plotted using WMAP5 best fit parameters.

Chapter 5

Summary and discussions

In this thesis, two aspects in the theory of modern cosmology are examined. First of which is the issue of testing the CP. Then we turned our attention to non-linear cosmological perturbation theory - in particular the second order vector modes sourced by quadratic linear scalar modes.

In chapter 2, we briefly introduced the general spherically symmetric metric for an irrotational dust matter source in synchronous comoving coordinates - the LTB metric. Different from the usual FLRW models being homogeneous and isotropic, the LTB models are spatially inhomogeneous. In fact, the LTB models are the simplest inhomogeneous models. After introducing the LTB model, we then presented a new, straightforward, test of the CP which may play an important role in our understanding of dark energy.

While we strive to determine the time varying EOS $w(z)$, we have shown that we can simultaneously constrain our Copernican function $\mathcal{C}(z)$ to a similar degree of accuracy. At any redshift, a measurement of $\mathcal{C}(z) \neq 0$ would imply that the FLRW models are the wrong foundation for cosmology and that something more sophisticated must be considered instead. Even if the geometry of the universe is FLRW on average, measurement of $\mathcal{C}(z)$ at small redshifts will allow us to probe the scale at which homogeneity sets in.

This proposed test does not depend on any theory of gravity nor on our understanding of dark energy, but relies only on the geometry of the FLRW models themselves. We have also illustrated that with much freedom exists in choosing of the functional forms of the three arbitrary functions in the LTB model, we are expecting to have $\mathcal{C}(z) \neq 0$ with perhaps a very limited subclass of LTB models that will give us $\mathcal{C}(z) = 0$. Indeed we have presented a figure demonstrating non-zero $\mathcal{C}(z)$ for three chosen LTB models and $\mathcal{C}(z) = 0$ for flat ΛCDM.

Apart from the key test proposed we also presented two other approaches that might help us in understanding the issue of dark energy. However, on what timescale can we expect these various tests to be implemented? Future BAO surveys such as Wide-Field Multi-Object Spectrograph (WFMOS) [231] will measure $d_A(z)$ and $H(z)$ to better than 2% and large radio surveys such as Hubble Sphere Hydrogen Survey (HSHS) [101] and

Square Kilometre Array (SKA) [202] will measure them to better than 1% in redshift bins of width $\triangle z \sim 0.2$ [29, 50]. At its simplest our test can be implemented by measuring Ω_k at two different redshifts. Combinations of future all sky lensing, BAO and SNIa surveys will allow a measurement of Ω_k with accuracy ~ 0.04 [24] which sets the approximate scale of how well we will test the CP in the next decade and which should allow us to strongly rule out inhomogeneity as the source of oversized cosmic distances. Beyond these surveys one can envisage large, low frequency HI surveys able to measure $d_A(z)$ and $H(z)$ at high redshift, $z \sim 10 - 100$ which will allow the testing of the CP in the first billion years of cosmic history when most perturbation modes were still in the linear regime.

While the Copernican assumption is unlikely to be dramatically wrong in our Hubble sphere, it is possible that the dark energy phenomenon is actually concealing something even more bizarre than a misconception of fundamental physics. Indeed, with suggestions such as chaotic inflation, everlasting bouncing universes and the like, it is statistically possible that our part of the universe has some unusual features on a spatial, instead of a purely temporal, dimension, see e.g. [131]. This cannot be ruled out at the moment on anything other than philosophical grounds.

After we have addressed the issue of testing the CP, we then briefly introduce some ideas in the standard cosmological perturbation, at the background and linear levels. We considered the FLRW model at the background level and performed a linear perturbation around it. We presented its line element and the energy momentum tensor in order to calculat the trace-reversed Einstein field equations up to linear order. The issue of coordinate transformation and gauge choices were also briefly reviewed. The validity of scalar-vector-tensor decomposition in the usual practice of cosmological perturbation theory was also discussed in brief. Furthermore, it is necessary to present the definition of the power spectrum, the matter transfer function and introduce the features of the scalar, vector and tensor modes in linear theory. Last but not least, some basics of the 1+3 covariant formalism was also presented which was of great help to us in presenting our arguments as to why there was no vorticity generation at second order in our study.

Next we move onto the main body of the work presented in this thesis. As an naive expectation of inflation is the idea that it does not produce vector modes: if they were observed to have a similar spectrum and amplitude to the scalars then this could prove difficult for inflation, and lend favor to other theories of the early universe, e.g. Pre Big Bang scenarios and Ekpyrotic models [152, 20, 30]. However, what we have presented in this thesis is that there is actually a background of vector modes with χ^2 statistics produced by inflation as a consequence of the non-linear interaction of scalar modes.

In chapter 4, we have first investigated the generation of vector modes induced by primordial density perturbations during the radiation dominated era. Performing a perturbative expansion to second order, we isolated the scalar terms which source the vector perturbations. We then calculated the power spectrum of the metric vector perturbation,

and analysed its form. In order to understand the generation of modes we investigated individual scalar modes generating vectors, and demonstrated that, contrary to the case of gravitational waves, vector modes cannot be generated by an isotropic distribution of scalars of a single wavelength, owing to the spin-1 nature of vector modes: rotational degrees of freedom must be generated by scattering of non-parallel input modes. We then demonstrated that vectors are generated by modes of differing wavelength whenever one of the two scalar modes is entering the Hubble radius. The amplitude of the generated modes depends on the ratio of input wavenumbers; maximum power is generated when the modes are not too widely separated. After investigating the generation of vector modes, we then presented the power spectrum for scale invariant scalar modes, displaying our results in terms of the variable $x = k\eta$: i.e., they may be interpreted the temporal evolution of a single scalar mode, or the power at a fixed time. Interestingly the maximum power generated is the same at all times, but the position of this peak changes with wavelength, such that $x \sim 1 \Rightarrow k \sim 1/\eta$. This is due to the fact that the modes are efficiently generated as they enter the Hubble radius, and are not generated significantly while outside.

We then computed the power spectra for the metric vector perturbations and vector shear at second order, generated by first order scalar perturbations in a ΛCDM model. In addition, we used a covariant approach to show explicitly how vorticity is not generated in a adiabatic perfect fluid at any perturbative order by first order scalar perturbations, so that there is no vorticity in the matter. In order to generate vorticity, one requires either an imperfect fluid, or momentum exchange between the fluid and another fluid. Momentum exchange (via Compton and Coulomb interactions) between electrons, protons and photons in the radiation and recombination eras can generate vorticity and magnetic fields at second order [147, 88, 211, 106, 199, 115, 140]. Another way to generate vorticity is via entropy gradients as it is well known in fluid dynamics and it was first pointed out in [59]. However, it has only until recently been studied at second order in cosmological perturbation theory as a natural extension to a cosmological setting [52].

In order to obtain the vector quantities $S_{(2)i}$ and $v_{(2)i}$, we used the vanishing of vorticity Eq. (4.86) and the $0i$ Einstein constraint Eq. (4.24). Alternatively, one could also use the ij Einstein equation Eq. (4.25) and the momentum conservation equation Eq. (4.19).

The cosmological background of vector modes is small, especially if measured in terms of the dimensionless shear density, as can be seen from the figures shown in chapter 4. However, given that the amplitude of the vector modes in the metric is as large as $\sim 1\%$ of the metric first order scalar modes, in principle these vector modes will have an effect on various cosmological observations. In particular:

- *Redshift-space distortions* [203]: the divergenceless velocity perturbation at second order $v_{(2)i}$ will make a contribution to radial peculiar velocities and thus to redshift-space distortions. With data from future large spectroscopic surveys, we should be able to probe deeper into this issue. Therefore, it is important to investigate and

understand contributions at second order.

- *Large angle CMB temperature anisotropies* [156, 218]: the vector modes will contribute to the Doppler and integrated Sachs-Wolfe effects:

$$\delta^{(2)}T = \frac{1}{2}\left\{v_{(2)i} - S_{(2)i}\right\} e^i|_E^O + \frac{1}{2}\int_E^O d\lambda \partial_i S_{(2)j} e^i e^j, \tag{5.1}$$

  where we have used O to denote observation and E to denote emission. Although we do expect small contribution to CMB temperature anisotropies from second order vector modes, with future observations to have better sensitivity level, we will not be able to neglect these contributions far into the future. It is perhaps timely to get a better understanding of these second order vector modes and their possible effects on the CMB.

- *Weak lensing* [194, 65]: vector modes produce a deflection angle

$$\bar{\alpha} = \int_E^O d\lambda \left(\vec{\nabla} \times \vec{S}\right) \times \vec{e}. \tag{5.2}$$

- *CMB polarization* [155, 111]: the vector modes will leave a characteristic imprint on the B-mode polarization in the CMB. It could become the dominant contribution when compared with the second order gravitational waves as pointed out in [155]. Therefore, it is important to understand this effect in great detail.

Further work is needed to compute the size of these vector corrections. They are likely to be significant mainly below ~ 10Mpc, but in this regime the scalar non-linear effects are important and likely to dominate. With better sensitivity level for the future observations, these vector mode contributions will have to be taken into consideration.

The vector degree of freedom forms an integral part of the perturbative expansion when one goes beyond linear order. At the order we have considered, vectors must be present essentially through a constraint in the field equations arising at order $(\Phi^{(1)})^2$, even though vectors have no independent propagating degrees of freedom. This is distinct from the intrinsically propagating degree of freedom in the scalar induced gravitational wave background [22, 7, 144]. We have shown that the vector mode background has maximum power around the equality scale, similar to the induced gravitational wave background, and the metric vector modes achieve their maximal fraction of the linear metric scalar modes on scales below the Silk scale. The size of the vector contribution to the full non-linear power spectrum relevant for structure formation remains to be calculated.

The work presented in this thesis is a small part of the ongoing detailed investigation of second order perturbation theory. As an extension of work presented in this thesis and those presented in [7, 22], we have started looking at the case of second order tensor modes sourced by linear order vector modes. Although it has been pointed out earlier in this

thesis that a scalar field cannot support vector modes at linear order. Even if vector modes are produced during inflation, once they leave the Hubble radius during the inflationary phase they will decay very rapidly. However, should inflation turns out not to be the model for the early universe, then it might be possible to produce vector modes at linear order. These linear order vector modes will leave an imprint on the second order tensor modes via coupled linear vector modes. We might be able to constrain the amplitude of these linear vector modes by studying second order tensor modes. However, at the time of writing up this thesis, no conclusive results have been reached and only some derivations have been done. Nevertheless, we presented our current progress of this work in detail in Appendix C and we shall briefly summarise it here.

The evolution equation of these second order tensor modes from coupled linear vector modes (in radiation era) is

$$\begin{aligned} h_{ij}^{(2)''} + 2\mathcal{H}h_{ij}^{(2)'} - \nabla^2 h_{ij}^{(2)} &= 4S^{(1)m}\partial_i\partial_j S_m^{(1)} - 2S^{(1)m}\partial_m\partial_{(i}S_{j)}^{(1)} + 2\partial_i S^{m(1)}\partial_j S_m^{(1)} \\ &\quad + 2\partial_m S_i^{(1)}\partial^m S_j^{(1)} + \frac{1}{4\mathcal{H}^2}\nabla^2 S_i^{(1)}\nabla^2 S_j^{(1)} \\ &\quad + 4\left(\mathcal{H}^2 S_m^{(1)}S^{m(1)} + \mathcal{H}S^{m(1)}S_m^{(1)'}\right)\gamma_{ij}. \end{aligned} \tag{5.3}$$

Note that the right hand side of this expression is not a pure tensor quantity. Similar to the approach adopted to our studies on second order vector modes, we shall extract out the pure tensor part by using a tensor extraction operator. This will provide us with an evolution equation for the second order tensor modes in Fourier space:

$$h''(\boldsymbol{k},\eta) + 2\mathcal{H}h'(\boldsymbol{k},\eta) + k^2 h(\boldsymbol{k},\eta) = \Upsilon(\boldsymbol{k},\eta), \tag{5.4}$$

where

$$\begin{aligned} \Upsilon(\boldsymbol{k},\eta) = \frac{-q^{ij}(\boldsymbol{k})}{(2\pi)^{3/2}}\int d^3k' S(\boldsymbol{k'},\eta)S(\boldsymbol{k}-\boldsymbol{k'},\eta)\left\{2e_m(\boldsymbol{k'})e^m(\boldsymbol{k}-\boldsymbol{k'})k'_i k'_j\right. \\ - 2\left[e_j(\boldsymbol{k'})k'_i + e_i(\boldsymbol{k'})k'_j\right]e^m(\boldsymbol{k}-\boldsymbol{k'})k'_m + 2e_i(\boldsymbol{k'})e_j(\boldsymbol{k}-\boldsymbol{k'}) \\ \left.\times(k'_m k^m - k'^2) - \frac{1}{4\mathcal{H}^2}e_i(\boldsymbol{k'})e_j(\boldsymbol{k}-\boldsymbol{k'})k'^2|\boldsymbol{k}-\boldsymbol{k'}|^2\right\}. \end{aligned} \tag{5.5}$$

The next stage in this project is to find a way to calculate power spectrum of these second order tensor modes. Regrettably, at the time of writing up this thesis, we have not been able to do simplify our power spectrum expression to a level that will be useable for numerical analysis (Eq. (C.41) shows the complexity of the current expression for our power spectrum calculation).

Appendix A

The connection coefficients and the projection tensor

In this appendix, we show the components of the connection coefficients and the projection tensor. Note however that the expressions shown here is what one arrives at when one keeps scalar quantities at first order and the second order vectors.

A.1 The connection coefficients

A.1.1 Zeroth order connection coefficients

The connection coefficients in the flat FLRW background are

$$\begin{aligned}\Gamma^0_{00} &= \mathcal{H}\\ \Gamma^i_{0j} &= \mathcal{H}\delta^i_j\\ \Gamma^0_{ij} &= \mathcal{H}\gamma_{ij}\\ \Gamma^i_{00} &= \Gamma^0_{0i} = \Gamma^0_{i0} = \Gamma^i_{jk} = 0.\end{aligned} \tag{A.1}$$

A.1.2 First order connection coefficients

The first order perturbed connection coefficients (before a gauge choice) have expressions as

$$\delta^{(1)}\Gamma^0_{00} = \phi^{(1)\prime}, \tag{A.2}$$

$$\delta^{(1)}\Gamma^0_{0i} = \partial_i\phi^{(1)} + \mathcal{H}\partial_i B^{(1)}, \tag{A.3}$$

$$\delta^{(1)}\Gamma^i_{00} = \mathcal{H}\partial^i B^{(1)} + \partial^i B^{(1)\prime} + \partial^i\phi^{(1)}, \tag{A.4}$$

$$\delta^{(1)}\Gamma^0_{ij} = \left[-\psi^{(1)\prime} - 2\mathcal{H}\left(\psi^{(1)} + \phi^{(1)}\right)\right]\gamma_{ij} + 2\mathcal{H}\partial_i\partial_j E^{(1)} + \partial_i\partial_j\left(E^{(1)\prime} - B^{(1)}\right), \tag{A.5}$$

$$\delta^{(1)}\Gamma^i_{0j} = -\psi^{(1)\prime}\delta^i_j + \partial^i\partial_j E^{(1)\prime}, \tag{A.6}$$

$$\delta^{(1)}\Gamma^i_{jk} = \left[\partial^i\psi^{(1)} - \mathcal{H}\partial^i B^{(1)}\right]\gamma_{jk} + \partial^i\partial_j\partial_k E^{(1)} - \partial_j\psi^{(1)}\delta^i_k - \partial_k\psi^{(1)}\delta^i_j. \tag{A.7}$$

A.1.3 Second order connection coefficients

The first order perturbed connection coefficients (before a gauge choice) have expressions as

$$\delta^{(2)}\Gamma^0_{00} = -2\phi^{(1)}\phi^{(1)\prime} + \partial^i B^{(1)}\left[\mathcal{H}\partial_i B^{(1)} + \partial_i B^{(1)\prime} + \partial_i\phi^{(1)}\right], \tag{A.8}$$

$$\begin{aligned}\delta^{(2)}\Gamma^0_{0i} = &-2\phi^{(1)}\partial_i\phi^{(1)} - \partial_i B^{(1)}\left[\psi^{(1)\prime} + 2\mathcal{H}\phi^{(1)}\right] - \frac{1}{2}\mathcal{H}S^{(2)}_i \\ &+ \partial^j B^{(1)}\partial_i\partial_j E^{(1)\prime},\end{aligned} \tag{A.9}$$

$$\begin{aligned}\delta^{(2)}\Gamma^i_{00} = &-\frac{1}{2}\left[\mathcal{H}S^{(2)i} + S^{(2)i\prime}\right] + 2\psi^{(1)}\left[\partial^i B^{(1)\prime} + \partial^i\phi^{(1)} + \partial^i B^{(1)}\right] \\ &- 2\partial^i\partial^j E^{(1)}\left[\partial_j B^{(1)\prime} + \partial_j\phi^{(1)} + \mathcal{H}\partial_j B^{(1)}\right] - \phi^{(1)\prime}\partial^i B^{(1)},\end{aligned} \tag{A.10}$$

$$\begin{aligned}\delta^{(2)}\Gamma^0_{ij} = &\left[4\mathcal{H}\phi^{(1)}\psi^{(1)} + 2\phi^{(1)}\psi^{(1)\prime} + 4\mathcal{H}\left(\phi^{(1)}\right)^2 + \partial^m B^{(1)}\partial_m\psi^{(1)} - \mathcal{H}\partial_m B^{(1)}\partial^m B^{(1)}\right]\gamma_{ij} \\ &+ \frac{1}{2}\partial_{(i}S^{(2)}_{j)} + \mathcal{H}\partial_{(i}F^{(2)}_{j)} + \frac{1}{2}\partial_{(i}F^{(2)\prime}_{j)} + 2\phi^{(1)}\left[\partial_i\partial_j B^{(1)} - 4\mathcal{H}\partial_i\partial_j E^{(1)} - \partial_i\partial_j E^{(1)\prime}\right] \\ &- \partial_j B^{(1)}\partial_i\psi^{(1)} + \partial^k B^{(1)}\partial_i\partial_k\partial_j E^{(1)} - \partial_i B^{(1)}\partial_j\psi^{(1)},\end{aligned} \tag{A.11}$$

$$\begin{aligned}\delta^{(2)}\Gamma^i_{0j} = &\frac{1}{2}\partial_{(j}F^{(2)i)\prime} + \frac{1}{2}\partial^{[i}S^{(2)}_{j]} - \partial^i B^{(1)}\partial_j\phi^{(1)} - 2\psi^{(1)}\psi^{(1)\prime}\delta^i_j + 2\psi^{(1)}\partial^i\partial_j E^{(1)\prime} \\ &- \mathcal{H}\partial^i B^{(1)}\partial_j B^{(1)} + 2\psi^{(1)\prime}\partial^i\partial_j E^{(1)} - 2\partial^i\partial^k E^{(1)}\partial_k\partial_j E^{(1)\prime},\end{aligned} \tag{A.12}$$

$$\begin{aligned}\delta^{(2)}\Gamma^i_{jk} = &\Big[\psi^{(1)\prime}\partial^i B^{(1)} + 2\mathcal{H}\phi^{(1)}\partial^i B^{(1)} + 2\mathcal{H}\partial_m B^{(1)}\partial^m\partial^i E^{(1)} + 2\psi^{(1)}\partial^i\psi^{(1)} + \frac{1}{2}\mathcal{H}S^{(2)i} \\ &-2\partial_m\psi^{(1)}\partial^i\partial^m E^{(1)}\Big]\gamma_{jk} + \partial^i B^{(1)}\left[\partial_j\partial_k B^{(1)} - 2\mathcal{H}\partial_j\partial_k E^{(1)} - \partial_j\partial_k E^{(1)\prime}\right] \\ &- 2\psi^{(1)}\partial_j\psi^{(1)}\delta^i_k - 2\psi^{(1)}\partial_k\psi^{(1)}\delta^i_j + 2\psi^{(1)}\partial_k\partial_j\partial^i E^{(1)} + 2\partial_j\psi^{(1)}\partial^i\partial_k E^{(1)} \\ &- 2\partial^i\partial^m E^{(1)}\partial_j\partial_m\partial_k E^{(1)} + 2\partial_k\psi^{(1)}\partial^i\partial_j E^{(1)} + \frac{1}{2}\partial_j\partial_k F^{(2)i}.\end{aligned} \tag{A.13}$$

A.2 The projection tensor

As mentioned earlier, the projection tensor projects into the instantaneous fluid rest space and is expressed as

$$\bar{h}_{\alpha\beta} = \bar{g}_{\alpha\beta} + \bar{u}_\alpha\bar{u}_\beta. \tag{A.14}$$

Expanding this expression and collecting the terms at the same order we can then calculate the expression for the projection tensor at each order. It's contravariant form can then be calculated from

$$\bar{h}^{\mu\nu} = \bar{g}^{\mu\alpha}\bar{g}^{\nu\beta}\bar{h}_{\alpha\beta}. \tag{A.15}$$

Below we show the expressions for their components at each order. Note however that all the components for the projection tensor presented here only suitable for the case we are considering since their expressions depend on how the metric components and four velocity components are set up to be.

A.2.1 Zeroth order projection tensor and its contravariant form

At zeroth order we have

$$h_{\alpha\beta} = g_{\alpha\beta} + u_\alpha u_\beta, \tag{A.16}$$

and

$$h_{\mu\nu} = g^{\mu\alpha} g^{\nu\beta} h_{\alpha\beta}. \tag{A.17}$$

Therefore, in our gauge choice and perfect fluid background we can calculate their components to be

$$h_{00} = 0,\ h_{0j} = 0,\ \text{and}\ h_{ij} = a^2\gamma_{ij}, \tag{A.18}$$

and

$$h^{00} = 0,\ h^{0j} = 0,\ \text{and}\ h^{ij} = a^{-2}\gamma^{ij}. \tag{A.19}$$

A.2.2 First order projection tensor and its contravariant form

At first order we have

$$\delta^{(1)} h_{\alpha\beta} = \delta^{(1)} g_{\alpha\beta} + u_\alpha \delta^{(1)} u_\beta + \delta^{(1)} u_\alpha u_\beta, \tag{A.20}$$

and

$$\delta^{(1)} h^{\mu\nu} = g^{\mu\alpha} g^{\nu\beta} \delta^{(1)} h_{\alpha\beta} + \delta^{(1)} g^{\mu\alpha} g^{\nu\beta} h_{\alpha\beta} + g^{\mu\alpha} \delta^{(1)} g^{\nu\beta} h_{\alpha\beta}. \tag{A.21}$$

Therefore, in our gauge choice and perfect fluid background we can calculate their components to be

$$\delta^{(1)} h_{00} = 0,\ \delta^{(1)} h_{0j} = -a^2 \partial_j v_{(1)},\ \text{and}\ \delta^{(1)} h_{ij} = -2a^2 \Phi^{(1)} \gamma_{ij}, \tag{A.22}$$

and

$$\delta^{(1)} h^{00} = 0,\ \delta^{(1)} h^{0j} = a^{-2} \partial^j v_{(1)},\ \text{and}\ \delta^{(1)} h^{ij} = 2a^{-2} \Phi^{(1)} \gamma^{ij}. \tag{A.23}$$

A.2.3 Second order projection tensor and its contravariant form

At second order we have

$$\delta^{(2)} h_{\alpha\beta} = \delta^{(2)} g_{\alpha\beta} + u_\alpha \delta^{(2)} u_\beta + \delta^{(1)} u_\alpha \delta^{(1)} u_\beta + \delta^{(2)} u_\alpha u_\beta, \tag{A.24}$$

and

$$\delta^{(2)}h^{\mu\nu} = g^{\mu\alpha}g^{\nu\beta}\delta^{(2)}h_{\alpha\beta} + g^{\mu\alpha}\delta^{(1)}g^{\nu\beta}\delta^{(1)}h_{\alpha\beta} + \delta^{(1)}g^{\mu\alpha}g^{\nu\beta}\delta^{(1)}h_{\alpha\beta} + \delta^{(1)}g^{\mu\alpha}\delta^{(1)}g^{\nu\beta}h_{\alpha\beta} + \delta^{(2)}g^{\mu\alpha}g^{\nu\beta}h_{\alpha\beta} + g^{\mu\alpha}\delta^{(2)}g^{\nu\beta}h_{\alpha\beta}. \tag{A.25}$$

Therefore, in our gauge choice and perfect fluid background we can calculate their components to be

$$\begin{aligned} \delta^{(2)}h_{00} &= a^2\partial^m v_{(1)}\partial_m v_{(1)}, \\ \delta^{(2)}h_{0j} &= -\frac{a^2}{2}v_{(2)j} + a^2\Phi^{(1)}\partial_j v_{(1)}, \\ \delta^{(2)}h_{ij} &= a^2\partial_i v_{(1)}\partial_j v_{(1)}, \end{aligned} \tag{A.26}$$

and

$$\begin{aligned} \delta^{(2)}h^{00} &= a^{-2}\partial^m v_{(1)}\partial_m v_{(1)}, \\ \delta^{(2)}h^{0j} &= \frac{1}{2}a^{-2}\left(v^j_{(2)} - S^j_{(2)}\right) - a^{-2}\Phi^{(1)}\partial^j v_{(1)}, \\ \delta^{(2)}h^{ij} &= a^{-2}\partial^i v_{(1)}\partial^j v_{(1)} + 4a^{-2}\left(\Phi^{(1)}\right)^2\gamma^{ij}. \end{aligned} \tag{A.27}$$

Appendix B

Fourier decomposition and the extraction operators

In this appendix we define the scalar, vector and tensor harmonic basis in flat space. This is necessary to develop the extraction operator presented in the second half of this appendix.

The extraction operator is essential for our second order studies since although *true* second order modes decouple, we can still get second order terms formed from two coupled first order modes. Usually we only wish to study the properties of a particular type of mode due to the complexity of the theory at second order. The extraction operator allows us to do this by, for example, isolating the pure vector part from coupled scalar-scalar modes. Only once we have set up the respective extraction operators, are we able to extract the scalar, vector and tensor quantities separately from second order quantities which have all three types coupled together.

Here we follow the presentation of [12], but it was shown in much more details in [6]. The extration operators were studied in detail in [6]. Due to their importance and for the completion of this thesis, we will present them again in detail here, mostly following [6].

B.1 Fourier decomposition

B.1.1 The scalar basis

The scalar basis is defined by the scalar Helmholtz equation

$$\nabla^2 Q(\boldsymbol{k}) = -k^2 Q(\boldsymbol{k}), \tag{B.1}$$

Thus they are just scalar eigenfunctions of the Laplacian. It is easy to follow that there is an additional constraint $\frac{d}{d\eta} Q(\boldsymbol{k}) = 0$. The complex conjugate of the time independent basis

function is $Q^*(\boldsymbol{k}) = Q(-\boldsymbol{k})$. We choose an orthonormal basis so that

$$\int d^3x\ Q(\boldsymbol{k})Q^*(\boldsymbol{k}') = \delta^3(\boldsymbol{k}-\boldsymbol{k}'). \tag{B.2}$$

Note that d^3x is used to represent the real space. Then the scalar basis consists of the exponentials

$$Q(\boldsymbol{k}) = \frac{1}{(2\pi)^{3/2}} e^{i\boldsymbol{k}\cdot\boldsymbol{x}}. \tag{B.3}$$

We can construct a one-index object from the scalar basis:

$$Q_i^{(s)}(\boldsymbol{k}) = \partial_i Q(\boldsymbol{k}) = ik_i Q(\boldsymbol{k}). \tag{B.4}$$

This provides us with a scalar type vector and it can be applied on a gradient. We can also construct a two-index object:

$$Q_{ij}^{(s)}(\boldsymbol{k}) = \left[\partial_i\partial_j - \frac{1}{3}\gamma_{ij}\nabla^2\right] Q(\boldsymbol{k}) = \left[-k_ik_j + \frac{1}{3}\gamma_{ij}k^2\right] Q(\boldsymbol{k}). \tag{B.5}$$

This is the scalar type symmetric trace-free tensor. Additionally, we can see that

$$k^ik^jQ_{ij}^{(s)}(\boldsymbol{k}) = -\frac{2}{3}k^4Q(\boldsymbol{k}). \tag{B.6}$$

The Fourier decomposition of an arbitrary scalar in real space can be expressed as

$$S(\boldsymbol{x},\eta) = \int d^3k S(\boldsymbol{k},\eta)\, Q(\boldsymbol{k}) = \frac{1}{(2\pi)^{3/2}} \int d^3k S(\boldsymbol{k},\eta)\, e^{i\boldsymbol{k}\cdot\boldsymbol{x}}. \tag{B.7}$$

The inverse of the above Fourier integral is then

$$S(\boldsymbol{k},\eta) = \int d^3x S(\boldsymbol{x},\eta)\, Q^*(\boldsymbol{k}) = \frac{1}{(2\pi)^{3/2}} \int d^3x S(\boldsymbol{x},\eta)\, e^{-i\boldsymbol{k}\cdot\boldsymbol{x}}. \tag{B.8}$$

We require $S^*(-\boldsymbol{k},\eta) = S(\boldsymbol{k},\eta)$ to ensure that $S(\boldsymbol{x},\eta)$ is real.

B.1.2 The vector basis

Similarly, the vector basis must satisfy the vector Helmholtz equation

$$\nabla^2 Q_i(\boldsymbol{k}) = -k^2 Q_i(\boldsymbol{k}), \tag{B.9}$$

These are just the vector eigenfunctions of the Laplacian. We impose additional constraints such that $\frac{d}{d\eta}Q_i = 0$ and $\partial^i Q_i = 0$. The vector basis come in two sets called parities denoted

Q_i and $\tilde{Q}_i$. Like the scalar basis, the vector basis must satisfy the orthonormality conditions:

$$\begin{aligned}\int d^3x\ Q^i(\boldsymbol{k})Q_i^*(\boldsymbol{k}') &= \delta^3(\boldsymbol{k}-\boldsymbol{k}'),\\ \int d^3x\ \tilde{Q}^i(\boldsymbol{k})\tilde{Q}_i^*(\boldsymbol{k}') &= \delta^3(\boldsymbol{k}-\boldsymbol{k}'),\\ \int d^3x\ Q^i(\boldsymbol{k})\tilde{Q}_i^*(\boldsymbol{k}') &= 0.\end{aligned} \tag{B.10}$$

The vector basis for each parity is then

$$Q_i(\boldsymbol{k}) = \frac{e_i(\boldsymbol{k})}{(2\pi)^{3/2}}e^{i\boldsymbol{k}\cdot\boldsymbol{x}},\ \text{and}\ \tilde{Q}_i(\boldsymbol{k}) = \frac{\tilde{e}_i(\boldsymbol{k})}{(2\pi)^{3/2}}e^{i\boldsymbol{k}\cdot\boldsymbol{x}}, \tag{B.11}$$

where e_i and $\tilde{e}_i$ are parity vectors. The parity vectors satisfy

$$e_i(\boldsymbol{k}) = e_i(-\boldsymbol{k}),\ \tilde{e}_i(-\boldsymbol{k}) = -\tilde{e}_i(\boldsymbol{k}), \tag{B.12}$$

and are orthogonal to the wave vector k^i

$$k^i e_i(\boldsymbol{k}) = 0,\ k^i\tilde{e}_i(\boldsymbol{k}) = 0. \tag{B.13}$$

Additionally, the two parity vectors are orthogonal to each other for all wave modes $\boldsymbol{k}$

$$e^i(\boldsymbol{k})\tilde{e}_i(\boldsymbol{k}) = 0,\ e^i(\boldsymbol{k})e_i(\boldsymbol{k}) = 0,\ \tilde{e}^i(\boldsymbol{k})\tilde{e}_i(\boldsymbol{k}) = 0. \tag{B.14}$$

A vector type symmetric trace free tensor can be constructed from the vector basis:

$$Q_{ij}^{(V)}(\boldsymbol{k}) = \partial_{(i}Q_{j)}(\boldsymbol{k}) = ik_{(i}Q_{j)}(\boldsymbol{k}). \tag{B.15}$$

Alternate parity tensors can be constructed in the same way using the vector basis $\tilde{Q}_i(\boldsymbol{k})$. A divergence free vector in real space can be expressed as a Fourier integral

$$\begin{aligned}V_i(\boldsymbol{x},\eta) &= \int d^3k\left[\tilde{V}(\boldsymbol{k},\eta)\tilde{Q}_i(\boldsymbol{k}) + V(\boldsymbol{k},\eta)Q_i(\boldsymbol{k})\right]\\ &= \frac{1}{(2\pi)^{3/2}}\int d^3k\left[\tilde{V}(\boldsymbol{k},\eta)\tilde{e}_i(\boldsymbol{k}) + V(\boldsymbol{k},\eta)e_i(\boldsymbol{k})\right]e^{i\boldsymbol{k}\cdot\boldsymbol{x}}.\end{aligned} \tag{B.16}$$

The inverse of the above Fourier integral decouples for the two parities:

$$\begin{aligned}V(\boldsymbol{k},\eta) &= \int d^3x V_i(\boldsymbol{x},\eta)Q^{*i}(\boldsymbol{k})\\ &= \frac{1}{(2\pi)^{3/2}}\int d^3x V_i(\boldsymbol{x},\eta)e^i(\boldsymbol{k})e^{-i\boldsymbol{k}\cdot\boldsymbol{x}},\end{aligned} \tag{B.17}$$

and

$$\begin{aligned}\tilde{V}(\boldsymbol{k},\eta) &= \int d^3x \tilde{V}_i(\boldsymbol{x},\eta)\tilde{Q}^{*i}(\boldsymbol{k}) \\ &= \frac{1}{(2\pi)^{3/2}}\int d^3x \tilde{V}_i(\boldsymbol{x},\eta)\tilde{e}^i(\boldsymbol{k})e^{-i\boldsymbol{k}\cdot\boldsymbol{x}}.\end{aligned} \tag{B.18}$$

In order for the vector function $V_i(\boldsymbol{x},\eta)$ to be real, we require that

$$\begin{aligned}V_i^*(-\boldsymbol{k},\eta) &= V_i(\boldsymbol{k},\eta), \\ \tilde{V}_i^*(-\boldsymbol{k},\eta) &= V_i(\boldsymbol{k},\eta).\end{aligned} \tag{B.19}$$

For any $\boldsymbol{k}$, we can form an orthonormal basis of $\mathbb{R}^3$:

$$e_i^{(\alpha)} = \left\{ e_i(\boldsymbol{k}),\ \tilde{e}_i(\boldsymbol{k}),\ \frac{k_i}{|\boldsymbol{k}|} \right\}. \tag{B.20}$$

B.1.3 The tensor basis

The tensor basis satisfies the tensor Helmholtz equation

$$\nabla^2 Q_{ij} = -k^2 Q_{ij} \tag{B.21}$$

with an additional constraint $\frac{d}{d\eta}Q_{ij} = 0$. They must also be transverse and traceless:

$$\partial^i Q_{ij} = 0,\ Q^i{}_i = 0. \tag{B.22}$$

We denote the two tensor polarizations by Q_{ij} and $\tilde{Q}_{ij}$. They must satisfy the normalisation conditions

$$\begin{aligned}\int d^3x\ Q^{ij}(\boldsymbol{k})Q^*_{ij}(\boldsymbol{k}') &= \delta^3(\boldsymbol{k}-\boldsymbol{k}'), \\ \int d^3x\ \tilde{Q}^{ij}(\boldsymbol{k})\tilde{Q}^*_{ij}(\boldsymbol{k}') &= \delta^3(\boldsymbol{k}-\boldsymbol{k}'), \\ \int d^3x\ Q^{ij}(\boldsymbol{k})\tilde{Q}^*_{ij}(\boldsymbol{k}') &= 0.\end{aligned} \tag{B.23}$$

The complete tensor basis is then

$$\begin{aligned}Q_{ij}(\boldsymbol{k}) &= \frac{q_{ij}(\boldsymbol{k})}{(2\pi)^{3/2}}e^{i\boldsymbol{k}\cdot\boldsymbol{x}}, \\ \tilde{Q}_{ij}(\boldsymbol{k}) &= \frac{\tilde{q}_{ij}(\boldsymbol{k})}{(2\pi)^{3/2}}e^{i\boldsymbol{k}\cdot\boldsymbol{x}},\end{aligned} \tag{B.24}$$

where the polarization tensors q_{ij} and $\tilde{q}_{ij}$ can be expressed in terms of the two parity vectors, $e_i(\boldsymbol{k})$ and $\tilde{e}_i(\boldsymbol{k})$, introduced earlier:

$$\begin{aligned} q_{ij}(\boldsymbol{k}) &= \frac{1}{\sqrt{2}}\left[e_i(\boldsymbol{k})e_j(\boldsymbol{k}) - \tilde{e}_i(\boldsymbol{k})\tilde{e}_j(\boldsymbol{k})\right], \\ \tilde{q}_{ij}(\boldsymbol{k}) &= \frac{1}{\sqrt{2}}\left[e_i(\boldsymbol{k})\tilde{e}_j(\boldsymbol{k}) - \tilde{e}_i(\boldsymbol{k})e_j(\boldsymbol{k})\right]. \end{aligned} \tag{B.25}$$

From the properties of the parity vectors, we can show that

$$\begin{aligned} q_{ij}(\boldsymbol{k}) &= q_{ij}(-\boldsymbol{k}), \\ \tilde{q}_{ij}(\boldsymbol{k}) &= -\tilde{q}_{ij}(\boldsymbol{k}), \end{aligned} \tag{B.26}$$

that polarization tensors q_{ij} and $\tilde{q}_{ij}$ are orthogonal to the wave vector k^i

$$k^i q_{ij}(\boldsymbol{k}) = 0,\ k^i \tilde{q}_{ij}(\boldsymbol{k}) = 0, \tag{B.27}$$

and that the polarization tensors are orthogonal to each other:

$$q^{ij}(\boldsymbol{k})\tilde{q}_{ij}(\boldsymbol{k}) = 0,\ q^{ij}(\boldsymbol{k})q_{ij}(\boldsymbol{k}) = 0,\ \tilde{q}^{ij}(\boldsymbol{k})\tilde{q}_{ij}(\boldsymbol{k}) = 0. \tag{B.28}$$

A transverse traceless tensor in real space can be expressed as a Fourier integral

$$\begin{aligned} T_{ij}(\boldsymbol{x},\eta) &= \int d^3k \left[T(\boldsymbol{k},\eta)Q_{ij}(\boldsymbol{k}) + \tilde{T}(\boldsymbol{k},\eta)\tilde{Q}_{ij}(\boldsymbol{k})\right] \\ &= \frac{1}{(2\pi)^{3/2}}\int d^3k \left[T(\boldsymbol{k},\eta)q_{ij}(\boldsymbol{k}) + \tilde{T}(\boldsymbol{k},\eta)\tilde{q}_{ij}(\boldsymbol{k})\right] e^{i\boldsymbol{k}\cdot\boldsymbol{x}}. \end{aligned} \tag{B.29}$$

The inverse of the above Fourier integral decouples for the two polarizations:

$$\begin{aligned} T(\boldsymbol{k},\eta) &= \int d^3x\ T_{ij}(\boldsymbol{x},\eta)Q^{*ij}(\boldsymbol{k}) \\ &= \frac{1}{(2\pi)^{3/2}}\int d^3x\ T_{ij}(\boldsymbol{x},\eta)q^{ij}(\boldsymbol{k})e^{-i\boldsymbol{k}\cdot\boldsymbol{x}}, \end{aligned} \tag{B.30}$$

and

$$\begin{aligned} \tilde{T}(\boldsymbol{k},\eta) &= \int d^3x\ \tilde{T}_{ij}(\boldsymbol{x},\eta)\tilde{Q}^{*ij}(\boldsymbol{k}) \\ &= \frac{1}{(2\pi)^{3/2}}\int d^3x\ \tilde{T}_{ij}(\boldsymbol{x},\eta)\tilde{q}^{ij}(\boldsymbol{k})e^{-i\boldsymbol{k}\cdot\boldsymbol{x}}. \end{aligned} \tag{B.31}$$

In order for the vector function $T_{ij}(\boldsymbol{x},\eta)$ to be real, we require that

$$T^*_{ij}(-\boldsymbol{k},\eta) = T_{ij}(\boldsymbol{k},\eta),\ \tilde{T}^*_{ij}(-\boldsymbol{k},\eta) = -\tilde{T}_{ij}(\boldsymbol{k},\eta). \tag{B.32}$$

B.2 Extraction operator

A generic second order quantity contains a pure second order quantity and a coupling of two linear order quantities. The coupling of two linear order quantities can be decomposed into scalar, vector and tensor quantities and such a decomposition is not trivial. Due to the complexity of second order studies, the most common approach is to study the properties of a single type of mode at a time. Hence, we need to develop a tool – the extraction operator – to help us isolate a single type of mode for analysis. In this subsection, we will introduce such extraction operators and demonstrate how they operate.

An arbitrary symmetric traceless spatial tensor in real space can be expressed as a combination of scalar, vector and tensor contributions:

$$A_{ij}(\boldsymbol{x},\eta) = \left[\partial_i\partial_j - \frac{1}{3}\gamma_{ij}\nabla^2\right] A^{(S)}(\boldsymbol{x},\eta) + \partial_{(i}A^{(V)}_{j)}(\boldsymbol{x},\eta) + A^{(T)}_{ij}(\boldsymbol{x},\eta). \tag{B.33}$$

This can also be expressed as the Fourier integral

$$\begin{aligned} A_{ij}(\boldsymbol{x},\eta) = \frac{1}{(2\pi)^{3/2}}\int d^3\boldsymbol{k}\ \Bigg\{\left[-k_ik_j + \frac{1}{3}\gamma_{ij}k^2\right] A^{(S)}(\boldsymbol{k},\eta) + iA^{(V)}(\boldsymbol{k},\eta)k_{(i}e_{j)} \\ +i\tilde{A}^{(V)}(\boldsymbol{k},\eta)k_{(i}\tilde{e}_{j)} + A^{(T)}(\boldsymbol{k},\eta)q_{ij} + \tilde{A}^{(T)}(\boldsymbol{k},\eta)\tilde{q}_{ij}\Bigg\} e^{i\boldsymbol{k}\cdot\boldsymbol{x}}. \end{aligned} \tag{B.34}$$

Note that we can extract the Fourier amplitude of the scalar and vector contributions using

$$A^{(S)}(\boldsymbol{k}',\eta) = -\frac{3}{2k'^4}\int d^3x\ A_{ij}(\boldsymbol{x},\eta)k'^ik'^jQ^*(\boldsymbol{k}'), \tag{B.35}$$

and

$$A^{(V)}(\boldsymbol{k}',\eta) = -\frac{2i}{k'^2}\int d^3x\ A_{ij}(\boldsymbol{x},\eta)k'^iQ^{*j}(\boldsymbol{k}'), \tag{B.36}$$

respectively. The alternate parity vector component can be extracted by replacing $Q^{*j}(\boldsymbol{k}')$ with $\tilde{Q}^{*j}(\boldsymbol{k}')$. The Fourier amplitude of the tensor contribution is given by

$$A^{(T)}(\boldsymbol{k}',\eta) = \int d^3x\ A_{ij}(\boldsymbol{x},\eta)Q^{*ij}(\boldsymbol{k}'). \tag{B.37}$$

As in the vector case, the alternate polarization component can be extracted by replacing $Q^{*ij}(\boldsymbol{k}')$ with $\tilde{Q}^{*ij}(\boldsymbol{k}')$.

Now we are ready to give complete expressions for the extraction operators. As usual, we will look at the scalar case first. We define the scalar extraction operator to be

$$\mathcal{S}^{ij}(\boldsymbol{x},\boldsymbol{x}') = -\frac{3}{2(2\pi)^3}\int d^3k'\ k'^{-4}k'^ik'^j\int d^3x'\ e^{i\boldsymbol{k}'\cdot(\boldsymbol{x}-\boldsymbol{x}')}. \tag{B.38}$$

If we apply $\mathcal{S}^{ij}(\boldsymbol{x},\boldsymbol{x}')$ to Eq. (B.33), then we get

$$\begin{aligned} A^{(S)}(\boldsymbol{x},\eta) &= \mathcal{S}^{ij}(\boldsymbol{x},\boldsymbol{x}')A_{ij}(\boldsymbol{x}',\eta) \\ &= -\frac{3}{2(2\pi)^3}\int d^3k'\ k'^{-4}k'^i k'^j \int d^3x'\ e^{i\boldsymbol{k}'\cdot(\boldsymbol{x}-\boldsymbol{x}')}A_{ij}(\boldsymbol{x}',\eta). \end{aligned} \tag{B.39}$$

The scalar extraction operator shown in Eq. (B.38) ensures that only scalar quantities are extracted from an expression with mixed scalar, vector and tensor quantities in real space. Next we define the even-parity vector extraction operator to be

$$\mathcal{V}_l^{ij}(\boldsymbol{x},\boldsymbol{x}') = -\frac{2i}{(2\pi)^3}\int d^3k'\ k'^{-2}k'^i\left[e_l(\boldsymbol{k}')e^j(\boldsymbol{k}')+\tilde{e}_l(\boldsymbol{k}')\tilde{e}^j(\boldsymbol{k}')\right]\int d^3x'\ e^{i\boldsymbol{k}'\cdot(\boldsymbol{x}-\boldsymbol{x}')}. \tag{B.40}$$

Applying $\mathcal{V}_l^{ij}(\boldsymbol{x},\boldsymbol{x}')$ to Eq. (B.33) gives

$$\begin{aligned} A_l^{(V)}(\boldsymbol{x},\eta) &= \mathcal{V}_l^{ij}(\boldsymbol{x},\boldsymbol{x}')A_{ij}(\boldsymbol{x}',\eta) \\ &= -\frac{2i}{(2\pi)^3}\int d^3k'\ k'^{-2}k'^i\left[e_l(\boldsymbol{k}')e^j(\boldsymbol{k}')+\tilde{e}_l(\boldsymbol{k}')\tilde{e}^j(\boldsymbol{k}')\right]\int d^3x'\ e^{i\boldsymbol{k}'\cdot(\boldsymbol{x}-\boldsymbol{x}')}A_{ij}(\boldsymbol{x}',\eta). \end{aligned} \tag{B.41}$$

The vector extraction operator shown in Eq. (B.40) ensures that only vector quantities are extracted from an expression with mixed scalar, vector and tensor quantities in real space. Finally, the tensor extraction operator is defined by

$$\mathcal{T}_{lm}^{\ ij}(\boldsymbol{x},\boldsymbol{x}') = \frac{1}{(2\pi)^3}\int d^3k'\ \left[q_{lm}(\boldsymbol{k}')q^{ij}(\boldsymbol{k}')+\tilde{q}_{lm}(\boldsymbol{k}')\tilde{q}^{ij}(\boldsymbol{k}')\right]\int d^3x'\ e^{i\boldsymbol{k}'\cdot(\boldsymbol{x}-\boldsymbol{x}')}. \tag{B.42}$$

Applying $\mathcal{T}_{lm}^{ij}(\boldsymbol{x},\boldsymbol{x}')$ to Eq. (B.33) gives

$$\begin{aligned} A_{lm}^{(T)}(\boldsymbol{x},\eta) &= \mathcal{T}_{lm}^{ij}(\boldsymbol{x},\boldsymbol{x}')A_{ij}(\boldsymbol{x}',\eta) \\ &= \frac{1}{(2\pi)^3}\int d^3k'\ \left[q_{lm}(\boldsymbol{k}')q^{ij}(\boldsymbol{k}')+\tilde{q}_{lm}(\boldsymbol{k}')\tilde{q}^{ij}(\boldsymbol{k}')\right]\int d^3x'\ e^{i\boldsymbol{k}'\cdot(\boldsymbol{x}-\boldsymbol{x}')}A_{ij}(\boldsymbol{x}',\eta). \end{aligned} \tag{B.43}$$

The tensor extraction operator presented in Eq. (B.42) ensures that only tensor quantities are extracted from an expression with mixed scalar, vector and tensor quantities in real space. This extraction of the scalar, vector and tensor components is made possible by the various properties of the parity vectors (e_i and $\tilde{e}_i$) and polarization tensors (q_{ij} and $\tilde{q}_{ij}$).

However, scalar, vector and tensor extraction operators for extracting the Fourier amplitude of the scalar, vector and tensor contribution separately are of the forms:

$$\hat{\mathcal{S}}^{ij}(\boldsymbol{k},\boldsymbol{x}) = -\frac{1}{(2\pi)^{3/2}}\frac{3}{2k^4}\int d^3x\ k^i k^j e^{-i\boldsymbol{k}\cdot\boldsymbol{x}}, \tag{B.44}$$

and

$$\hat{\mathcal{V}}^{ij}(\boldsymbol{k},\boldsymbol{x}) = -\frac{1}{(2\pi)^{3/2}}\frac{2i}{k^2}\int d^3x\ k^i e^j(\boldsymbol{k})e^{-i\boldsymbol{k}\cdot\boldsymbol{x}}, \tag{B.45}$$

respectively. The alternate parity vector component can be extracted by replacing $e^j(\boldsymbol{k})$ with $\tilde{e}^j(\boldsymbol{k})$. The Fourier amplitude of the tensor contribution is given by

$$\hat{\mathcal{T}}^{ij}(\boldsymbol{k},\boldsymbol{x}) = \frac{1}{(2\pi)^{3/2}}\int d^3x\ q^{ij}(\boldsymbol{k})e^{-i\boldsymbol{k}\cdot\boldsymbol{x}}. \tag{B.46}$$

Similar to the vector case, the alternate polarization tensor component can be extracted by replacing $q^{ij}(\boldsymbol{k})$ with $\tilde{q}^{ij}(\boldsymbol{k})$. These extraction operators in Fourier space have been used in Eqs. (B.35), (B.36) and (B.37).

Now we will give an example to show exactly how these operators work. Consider a term of the type

$$\left[\Phi\partial_i\partial_j\Phi\right](\boldsymbol{x},\eta) = \frac{1}{(2\pi)^3}\left[\int d^3k_1\ \Phi(\boldsymbol{k}_1,\eta)e^{i\boldsymbol{k}_1\cdot\boldsymbol{x}}\right]\left[\int d^3k_2\ \Phi(\boldsymbol{k}_2,\eta)\left(-k_{2i}k_{2j}\right)e^{i\boldsymbol{k}_2\cdot\boldsymbol{x}}\right]. \tag{B.47}$$

The vector Fourier amplitude is then

$$\begin{aligned}\left[\Phi\partial_i\partial_j\Phi\right]^{(V)}(\boldsymbol{k},\eta) &= \hat{\mathcal{V}}^{ij}(\boldsymbol{k},\boldsymbol{x})\left[\Phi\partial_i\partial_j\Phi\right](\boldsymbol{x},\eta)\\ &= \frac{2i}{(2\pi)^{3/2}}\int d^3k_2\ \Phi(\boldsymbol{k}-\boldsymbol{k}_2,\eta)\Phi(\boldsymbol{k}_2,\eta)\frac{k^i\left[e^j(\boldsymbol{k})+\tilde{e}^j(\boldsymbol{k})\right]k_{2i}k_{2j}}{k^2},\end{aligned} \tag{B.48}$$

where we have made use of the aforementioned properties of the parity vectors and polarization tensors, and carried out the real space and k space integrals.

Appendix C

Second order tensors from linear vector modes

As mentioned in chapter 5, in this appendix we present current progress on the project on second order tensor modes sourced by linear vector modes.

C.1 The metric

The perturbed metric around background FLRW metric including first order vector quantities and second order tensor is shown below:

$$\bar{g}_{00} = -a^2,\ \bar{g}_{0i} = a^2\left[-S_i^{(1)}\right],\ \text{and}\ \bar{g}_{ij} = a^2\left[\gamma_{ij} + 2\partial_{(i}F_{j)}^{(1)} + \frac{1}{2}\,h_{ij}^{(2)}\right], \tag{C.1}$$

where $S_i^{(1)}$ and $F_i^{(1)}$ are first order divergenceless vectors, i.e. $\partial^i S_i^{(1)} = 0$ and $\partial^i F_i^{(1)} = 0$; $h_{ij}^{(2)}$ is the second order tracefree and divergenceless tensor, i.e. $\gamma^{ij}h_{ij}^{(2)} = 0$ and $\partial^j h_{ij}^{(2)} = 0$.

The components of the contravariant form of the metric are given

$$\bar{g}^{00} = -a^{-2}\left[1 - S_k^{(1)}S^{(1)k}\right],\ \bar{g}^{0i} = a^{-2}\left[-S^{(1)i} + 2S_k^{(1)}\partial^{(k}F^{(1)i)}\right], \tag{C.2}$$

and

$$\bar{g}^{ij} = a^{-2}\left[\gamma^{ij} - 2\partial^{(i}F^{(1)j)} - S^{(1)i}S^{(1)j} + 2\left(\partial^i F_k^{(1)} + \partial_k F^{(1)i}\right)\partial^{(k}F^{(1)j)} - \frac{1}{2}\,h^{(2)ij}\right]. \tag{C.3}$$

The components for the connection coefficients , at first order, in this case are

$$\delta^{(1)}\Gamma^0_{00} = 0,\ \delta^{(1)}\Gamma^0_{0i} = -\mathcal{H}S_i^{(1)},\ \delta^{(1)}\Gamma^i_{00} = -\mathcal{H}S^{(1)i} - S^{(1)i\prime}, \tag{C.4}$$

$$\begin{aligned}\delta^{(1)}\Gamma^0_{ij} &= \partial_{(i}S_{j)}^{(1)} + 2\mathcal{H}\partial_{(i}F_{j)}^{(1)} + \partial_{(i}F_{j)}^{(1)\prime},\\ \delta^{(1)}\Gamma^i_{0j} &= \frac{1}{2}\left[\left(\partial^i F_j^{(1)\prime} + \partial_j F^{(1)i\prime}\right) - \left(\partial_j S^{(1)i} - \partial^i S_j^{(1)}\right)\right],\end{aligned} \tag{C.5}$$

and

$$\delta^{(1)}\Gamma^{i}_{jk} = \partial_j\partial_k F^{(1)i} + \mathcal{H}S^{(1)i}\gamma_{jk}, \tag{C.6}$$

whereas at second order we have

$$\delta^{(2)}\Gamma^{0}_{00} = \mathcal{H}S^{(1)k}S^{(1)}_{k} + S^{(1)k}S^{(1)'}_{k},\ \delta^{(2)}\Gamma^{0}_{0i} = -S^{(1)k}\left[\partial_{(k}F^{(1)'}_{i)} - \partial_{[i}S^{(1)}_{k]}\right], \tag{C.7}$$

$$\delta^{(2)}\Gamma^{i}_{00} = 2\partial^{(i}F^{(1)k)}\left(S^{(1)'}_{k} + \mathcal{H}S^{(1)}_{k}\right), \tag{C.8}$$

$$\delta^{(2)}\Gamma^{0}_{ij} = \frac{1}{2}\mathcal{H}h^{(2)}_{ij} + \frac{1}{4}h^{(2)'}_{ij} - \mathcal{H}S^{(1)}_{k}S^{(1)k}\gamma_{ij} - S^{(1)k}\partial_i\partial_j F^{(1)}_{k}, \tag{C.9}$$

$$\delta^{(2)}\Gamma^{i}_{0j} = \frac{1}{4}h^{(2)i'}_{\ \ j} - \mathcal{H}S^{(1)i}S^{(1)}_{j} - 2\partial^{(i}F^{(1)k)}\left[\partial_{(k}F^{(1)'}_{j)} - \partial_{[j}S^{(1)}_{k]}\right], \tag{C.10}$$

$$\begin{aligned}\delta^{(2)}\Gamma^{i}_{jk} = {}& \frac{1}{4}\left(\partial_j h^{i(2)}_{\ \ k} + \partial_k h^{i(2)}_{\ \ j} - \partial^i h^{(2)}_{jk}\right) - 2\mathcal{H}S^{(1)}_{m}\partial^{(m}F^{(1)i)}\gamma_{jk} + S^{(1)i}\left[\partial_{(j}S^{(1)}_{k)}\right.\\ &\left. + 2\,\mathcal{H}\partial_{(j}F^{(1)}_{k)} + \partial_{(j}F^{(1)'}_{k)}\right] - 2\partial^{(i}F^{(1)m)}\partial_j\partial_k F^{(1)}_{m}.\end{aligned} \tag{C.11}$$

The components of the Ricci tensor at second order can now then be calculated

$$\begin{aligned}\delta^{(2)}R_{00} = {}& 2\partial^{(m}F^{(1)k)}\left(\partial_k F^{(1)''}_{m} + \mathcal{H}\partial_k F^{(1)'}_{m} + \partial_m S^{(1)'}_{k} + \mathcal{H}\partial_m S^{(1)}_{k}\right)\\ &+ \nabla^2 F^{(1)k}\left(S^{(1)'}_{k} + \mathcal{H}S^{(1)}_{k}\right) + 3\mathcal{H}S^{(1)m'}S^{(1)}_{m} + \partial^{(m}F^{(1)k)'}\partial_k F^{(1)'}_{m}\\ &+ \left[\frac{a''}{a} + \mathcal{H}^2\right]S^{(1)m}S^{(1)}_{m} - \frac{1}{2}\left(\partial_k S^{(1)m} - \partial^m S^{(1)}_{k}\right)\partial_i S^{j(1)},\end{aligned} \tag{C.12}$$

$$\begin{aligned}\delta^{(2)}R_{0i} = {}& -2\left(\mathcal{H}S^{m(1)} + \frac{1}{2}\nabla^2 F^{m(1)}\right)\left(\partial_{(m}F^{(1)'}_{i)} + \partial_{[m}S^{(1)}_{i]}\right) + \left(\partial_i\partial_j F^{(1)'}_{m}\right.\\ &\left. - \partial_j\partial_m F^{(1)'}_{i} + \partial_j\partial_i S^{(1)}_{m} - \partial_j\partial_m S^{(1)}_{i}\right)\partial^{(j}F^{(1)m)}\\ &- S^{(1)j}\left(\partial_{(i}F^{(1)''}_{j)} + \partial_{(i}S^{(1)'}_{j)}\right) + \partial_i\partial_j F^{(1)}_{m}\left(\partial^{(j}F^{(1)m)'} + \partial^{[m}S^{(1)j]}\right)\\ &+ 2\left[\frac{a''}{a} - \mathcal{H}^2\right]S^{(1)}_{m}\left(\partial^m F^{(1)}_{i} + \partial_i F^{(1)m}\right).\end{aligned} \tag{C.13}$$

$$\begin{aligned}\delta^{(2)}R_{ij} = {}& \frac{1}{4}h^{(2)''}_{ij} + \frac{1}{2}\mathcal{H}h^{(2)'}_{ij} + \frac{1}{2}\left[\frac{a''}{a} + \mathcal{H}^2\right]h^{(2)}_{ij} - \frac{1}{4}\nabla^2 h^{(2)}_{ij} - \partial_i\partial_j F^{(1)}_{m}\left(S^{(1)m'}\right.\\ &\left. + 2\mathcal{H}S^{(1)m} + \nabla^2 F^{(1)m}\right) - S^{(1)m}\left[\partial_i\partial_j F^{(1)'}_{m} - \partial_m\partial_{(i}F^{(1)'}_{j)} + \partial_i\partial_j S^{(1)}_{m}\right.\\ &\left. - \partial_m\partial_{(i}S^{(1)}_{j)}\right] - \frac{1}{2}\partial_i S^{(1)m}\partial_j S^{(1)}_{m} + \partial_i\partial^k F^{(1)m}\partial_j\partial_k F^{(1)}_{m} - \frac{1}{2}\left(\partial^k S^{(1)}_{j}\right.\\ &\left. + \partial^k F^{(1)'}_{j} + \partial_j F^{(1)k'}\right)\left(\partial_k S^{(1)}_{i} + 2\partial_{(i}F^{(1)'}_{k)}\right) - \mathcal{H}\left[2\partial^{(m}F^{(1)k)}\left(\partial_k S^{(1)}_{m}\right.\right.\\ &\left.\left. + \partial_m F^{(1)'}_{k}\right) + S^{(1)m}\left(\nabla^2 F^{(1)}_{m} + S^{(1)'}_{m}\right) + \left[\frac{a''}{a'} + \mathcal{H}\right]S^{(1)}_{m}S^{(1)m}\right]\gamma_{ij}.\end{aligned} \tag{C.14}$$

C.2 The EMT

Again we have perfect fluid at background level. Note that the three-velocity perturbation can be split into a scalar and vector part. However since only vector perturbation is taken into account at first order, here we have

$$\delta^{(1)}u^i = v^i_{(1)}, \tag{C.15}$$

where $v^i_{(1)}$ is divergencefree, i.e. $\partial_i v^i_{(1)} = 0$. Similar to the three-velocity perturbation, the energy flux $\delta^{(1)}q_j$ can also be split into a scalar and vector part. Again with only the vector quantity is taken into account at first order, we have

$$\delta^{(1)}q_i = q_{(1)i}, \tag{C.16}$$

where $q_{(1)i}$ is also divergencefree, i.e. $\partial^i q_{(1)i} = 0$. The perturbed spatial anisotropic pressure can be split into a scalar, vector and tensor part at each order. Keeping only the vector quantity at first order and the tensor quantity at second order, we then have

$$\delta^{(1)}\pi_{ij} = \partial_{(i}\pi_{(1)j)}, \tag{C.17}$$

and

$$\delta^{(2)}\pi_{ij} = \frac{1}{2}\pi_{(2)ij}, \tag{C.18}$$

at first and second order respectively. Note that the vector $\pi_{(1)j}$ is divergencefree, i.e. $\partial^i\pi_{(1)i} = 0$ and the tensor $\pi_{(2)ij}$ is divergencefree and tracefree, i.e. $\partial^j\pi_{(2)ij} = 0$ and $\gamma^{ij}\pi_{(2)ij} = 0$.

Components of the first order velocity perturbation and its contravariant form are

$$\delta^{(1)}u^\mu = \frac{1}{a}\left[0,\ v^i_{(1)}\right], \text{ and } \delta^{(1)}u_\mu = a\left[0,\ v_{(1)i} - S^{(1)}_i\right]. \tag{C.19}$$

At first order, the perturbed energy flux and its inverse has components of

$$\begin{aligned}\delta^{(1)}q_\mu &= \left[0,\ q_{(1)i}\right],\\ \delta^{(1)}q^\mu &= a^{-2}\left[0,\ q_{(1)i}\right],\end{aligned} \tag{C.20}$$

respectively. The anisotropic stress, at first order, therefore has components

$$\delta^{(1)}\pi_{00} = 0,\ \delta^{(1)}\pi_{0i} = 0,\ \delta^{(1)}\pi^k_{\ k} = 0, \tag{C.21}$$

whereas at second order we have

$$\begin{aligned}&\delta^{(2)}\pi_{00} = 0,\ \delta^{(2)}\pi_{0i} = -v^j_{(1)}\partial_{(j}\pi_{(1)i)},\\ &\delta^{(2)}\pi^k_{\ k} = 2\partial_{(i}\pi_{(1)j)}\partial^{(i}F^{(1)j)}.\end{aligned} \tag{C.22}$$

Now we can present the components of the EMT. At first order, they are

$$\begin{aligned}
&\delta^{(1)}T_{00} = 0,\\
&\delta^{(1)}T_{0i} = -a^2\left(\rho + P\right)v_{(1)i} + a^2\rho S^{(1)}_i - aq_{(1)i},\\
&\delta^{(1)}T_{ij} = 2a^2P\partial_{(i}F^{(1)}_{j)} + \partial_{(j}\pi_{(1)i)}.
\end{aligned} \tag{C.23}$$

And at second order they look like

$$\begin{aligned}
&\delta^{(2)}T_{00} = 0,\ \delta^{(2)}T_{0i} = -v^j_{(1)}\partial_{(j}\pi_{(1)i)},\\
&\delta^{(2)}T_{ij} = \frac{1}{2}a^2Ph^{(2)}_{ij} + 2aq_{(1)(i}\left(v_{(1)j)} - S^{(1)}_{j)}\right) + \frac{1}{2}\pi_{(2)ij}\\
&\qquad\qquad + a^2\left(\rho + P\right)\left(v_{(1)i} - S^{(1)}_i\right)\left(v_{(1)j} - S^{(1)}_j\right).
\end{aligned} \tag{C.24}$$

Expressions for $\bar{T} = \bar{T}^{\alpha}_{\alpha}$ at first and second order are

$$\delta^{(1)}T = \rho S^{(1)}_k S^{(1)k}, \tag{C.25}$$

and

$$\delta^{(2)}T = -\rho S^{(1)k}S^{(1)}_k + \left(\rho + P\right)v^i_{(1)}v_{(1)i} + \frac{2}{a}q^i_{(1)}v_{(1)i} - \frac{2}{a^2}\partial^{(i}F^{(1)j)}\partial_{(i}\pi_{(1)j)}, \tag{C.26}$$

respectively.

C.3 The EFEs

If we consider again the choice of Poission gauge, together with perfect fluid background and no energy flux and anisotropic stress at first order, then the first order trace reversed EFEs provide us with the equations

$$\frac{1}{2}\nabla^2 S^{(1)}_i - \left[\frac{a''}{a} + \mathcal{H}^2\right]S^{(1)}_i = \kappa^2\left[-a^2(\rho + P)v_{(1)i} + \frac{a}{2}(\rho + 3P)S^{(1)}_i\right], \tag{C.27}$$

and

$$\partial_{(i}S^{(1)\prime}_{j)} + 2\mathcal{H}\partial_{(i}S^{(1)}_{j)} = 0, \tag{C.28}$$

where Eq. (C.27) gives us a relation between $v_{(1)i}$ and $S^{(1)}_i$ and Eq. (C.28) gives us an evolution equation for $S^{(1)}_i$. At second order we choose to derive the radiation era equation, we then have

$$\begin{aligned}
h^{(2)\prime\prime}_{ij} + 2\mathcal{H}h^{(2)\prime}_{ij} - \nabla^2 h^{(2)}_{ij} &= 4S^{(1)m}\partial_i\partial_j S^{(1)}_m - 2S^{(1)m}\partial_m\partial_{(i}S^{(1)}_{j)} + 2\partial_i S^{m(1)}\partial_j S^{(1)}_m\\
&\quad + 2\partial_m S^{(1)}_i\partial^m S^{(1)}_j + \frac{1}{4\mathcal{H}^2}\nabla^2 S^{(1)}_i\nabla^2 S^{(1)}_j\\
&\quad + 4\left(\mathcal{H}^2 S^{(1)}_m S^{m(1)} + \mathcal{H}S^{m(1)}S^{(1)\prime}_m\right)\gamma_{ij}.
\end{aligned} \tag{C.29}$$

C.4 Tensor modes evolution equation in Fourier space

Similar to the second order vector modes from linear scalar modes case, we now need to apply the projection operator in order to obtain the pure tensor quantity and also express Eq. (C.29) in Fourier space. However, this time a different projection operator applies to our case. Instead of using the vector projection operator shown in Eq. (B.45), we will now use the tensor projection operator $\hat{\mathcal{T}}^{ij}(\boldsymbol{k},\boldsymbol{x})$ shown in Eq. (B.46). If we apply $\hat{\mathcal{T}}^{ij}(\boldsymbol{k},\boldsymbol{x})$ to the left hand side of Eq. (C.29), the term $h_{ij}^{(2)'}$ will become

$$\begin{aligned}\hat{\mathcal{T}}^{ij}(\boldsymbol{k},\boldsymbol{x})\left[h_{ij}^{(2)'}\right](\boldsymbol{x},\eta) &= \frac{q^{ij}(\boldsymbol{k})}{(2\pi)^{3/2}}\frac{1}{(2\pi)^{3/2}}\int d^3k' h''(\boldsymbol{k'},\eta)q_{ij}(\boldsymbol{k'})\int d^3x e^{i(\boldsymbol{k'}-\boldsymbol{k})\cdot\boldsymbol{x}} \\ &= h'(\boldsymbol{k},\eta),\end{aligned} \tag{C.30}$$

where the last line is obtained using the fact that $q^{ij}(\boldsymbol{k})q_{ij}(\boldsymbol{k}) = 1$. Similar calculation can be done for the terms $h_{ij}^{(2)''}$ and $\nabla^2 h_{ij}^{(2)}$. As for the right hand side of Eq. (C.29), the term contains the factor γ_{ij} once $\hat{\mathcal{T}}^{ij}(\boldsymbol{k},\boldsymbol{x})$ is applied to it since $\gamma_{ij}q^{ij}(\boldsymbol{k}) = 0$. We shall now demonstrate how to calculate one of the other terms and the rest shall apply similarly. If we apply $\hat{\mathcal{T}}^{ij}(\boldsymbol{k},\boldsymbol{x})$ to the term $\nabla^2 S_i^{(1)}\nabla^2 S_j^{(1)}$, it will then become

$$\begin{aligned}\hat{\mathcal{T}}^{ij}(\boldsymbol{k},\boldsymbol{x})\left[\nabla^2 S_i^{(1)}\nabla^2 S_j^{(1)}\right](\boldsymbol{x},\eta) &= \frac{q^{ij}(\boldsymbol{k})}{(2\pi)^{3/2}}\frac{1}{(2\pi)^3}\int d^3k' S(\boldsymbol{k'},\eta)e_i(\boldsymbol{k'})k'_m k'^m \\ &\quad\times\int d^3\tilde{k} S(\tilde{\boldsymbol{k}},\eta)e_j(\tilde{\boldsymbol{k}})\tilde{k}^m\tilde{k}_m\int d^3x e^{i[\tilde{\boldsymbol{k}}-(\boldsymbol{k}-\boldsymbol{k'})]\cdot\boldsymbol{x}} \\ &= \frac{q^{ij}(\boldsymbol{k})}{(2\pi)^{3/2}}\int d^3k' S(\boldsymbol{k'},\eta)e_i(\boldsymbol{k'})S(\boldsymbol{k}-\boldsymbol{k'},\eta) \\ &\quad\times e_j(\boldsymbol{k}-\boldsymbol{k'})k'^2|\boldsymbol{k}-\boldsymbol{k'}|^2,\end{aligned} \tag{C.31}$$

where the last line is obtained from the fact that $k'_m k'^m = k'^2$. Collecting terms, Eq. (C.29) now becomes (in the Fourier space) that

$$h''(\boldsymbol{k},\eta) + 2\mathcal{H}h'(\boldsymbol{k},\eta) + k^2 h(\boldsymbol{k},\eta) = \Upsilon(\boldsymbol{k},\eta), \tag{C.32}$$

where

$$\begin{aligned}\Upsilon(\boldsymbol{k},\eta) = \frac{-q^{ij}(\boldsymbol{k})}{(2\pi)^{3/2}}\int d^3k' S(\boldsymbol{k'},\eta)S(\boldsymbol{k}-\boldsymbol{k'},\eta)\Big\{&2e_m(\boldsymbol{k'})e^m(\boldsymbol{k}-\boldsymbol{k'})k'_i k'_j \\ &- 2\left[e_j(\boldsymbol{k'})k'_i + e_i(\boldsymbol{k'})k'_j\right]e^m(\boldsymbol{k}-\boldsymbol{k'})k'_m + 2e_i(\boldsymbol{k'})e_j(\boldsymbol{k}-\boldsymbol{k'}) \\ &\times(k'_m k^m - k'^2) - \frac{1}{4\mathcal{H}^2}e_i(\boldsymbol{k'})e_j(\boldsymbol{k}-\boldsymbol{k'})k'^2|\boldsymbol{k}-\boldsymbol{k'}|^2\Big\}.\end{aligned} \tag{C.33}$$

Eq. (C.32) is a wave equation with source terms that are represented as $\Upsilon(\boldsymbol{k},\eta)$. What we then wish to do is to solve this wave equation in order to find a solution for $h(\boldsymbol{k},\eta)$

and hence to be able to calculate the power spectrum of $h(\boldsymbol{k},\eta)$. However, we notice from expression presented in Eq. (C.33) that a solution is needed for $S(\boldsymbol{k},\eta)$. This can be achieved by applying the vector extraction operator $\mathcal{V}_l^{ij}(\boldsymbol{x},\boldsymbol{x}')$ from Eq. (B.45) to Eq. (C.28). Therefore, the Fourier convolution of Eq. (C.28) is

$$S'(\boldsymbol{k},\eta) + 2\mathcal{H}S(\boldsymbol{k},\eta) = 0. \tag{C.34}$$

This can easily be solved with some initial condition at η_0 as

$$S(\boldsymbol{k},\eta) = a_0^2 S_0(\boldsymbol{k}) a^{-2}(\eta), \tag{C.35}$$

where $a_0 = a(\eta_0)$ and $S_0(\boldsymbol{k}) = S(\boldsymbol{k},\eta_0)$.

C.5 Solving the wave equation with a source

Here we will show how one can solve the wave equation Eq. (C.32) in order to obtain a solution for $h(\boldsymbol{k},\eta)$. This can be done using the Green's function method. But first we introduce a new variable $u(\boldsymbol{k},\eta) = a(\eta)h(\boldsymbol{k},\eta)$ and rewrite Eq. (C.32) with the new variable we obtain (considering radiation era with $a''/a = 0$):

$$u''(\boldsymbol{k},\eta) + k^2 u(\boldsymbol{k},\eta) = a(\eta)\Upsilon(\boldsymbol{k},\eta). \tag{C.36}$$

We can solve Eq. (C.36) using a Wronskian Green's function method and obtain its solution

$$\begin{aligned} u(\boldsymbol{k},\eta) &= \int_{\eta_0}^{\eta} G_u(\eta,\tilde{\eta}) a(\tilde{\eta}) \Upsilon(\boldsymbol{k},\tilde{\eta}) d\tilde{\eta} \\ &= \frac{1}{|k|}\int_{\eta_0}^{\eta} \sin\left(|k|(\eta-\tilde{\eta})\right) a(\tilde{\eta})\Upsilon(\boldsymbol{k},\tilde{\eta}) d\tilde{\eta}, \end{aligned} \tag{C.37}$$

where $G_u(\eta,\tilde{\eta})$ is the Green's function for $u(\boldsymbol{k},\eta)$. Therefore, a solution for $h(\boldsymbol{k},\eta)$ is:

$$\begin{aligned} h(\boldsymbol{k},\eta) &= \frac{1}{a(\eta)} u(\boldsymbol{k},\eta) \\ &= \frac{1}{|k|a(\eta)}\int_{\eta_0}^{\eta} \sin\left(|k|(\eta-\tilde{\eta})\right) a(\tilde{\eta})\Upsilon(\boldsymbol{k},\tilde{\eta}) d\tilde{\eta}. \end{aligned} \tag{C.38}$$

C.6 Tensor mode power spectrum

Here we shall use the same definition for tensor mode power spectrum as shown in Eq. (3.69):

$$\langle h^*(\boldsymbol{k_1},\eta) h(\boldsymbol{k_2},\eta)\rangle = \frac{2\pi^2}{k^3}\delta^3(\boldsymbol{k_1}-\boldsymbol{k_2})\mathcal{P}_h(k,\eta). \tag{C.39}$$

From Eq. (C.38) we can calculate the left hand side of Eq. (C.39):

$$\begin{aligned}\langle h^*(\boldsymbol{k_1},\eta)h(\boldsymbol{k_2},\eta)\rangle = &\frac{1}{k^2a^2(\eta)}\int_{\eta_0}^{\eta}d\tilde{\eta}_2\int_{\eta_0}^{\eta}d\tilde{\eta}_1\sin\left(k(\eta-\tilde{\eta}_1)\right)\sin\left(k(\eta-\tilde{\eta}_2)\right)a(\tilde{\eta}_1)a(\tilde{\eta}_1)\\ &\frac{{a_0}^4q^{*ij}(\boldsymbol{k_1})q^{ab}(\boldsymbol{k_2})}{a^2(\tilde{\eta}_1)a^2(\tilde{\eta}_2)}\int d^3k_1'\int d^3k_2'\ S_0(k_1')S_0(k_1-k_1')S_0(k_2')S_0(k_2-k_2')\\ &\left\{2e_m(\boldsymbol{k_1'})e^m(\boldsymbol{k_1}-\boldsymbol{k_1'})k_{1i}'k_{1j}'-2\left[e_j(\boldsymbol{k_1'})k_{1i}'+e_i(\boldsymbol{k_1'})k_{1j}'\right]e^m(\boldsymbol{k_1}-\boldsymbol{k_1'})\right.\\ &\times k_{1m}'+2e_i(\boldsymbol{k_1'})e_j(\boldsymbol{k_1}-\boldsymbol{k_1'})(k_{1m}'k_1^m-k_1^{'2})-\frac{1}{4H^2}e_i(\boldsymbol{k_1'})e_j(\boldsymbol{k_1}-\boldsymbol{k_1'})\\ &\left.\times\ k_1^{'2}|\boldsymbol{k}_1-\boldsymbol{k_1'}|^2\right\}\left\{2e_m(\boldsymbol{k_2'})e^m(\boldsymbol{k_2}-\boldsymbol{k_2'})k_{2a}'k_{2b}'+2e_a(\boldsymbol{k_2'})e_b(\boldsymbol{k_2}-\boldsymbol{k_2'})\right.\\ &\times(k_{2m}'k_2^m-k_2^{'2})-2\left[e_b(\boldsymbol{k_2'})k_{2a}'+e_a(\boldsymbol{k_2'})k_{2b}'\right]e^m(\boldsymbol{k_2}-\boldsymbol{k_2'})k_{2m}'\\ &\left.-\frac{1}{4H^2}e_a(\boldsymbol{k_2'})e_b(\boldsymbol{k_2}-\boldsymbol{k_2'})k_2^{'2}|\boldsymbol{k}_2-\boldsymbol{k_2'}|^2\right\}\\ &\times\langle\hat{E}^*(\boldsymbol{k_1'})\hat{E}^*(\boldsymbol{k_1}-\boldsymbol{k_1'})\hat{E}(\boldsymbol{k_2'})\hat{E}(\boldsymbol{k_2}-\boldsymbol{k_2'})\rangle.\end{aligned}\tag{C.40}$$

Again, using Wick's theorem and the properties that $e^a(\boldsymbol{k})\bar{e}_a(\boldsymbol{k})=0$, $e^a(\boldsymbol{k})e_a(\boldsymbol{k})=1$, $\bar{e}^a(\boldsymbol{k})\bar{e}_a(\boldsymbol{k})=1$, $k^ae_a(\boldsymbol{k})=0$, $k^a\bar{e}_a(\boldsymbol{k})=0$, $k^aq_{ab}(\boldsymbol{k})=0$ and $k^a\bar{q}_{ab}(\boldsymbol{k})=0$, we can solve for one of the k integral and arrive at the expression

$$\begin{aligned}\mathcal{P}_h(k,\eta) = &\frac{{a_0}^4k}{2\pi^2a^2(\eta)}\int_{\eta_0}^{\eta}d\tilde{\eta}_2\int_{\eta_0}^{\eta}d\tilde{\eta}_1\sin\left(k(\eta-\tilde{\eta}_1)\right)\sin\left(k(\eta-\tilde{\eta}_2)\right)\frac{1}{a(\tilde{\eta}_1)a(\tilde{\eta}_2)}\\ &\times\int d^3k'q^{*ij}(\boldsymbol{k})q^{ab}(\boldsymbol{k}){S_0}^2(k'){S_0}^2(k-k')\left\{2e_m(\boldsymbol{k'})e^m(\boldsymbol{k}-\boldsymbol{k'})k_a'k_b'\right.\\ &-2\left[e_b(\boldsymbol{k'})k_a'+e_a(\boldsymbol{k'})k_b'\right]e^m(\boldsymbol{k}-\boldsymbol{k'})k_m'+2e_a(\boldsymbol{k'})e_b(\boldsymbol{k}-\boldsymbol{k'})(k_m'k^m-k^{'2})\\ &-\frac{1}{4\mathcal{H}^2}e_a(\boldsymbol{k'})e_b(\boldsymbol{k}-\boldsymbol{k'})k^{'2}(k-k')^2+2e_m(\boldsymbol{k}-\boldsymbol{k'})e^m(\boldsymbol{k'})k_a'k_b'\\ &-2\left[e_b(\boldsymbol{k}-\boldsymbol{k'})k_a'+e_a(\boldsymbol{k}-\boldsymbol{k'})k_b'\right]e^m(\boldsymbol{k'})k_m-\frac{1}{4\mathcal{H}^2}e_a(\boldsymbol{k}-\boldsymbol{k'})e_b(\boldsymbol{k'})\\ &\left.\times k^{'2}(k-k')^2+2e_a(\boldsymbol{k}-\boldsymbol{k'})e_b(\boldsymbol{k'})[k^2-k_m'k^m-(k-k')^2]\right\}\\ &\times\left\{2e_m(\boldsymbol{k'})e^m(\boldsymbol{k}-\boldsymbol{k'})k_i'k_j'-2\left[e_j(\boldsymbol{k'})k_i'+e_i(\boldsymbol{k'})k_j'\right]e^m(\boldsymbol{k}-\boldsymbol{k'})k_m'\right.\\ &\left.+2e_i(\boldsymbol{k'})e_j(\boldsymbol{k}-\boldsymbol{k'})(k_m'k^m-k^{'2})-\frac{1}{4\mathcal{H}^2}e_i(\boldsymbol{k'})e_j(\boldsymbol{k}-\boldsymbol{k'})k^{'2}(k-k')^2\right\}.\end{aligned}\tag{C.41}$$

This is where we have reached at the time of writing up this thesis. Note however that it is probably not possible to solve the k integral in Eq. (C.41) analytically, and hence approximate solution is needed.

Bibliography

[1] Albrecht, A., *et al.*, arXiv:astro-ph/0609591.

[2] Alcock, C., and Paczynski, B., Nature 281 (1979) 358.

[3] Alexander, S., Biswas, T., Notari, A., and Vaid, D., arXiv: 0712.0370.

[4] Alnes, H., Amarzguioui, M., and Gron, O., *Phys. Rev.* **D** 73 (2006) 083519.

[5] Amendola, L., and Tocchini-Valentini, D., *Phys. Rev.* **D** 66 (2002) 043528.

[6] Ananda, K.N., Exact and perturbative cosmological dynamics, PhD thesis, University of Portsmouth, 2006.

[7] Ananda, K.N., Clarkson, C., and Wands, D., *Phys. Rev.* **D** 75 (2007) 123518.

[8] Arroja, F., Assadullahi, H., Koyama, K., and Wands, D., arXiv: 0907.3618 [astro-ph.CO].

[9] Assadullahi, H., and Wands, D., arXiv: 0901.0989 [astro-ph.CO].

[10] Assadullahi, H., and Wands, D., arXiv: 0907.4073 [astro-ph.CO].

[11] Astier, P., *et al.*, *Astron. Astrophys.* 447 (2006) 31.

[12] Bardeen, J.M., *Phys. Rev.* **D** 22 (1980) 1882.

[13] Bardeen, J.M., Bond, J.R., Kaiser, N., and Szalay, A.S., *Astrophys. J.* 304 (1986) 15.

[14] Bartolo, N., Komatsu, E., Matarrese, S., and Riotto, A., *Phys. Reports* 402 (2004) 103.

[15] Bartolo, N., Matarrese, S., and Riotto, A., *JCAP* 0508 (2005) 010.

[16] Bartolo, N., Matarrese, S., and Riotto, A., *JCAP* 0510 (2005) 010.

[17] Bassett, B.A., and Kunz, M., *Astrophys. J.* 607 (2004) 661.

[18] Bassett, B.A., and Kunz, M., *Phys. Rev.* **D** 69 (2004) 101305.

[19] Bassett, B.A., Tsujikawa, S., and Wands, D., *Rev. Mod. Phys.* 78 (2006) 537.

[20] Battefeld, T.J., and Brandenberger, R., *Phys. Rev.* **D** 70 (2004) 121302.

[21] Baumann, D., arXiv:0907.5424 [hep-th].

[22] Baumann, D., Steinhardt, P.J., Takahashi, K., and Ichiki, K., *Phys. Rev.* **D** 76 (2007) 084019.

[23] Bennett, C.L., *et al. Astrophys. J.* 464 (1996) L1.

[24] Bernstein, G., *Astrophys. J.* 637 (2006) 598.

[25] Bertolami, O., Gil Pedro, F., and Le Delliou, M., *Phys. Letts. B* 654 (2007) 165.

[26] Bertschinger, E., astro-ph/9503125.

[27] Billyard, A.P., and Coley, A.A., *Phys. Rev.* **D** 61 (2000) 083503.

[28] Biswas, T., Mansouri, R., and Notari, A., *JCAP* 0712 (2007) 017.

[29] Blake, C.A., Abdalla, F.B., Bridle, S.L., and Rawlings, S., *New Astron. Rev.* 48 (2004) 1063.

[30] Bojowald, M., and Hossain, G.M., *Class. Quantum Grav.* 24 (2007) 4816.

[31] Bolejko, K., and Wyithe, J.S.B., *JCAP* 02 (2009) 020.

[32] Bondi, H., *Mon. Not. Roy. Astr. Soc.* 107 (1947) 410; reprinted in *Gen. Rel. Grav.* 11 (1999) 1783.

[33] Bonvin, C., Durrer, R., and Kunz, M., *Phys. Rev. Lett.* 96 (2006) 191302.

[34] Boyle, L.A., Steinhardt, P.J., and Turok, N., *Phys. Rev.* **D** 69 (2004) 127302.

[35] Brandenberger, R., Kahn, R., and Press, W., *Phys. Rev.* **D** 28 (1983) 1809.

[36] Bruni, M., Dunsby, P.K.S., and Ellis, G.F.R., *Astrophys. J.* 395 (1992) 34.

[37] Bruni, M., Ellis, G.F.R., and Dunsby, P.K.S., *Class. Quantum Grav.* 9 (1992) 921.

[38] Bruni, M., Matarrese, S., Mollerach, S., and Sonego, S., *Class. Quantum Grav.* 14 (1997) 2585.

[39] Bruni, M., and Sopuerta, C.F., *Class. Quantum Grav.* 16 (1999) L29.

[40] Bruni, M., Gualtier, L., and Sopuerta, C.F., *Class. Quantum Grav.* 20 (2003) 535.

[41] Bucher, M., Moodley, K., and Turok, N., *Phys. Rev.* **D** 62 (2000) 083508.

[42] Buchert, T., *Gen. Rel. Grav.* 32 (2000) 105.

[43] Buchert, T., *Gen. Rel. Grav.* 40 (2008) 467.

[44] Caldwell, R.R., and Stebbins, A., *Phys. Rev. Lett.* 100 (2008) 191302.

[45] Carbone, C., and Matarrese, S., *Phys. Rev.* **D** 71 (2005) 043508.

[46] Carbone, C., Baccigalupi, C., and Matarrese, S., *Phys. Rev.* **D** 73 (2006) 063503.

[47] Carroll, S.M., Press, W.H., and Turner, E.L., *Ann. Rev. Astr. Astrophys.* 30 (1992) 499.

[48] Célérier, M.-N., *Astron. Astrophys.* 353 (2000) 63.

[49] Célérier, M.-N., *New Advances in Physics* 1 (2007) 29.

[50] Chang, T.-C., Pen, U.-L., Peterson, J.B., and McDonald, P., *Phys. Rev. Lett.* 100 (2008) 091303.

[51] Chibisov, G., and Mukhanov, V., *Mon. Not. Roy. Astr. Soc.* 200 (1982) 535.

[52] Christopherson, A.J., Malik, K.A., and Matravers, D.R., *Phys. Rev.* **D** 79 (2009) 123523.

[53] Chung, D.J.H., and Romano, A.E., *Phys. Rev.* **D** 74 (2006) 103507.

[54] Clarkson, C., Cortês, M., and Bassett, B., *JCAP* 8 (2007) 11.

[55] Clifton, T., Ferreira, P.G., and Land, K., *Phys. Rev. Lett.* 101 (2008) 131302.

[56] Clifton, T., and Ferreira, P.G., *JCAP* 10 (2009) 26.

[57] Coles, P., and Lucchin, F., 2002, *The Origin and Evolution of Cosmic Structure*, (John Wiley & Sons, Ltd).

[58] Cooray, A.R., and Huterer, D., *Astrophys. J.* 513 (1999) L95.

[59] Crocco, L., ZAMM 17 (1937) 1.

[60] Davis, M., and Peebles, P.J.E., *Astrophys. J.* 267 (1983) 465.

[61] Dodelson, S., 2003, *Modern Cosmology*, (Academic Press).

[62] Dufaux, J.F., Bergman, A., Felder, G.N., Kofman, L., and Uzan, J.-P., *Phys. Rev.* **D** 76 (2007) 123517.

[63] Dunkley, J., *et al.* [WMAP5 Collaboration], *Astrophys. J. Suppl.* 180 (2009) 306.

[64] Dunsby, P.K.S., Bruni, M., and Ellis, G.F.R., *Astrophys. J.* 395 (1992) 54.

[65] Durrer, R., *Phys. Rev. Lett.* 72 (1994) 3301.

[66] Durrer, R., 2008, *The Cosmic Microwave Background*, (Cambridge University Press, Cambridge).

[67] Easther, R., Giblin, J.T., and Lim, E.A., *Phys. Rev. Lett.* 99 (2007) 221301.

[68] Efstathiou, G., *Mon. Not. Roy. Astr. Soc.* 310 (1999) 842.

[69] Ehlers, J., *Gen. Rel. Grav.* 25 (1993) 1225.

[70] Eisenstein, D.J., *et al.*, *Astrophys. J.* 633 (2005) 560.

[71] Eisenstein, D.J., and Hu, W., *Astrophys. J.* 496 (1998) 605.

[72] Ellis, G.F.R., Proceedings of the XLVII Enrico Fermi Summer School, edited by Sachs, R.K., 1971.

[73] Ellis, G.F.R., Cargese Lecturs in Physics, edited by Schatzman, E., New York, US, 1973, Gordan and Breach.

[74] Ellis, G.F.R., and Bruni, M., *Phys. Rev.* **D** 40 (1989) 1804.

[75] Ellis, G.F.R., Bruni, M., and Hwang, J., *Phys. Rev.* **D** 42 (1990) 1035.

[76] Ellis, G.F.R., Hwang, J., and Bruni, M., *Phys. Rev.* **D** 40 (1989) 1819.

[77] Ellis, G.F.R., and van Elst, H., gr-qc/9812046.

[78] Enqvist, K., and Mattsson, T., *JCAP* 0702 (2007) 019.

[79] Farrar, G.R., and Peebles, P.J.E., *Astrophys. J.* 604 (2004) 1.

[80] February, S., Clarkson, C., Larena, J., and Smith, M., in preparation.

[81] Feldman, H., and Brandenberger, R., *Phys. Letts. B* 227 (1989) 359.

[82] Freedman, W.L., et. al., *Astrophys. J.* 553 (2001) 47.

[83] Garcia-Bellido, J., and Haugbølle, T., *JCAP* 0804 (2008) 003.

[84] Gasperini, M., and Veneziano, G., *Phys. Reports* 373 (2003) 1.

[85] Gerke, B.F., and Efstathiou, G., *Mon. Not. Roy. Astr. Soc.* 335 (2002) 33.

[86] Green, A.M., and Liddle, A.R., *Phys. Rev.* **D** 56 (1997) 6166.

[87] Goodman, J., *Phys. Rev.* **D** 52 (1995) 1821.

[88] Gopal, R., and Sethi, S., *Mon. Not. Roy. Astr. Soc.* 363 (2005) 521.

[89] Gorski, K.M., *et al. Astrophys. J.* 464 (1996) L11.

[90] Gouda, N., and Sasaki, M., *Prog. Theor. Phys.* 76 (1986) 1016.

[91] Guth, A.H., *Phys. Rev.* **D** 23 (1981) 347.

[92] Harrison, E.R., *Rev. Mod. Phys.* 39 (1967) 862.

[93] Harrison, E.R., *Phys. Rev.* **D** 1 (1970) 2726.

[94] Hawking, S.W., *Astrophys. J.* 145 (1966) 544.

[95] Heckman, G., and Schücking, E., *Zeitshrift fur Astroph.* 38 (1955) 95.

[96] Hinshaw, G., *et al.* [WMAP5 Collaboration], *Astrophys. J. Suppl.* 180 (2009) 225.

[97] Hlozek, R., Cortês, M., Clarkson, C., and Bassett, B., *Gen. Rel. Grav.* 40 (2008) 285.

[98] Hollenstein, L., Caprini, C., Crittenden, R., and Maartens, R., *Phys. Rev.* **D** 77 (2008) 063517.

[99] Hu, W., and Sugiyama, N., *Astrophys. J.* 471 (1996) 542.

[100] Huang, Z.-Y., Wang, B., and Su, R.-K., *Int. Journ. Mod. Phys. A* 22 (2007) 1819.

[101] http://h1survey.phys.cmu.edu/

[102] Hwang, J.C., *Phys. Rev.* **D** 48 (1993) 3544.

[103] Hwang, J., and Noh, H., *Phys. Rev.* **D** 76 (2007) 13527.

[104] Hwang, J., and Noh, H., *JCAP* 0712 (2007) 003.

[105] Hwang, J.C., and Vishniac, E., *Astrophys. J.* 353 (1990) 1.

[106] Ichiki, K., Ohno, H., Hanayama, H., and Sugiyama, N., Science 311 (2006) 827.

[107] Ishibashi, A., and Wald, R.M., *Class. Quantum Grav.* 23 (2006) 235.

[108] Jia, J., and Zhang, H., *JCAP* 12 (2008) 002.

[109] Jimenez, R., and Loeb, A., *Astrophys. J.* 537 (2002) 37.

[110] Kaiser, N., *Mon. Not. Roy. Astr. Soc.* **227** (1987) 1.

[111] Kamionkowski, M., Kosowsky, A., and Stebbins, A., *Phys. Rev. Lett.* 78 (1997) 2058.

[112] Kamionkowski, M., Kosowsky, A., and Stebbins, A., *Phys. Rev.* **D** 55 (1997) 7368.

[113] Kawamura, S., *et al.*, *J. Phys. Conf. Ser.* 120 (2008) 032004.

[114] Knox, L., and Song, Y.-S., *Phys. Rev. Lett.* 89 (2002) 011303.

[115] Kobayashi, T., Maartens, R., Shiromizu, T., and Takahashi, K., *Phys. Rev.* **D** 75 (2007) 103501.

[116] Kodama, H., and Sasaki, M., *Prog. Theor. Phys. Suppl.* 78 (1984) 1.

[117] Komatsu, E., *et al.* [WMAP5 Collaboration], *Astrophys. J. Suppl.* 180 (2009) 330.

[118] Kowalski, M., *et al.*, *Astrophys. J.* 686 (2008) 749.

[119] Kunz, M., astro-ph/0702615.

[120] Lemaître, G., *Ann. Soc. Sci. Bruxelles* A53 (1933) 51; reprinted in *Gen. Rel. Grav.* 29 (1997) 641.

[121] Lahav, O., Rees, M.J., Lilje, P.B., and Primack, J.R., *Mon. Not. Roy. Astr. Soc.* 251 (1991) 128.

[122] Lewis, A., *Phys. Rev.* **D** 70 (2004) 043518.

[123] Lewis, A., *Phys. Rev.* **D** 70 (2004) 043011.

[124] Li, C., Holz, D.E., and Cooray, A., *Phys. Rev.* **D** 75 (2007) 10353.

[125] Liddle, A.R., and Green, A.M., *Phys. Reports* 307 (1998) 125.

[126] Liddle, A.R., and Lyth, D.H., (2000) *Cosmological Inflation and Large-Scale Structure*, (Cambridge University Press, Cambridge).

[127] Liddle, A.R., and Lyth, D.H., *Phys. Letts. B* 291 (1992) 391.

[128] Lifshitz, E.M., *J. Phys. USSR* 10 (1946) 116.

[129] Lifshitz, E.M., and Khalatnikov, I., *Adv. Phys.* 12 (1963) 185.

[130] http://www.ligo.caltech.edu/

[131] Linde, A., Linde, D., and Mezhlumian, A., *Phys. Letts. B* 345 (1995) 203.

[132] Linder, E.V., *Phys. Rev. Lett.* 90 (2003) 091301.

[133] Linder, E.V., *Astropart. Phys.* 24 (2005) 391.

[134] http://lisa.jpl.nasa.gov/

[135] http://www.lisa.aei-hannover.de/

[136] Lu, T.H.-C., and Hellaby, C., *Class. Quantum Grav.* 24 (2007) 4107.

[137] Lyth, D.H., Malik, K.A., and Sasaki, M., *JCAP* 0505 (2005) 004.

[138] Lyth, D., and Riotto, A., *Phys. Reports* 314 (1999) 1.

[139] Ma, C.P., and Bertschinger, E., *Astrophys. J.* 455 (1995) 7.

[140] Maeda, S., Kitagawa, S., Kobayashi, T., and Shiromizu, T., *Class. Quantum Grav.* 26 (2009) 135014.

[141] Malik, K.A., and Matravers, D.R., *Class. Quantum Grav.* 25 (2008) 193001.

[142] Malik, K.A., and Wands, D., *Class. Quantum Grav.* 21 (2004) L65.

[143] Malik, K.A., and Wands, D., *Phys. Reports* 475 (2009) 1.

[144] Mangilli, A., Bartolo, N., Matarrese, S., and Riotto, A., *Phys. Rev.* **D** 78 (2008) 083517.

[145] Maor, I., Brustein, R., McMahon, J., and Steinhardt, P.J., *Phys. Rev.* **D** 65 (2002) 123003.

[146] Matarrese, S., Mollerach, S., and Bruni, M., *Phys. Rev.* **D** 58 (1998) 043504.

[147] Matarrese, S., Mollerach, S., Notari, A., and Riotto, A., *Phys. Rev.* **D** 71 (2005) 043502.

[148] Matarrese, S., Pantano, O., and Saez, D., *Phys. Rev.* **D** 47 (1993) 1311.

[149] Matarrese, S., Pantano, O., and Saez, D., *Phys. Rev. Lett.* 72 (1994) 320.

[150] Matsubara, T., and Suto, Y., *Astrophys. J.* 470 (1996) L1.

[151] McNamara, P., Vitale, S., and Danzmann, K., *Class. Quantum Grav.* 25 (2008) 114034.

[152] Mena, F.C., Mulryne, D.J., and Tavakol, R., *Class. Quantum Grav.* 24 (2007) 2721.

[153] Misner, C.W., Thorne, K.S., and Wheeler, J.A., Gravitation (W. H. Freeman, New York, 1973).

[154] Moffat, J.W., and Tatarski, D.C., *Astrophys. J.* 453 (1995) 17.

[155] Mollerach, S., Harari, D., and Matarrese, S., *Phys. Rev.* **D** 69 (2004) 063002.

[156] Mollerach, S., and Matarrese, S., *Phys. Rev.* **D** 56 (1997) 4494.

[157] Moody, T., *Phys. Letts. B* 149 (1984) 328.

[158] Mortonso, M.J., Hu, W., and Huterer, D., *Phys. Rev.* **D** 79 (2009) 023004.

[159] Mukhanov, V.F., Feldman, H.A., and Brandenberger, R.H., *Phys. Reports* 215 (1992) 203.

[160] Mustapha, N., Bassett, B.A., Hellaby, C., and Ellis, G.F.R., *Class. Quantum Grav.* 15 (1998) 2363.

[161] Mustapha, N., and Hellaby, C., *Gen. Rel. Grav.* 33 (2001) 455.

[162] Nakamura, K., *Prog. Theor. Phys.* 110 (2003) 723.

[163] Nakamura, K., arXiv: gr-qc/0402032.

[164] Nakamura, K., *Prog. Theor. Phys.* 113 (2005) 481.

[165] Nakamura, K., *Phys. Rev.* **D** 74 (2006) 101301(R).

[166] Nakamura, K., arXiv: gr-qc/0612040.

[167] Nakamura, K., *Prog. Theor. Phys.* 117 (2007) 17.

[168] Nariai, H., *Prog. Theor. Phys.* 41 (1969) 686.

[169] Noh, H., and Hwang, J., *Phys. Rev.* **D** 69 (2004) 104011.

[170] Olson, D.W., *Phys. Rev.* **D** 14 (1976) 327.

[171] Omer, G.C., *Proc. Nat. Acad. Sci. U.S.A.* 53 (1965) 1.

[172] Osano, B., Pitrou, C., Dunsby, P., Uzan, J.-P., and Clarkson, C., *JCAP* 4 (2007) 3.

[173] Padmanabhan, T., arXiv:astro-ph/0602117.

[174] Paranjape, A., and Singh, T.P., *Phys. Rev. Lett.* 101 (2008) 181101.

[175] Pascual-Sanchez, J.F., *Mod. Phys. Lett. A* 14 (1999) 1539.

[176] Peacock, J.A., and Dodds, S.J., *Mon. Not. Roy. Astr. Soc.* 280 (1996) L19.

[177] Percival, W.J., *et al. Mon. Not. Roy. Astr. Soc.* 381 (2007) 1053.

[178] Perlmutter, S., *et al.*, *Astrophys. J.* 517 (1999) 565.

[179] Pitrou, C., *Class. Quantum Grav.* 24 (2007) 6126.

[180] Pitrou, C., *Class. Quantum Grav.* 26 (2009) 065006.

[181] Pitrou, C., *Gen. Rel. Grav.* 41 (2009) 2587.

[182] Pogosian, L., Wasserman, I., and Wyman, M., arXiv: astro-ph/0604141.

[183] Press, W., *Phys. Scr.* 21 (1980) 702.

[184] Press, W.H., and Vishniac, E.T., *Astrophys. J.* 239 (1980) 1.

[185] Räsänen, S., *JCAP* 0804 (2008) 026.

[186] Raychauduri, A., *Zeitshrift fur Astroph.* 43 (1957) 161.

[187] Riess, A.G., *et al.*, *Astrophys. J.* 116 (1998) 1009.

[188] Roos, M., (2003), *Introduction to Cosmology*, (John Wiley & Sons, Ltd).

[189] Sakai, K., *Prog. Theor. Phys.* 41 (1969) 1461.

[190] Sandage, A., *et al.*, *Astrophys. J.* 653 (2006) 843.

[191] Sato, K., *Mon. Not. Roy. Astr. Soc.* 195 (1981) 467.

[192] Schmidt, B.P., *et al.*, *Astrophys. J.* 507 (1998) 46.

[193] Schimd, C., *et al.*, *Astron. Astrophys.* 463 (2007) 405.

[194] Schneider, P., Ehlers, J., and Falco, E.E., Gravitational Lenses (Springer-Verlag Berlin, 1992).

[195] Seljak, U., and Hirata, C.M., *Phys. Rev.* **D** 69 (2004) 043005.

[196] Seljak, U., and Zaldarriaga, M., *Phys. Rev. Lett.* 78 (1997) 2054.

[197] Seljak, U., and Zaldarriaga, M., *Phys. Rev.* **D** 55 (1997) 1830.

[198] Seo, H., and Eisenstein, D., *Astrophys. J.* 598 (2003) 720.

[199] Siegel, E.R., and Fry, J.N., *Astrophys. J.* 651 (2006) 627.

[200] Silk, J., *Astrophys. J.* 151 (1968) 459.

[201] Simon, J., Verde, L., and Jimenez, R., *Phys. Rev.* **D** 71 (2005) 123001.

[202] www.ska.ac.za

[203] Smith, R.E., Sheth, R.K., and Scoccimarro, R., *Phys. Rev.* **D** 78 (2008) 023523.

[204] Smoot, G.F., *et al. Astrophys. J.* 396 (1992) L1.

[205] Sonego, S., and Bruni, M., *Commun. Math. Phys.* 193 (1998) 209.

[206] Spergel, D.N., *et al.* [WMAP Collaboration], *Astrophys. J. Suppl.* 148 (2003) 175.

[207] Spergel, D.N., *et al.* [WMAP Collaboration], *Astrophys. J. Suppl.* 170 (2007) 377.

[208] Steinhardt, P.J., and Turok, N., *Phys. Rev.* **D** 65 (2002) 126003.

[209] Stewart, J.M., *Class. Quantum Grav.* 7 (1990) 1169.

[210] Subramanian, K., Seshadri, T.R., and Barrow, J.D., *Mon. Not. Roy. Astr. Soc.* 344 (2003) L31.

[211] Takahashi, K., Ichiki, K., Ohno, H., and Hanayama, H., *Phys. Rev. Lett.* 95 (2005) 121301.

[212] Tegmark, M., *et al.* [SDSS Collaboration], *Phys. Rev.* **D** 69 (2004) 103501.

[213] Tolley, A.J., Turok, N., and Stenhardt, P.J., *Phys. Rev.* **D** 69 (2004) 106005.

[214] Tolman, R.C., *Proc. Nat. Acad. Sci. U.S.A.* 20 (1934) 169; reprinted in *Gen. Rel. Grav.* 29 (1997) 935.

[215] Tomita, K., *Astrophys. J.* 529 (2000) 26.

[216] Tomita, K., *Mon. Not. Roy. Astr. Soc.* 326 (2001) 287.

[217] Tomita, K., *Prog. Theor. Phys.* 106 (2001) 929.

[218] Tomita, K., *Phys. Rev.* **D** 71 (2005) 083504.

[219] Tomita, K., *Phys. Rev.* **D** 72 (2005) 103506.

[220] Tomita, K., *Phys. Rev.* **D** 72 (2005) 043526.

[221] Tomita, K., and Inoue, K.T., arxiv: 0903.1541.

[222] Tsagas, C.G., Challinor, A., and Maartens, R., *Phys. Reports* 465 (2008) 61.

[223] Turner, M., *Phys. Rev.* **D** 48 (1993) 3502.

[224] Turner, M., White, M., and Lidsey, J.E., *Phys. Rev.* **D** 48 (1993) 4613.

[225] Uzan, J.-P., Aghanim, N. and Mellier, Y., *Phys. Rev.* **D** 70 (2004) 083533.

[226] Uzan, J.-P., Bernardeau, F., and Mellier, Y., *Phys. Rev.* **D** 77 (2008) 021301.

[227] Uzan, J.-P., Clarkson, C., and Ellis, G.F.R., *Phys. Rev. Lett.* 100 (2008) 191303.

[228] Valiviita, J., Majerotto, E., and Maartens, R., *JCAP* 0807 (2008) 020.

[229] Weinberg, S., *Phys. Rev. Lett.* 59 (1987) 2607.

[230] Weinberg, S., *Rev. Mod. Phys.* 61 (1989) 1.

[231] http://hetdex.org/other_projects/wfmos.php

[232] White, M., *Phys. Rev.* **D** 46 (1992) 4198.

[233] Wiltshire, L., *Phys. Rev. Lett.* 99 (2007) 251101.

[234] Wyman, M., Pogosian, L., and Wasserman, I., *Phys. Rev.* **D** 72 (2005) 023513.

[235] Yamamoto, K., *Mon. Not. Roy. Astr. Soc.* 341 (2003) 1199.

[236] Yamamoto, K., Bassett, B.A., and Nishioka, H., *Phys. Rev. Lett.* 94 (2005) 051301.

[237] Zel'dovich, Ya.B., Pis'ma Zh. Eksp. Teor. Fiz. 6 (1967) 883 [JETP Lett. 6 (1967) 316].

[238] Zel'dovich, Ya.B., *Astron. Astrophys.* 5 (1970) 84.

[239] Zel'dovich, Ya.B., *Mon. Not. Roy. Astr. Soc.* 160 (1972) 1.